AFWL-TR-88-102

AD-A203 394

THE IMPLEMENTATION OF A NONREFLECTING BOUNDARY INTO THE SAMSON2 CODE

B. L. Halverson
H. C. Sorensen

Washington State University
Department of Civil and Environmental Engineering
Pullman, WA 99164

November 1988

Final Report

AFWL

Approved for public release; distribution unlimited.

AIR FORCE WEAPONS LABORATORY
Air Force Systems Command
Kirtland Air Force Base, NM 87117-6008

AFWL-TR-88-102

This final report was prepared by Washington State University, Pullman, Washington, under Contract F29601-85-K-0050, Job Order 8809131A, with the Air Force Weapons Laboratory, Kirtland Air Force Base, New Mexico. Mr Douglas Seemann (AFWL/NTES) was the Laboratory Project Officer-in-Charge.

When Government drawings, specifications, or other data are used for any purpose other than in connection with a definitely Government-related procurement, the United States Government incurs no responsibility or any obligation whatsoever. The fact that the Government may have formulated or in any way supplied the said drawings, specifications, or other data, is not to be regarded by implication, or otherwise in any manner construed, as licensing the holder or any other person or corporation; or as conveying any rights or permission to manufacture, use, or sell any patented invention that may in any way be related thereto.

This report has been authored by a contractor of the United States Government. Accordingly, the United States Government retains a nonexclusive, royalty-free license to publish or reproduce the material contained herein, or allow others to do so, for the United States Government purposes.

If your address has changed, if you wish to be removed from our mailing list, or if your organization no longer employs the addressee, please notify AFWL/NTES, Kirtland AFB, NM 87117-6008 to help us maintain a current mailing list.

This technical report has been reviewed and is approved for publication.

Rodney G Galloway

RODNEY G. GALLOWAY
Project Officer

FOR THE COMMANDER

Thomas E Bretz

THOMAS E. BRETZ
Lt Col, USAF
Chief, Applications Branch

Carl L Davidson

CARL L. DAVIDSON
Col, USAF
Chief, Civil Engineering Rsch Div

DO NOT RETURN COPIES OF THIS REPORT UNLESS CONTRACTUAL OBLIGATIONS OR NOTICE ON A SPECIFIC DOCUMENT REQUIRES THAT IT BE RETURNED.

UNCLASSIFIED
SECURITY CLASSIFICATION OF THIS PAGE

ADA203394

REPORT DOCUMENTATION PAGE

Form Approved
OMB No 0704-0188

1a. REPORT SECURITY CLASSIFICATION Unclassified	1b. RESTRICTIVE MARKINGS
2a. SECURITY CLASSIFICATION AUTHORITY	3. DISTRIBUTION/AVAILABILITY OF REPORT Approved for public release, distribution unlimited.
2b. DECLASSIFICATION/DOWNGRADING SCHEDULE	
4. PERFORMING ORGANIZATION REPORT NUMBER(S)	5. MONITORING ORGANIZATION REPORT NUMBER(S) AFWL-TR-88-102
6a. NAME OF PERFORMING ORGANIZATION Washington State University 6b. OFFICE SYMBOL (If applicable)	7a. NAME OF MONITORING ORGANIZATION Air Force Weapons Laboratory
6c. ADDRESS (City, State, and ZIP Code) Department of Civil and Environmental Engrg Pullman, Washington 99164	7b. ADDRESS (City, State, and ZIP Code) Kirtland Air Force Base, New Mexico 87117-6008
8a. NAME OF FUNDING/SPONSORING ORGANIZATION 8b. OFFICE SYMBOL (If applicable)	9. PROCUREMENT INSTRUMENT IDENTIFICATION NUMBER F29601-85-K-0050
8c. ADDRESS (City, State, and ZIP Code)	10. SOURCE OF FUNDING NUMBERS

PROGRAM ELEMENT NO.	PROJECT NO.	TASK NO	WORK UNIT ACCESSION NO
62601F	8809	13	1A

11. TITLE (Include Security Classification)
THE IMPLEMENTATION OF A NONREFLECTING BOUNDARY INTO THE SAMSON2 CODE

12. PERSONAL AUTHOR(S)
Halverson, B. L.; Sorensen, H. C.

13a. TYPE OF REPORT	13b. TIME COVERED	14. DATE OF REPORT (Year, Month, Day)	15. PAGE COUNT
Final	FROM 02/17/87 TO 12/31/87	1988, November	180

16. SUPPLEMENTARY NOTATION

17. COSATI CODES			18. SUBJECT TERMS (Continue on reverse if necessary and identify by block number)
FIELD	GROUP	SUB-GROUP	Finite Elements, Viscous Boundaries, Dynamic Analysis, Transmitting Boundaries.
12	01		
20	11		

19. ABSTRACT (Continue on reverse if necessary and identify by block number)

A nonreflecting boundary has been implemented into a dynamic explicit finite element code called SAMSON2. The nonreflecting boundary is a practical application of a viscous boundary developed by Lysmer and Kuhlemeyer. The basic principle involves an introduction of a set of dissipative stresses applied normal to and tangentially along the boundary which match the impedences of the interior of the mesh. The original viscous boundary scheme is limited to a plane elastic isotropic medium. This study expanded the versatility of the viscous boundary by including a medium that is axisymmetric, inelastic and/or anisotropic. A series of tests were conducted to determine the effectiveness of the nonreflecting boundary under a variety of circumstances. The implemented nonreflecting boundary performed very well for normal values of Poisson's ratio and for axisymmetric problems. A decrease in the effectiveness was noticed for materials with high values of Poisson's ratio and when the nonreflecting boundary is placed too close to the axis of symmetry. Also, the effectiveness of the boundary decreases as the angle of incidence of the (over)

20. DISTRIBUTION/AVAILABILITY OF ABSTRACT	21. ABSTRACT SECURITY CLASSIFICATION
☒ UNCLASSIFIED/UNLIMITED ☐ SAME AS RPT ☐ DTIC USERS	Unclassified
22a. NAME OF RESPONSIBLE INDIVIDUAL Mr Rodney G. Galloway	22b. TELEPHONE (Include Area Code) (505) 844-9088
	22c. OFFICE SYMBOL NTES

DD Form 1473, JUN 86 — Previous editions are obsolete.

SECURITY CLASSIFICATION OF THIS PAGE
UNCLASSIFIED

19. ABSTRACT (Continued)

impinging stress wave increases. These results support conclusions from previous work. Large blast and impulse loads were applied to a continuum composed of Yuma soil and fiber-reinforced concrete. These two materials were modelled using a nonlinear constitutive relationship. The results indicate that the nonreflecting boundary is also capable of absorbing radiant inelastic wave energy.

Accession For	
NTIS GRA&I	☑
DTIC TAB	☐
Unannounced	☐
Justification	
By	
Distribution/	
Availability Codes	
Dist	Avail and/or Special
A-1	

Table of Contents

LIST OF FIGURES

LIST OF SYMBOLS

a = dimensionless parameter

b = dimensionless parameter

c = wave speed

c_d = dilatational wave speed

c_s = shear wave speed

E = Young's modulus

f = frequency

F_{x_i} = horizontal viscous force applied at node i

$F_{x_{i+1}}$ = horizontal viscous force applied at node $i+1$

F_{y_i} = vertical viscous force applied at node i

$F_{y_{i+1}}$ = vertical viscous force applied at node $i+1$

G = shear modulus

H_e = horizontal distance between node i and node $i+1$

ΔI = change in impulse on a load line

$\sqrt{J_2'}$ = square root of the second invariant of the deviatoric stress tensor

M = constrained modulus

n = number of nonreflective boundaries

$N_i(x)$ = horizontal interpolation function for node i

$N_{i+1}(x)$ = horizontal interpolation function for node $i+1$

$N_i(y)$ = vertical interpolation function for node i

$N_{i+1}(y)$ = vertical interpolation function for node $i+1$

R = distance nonreflecting boundary is from axis of symmetry

t = time

t = thickness

δt = time step

u = horizontal displacement variable

$\dot{u}_i$ = horizontal velocity of node i

$\dot{u}_{i+1}$ = horizontal velocity of node $i+1$

$\dot{u}_n$ = normal velocity on boundary

$\dot{u}_t$ = tangential velocity on boundary

$\dot{u}_x$ = horizontal velocity on boundary

$\dot{v}_i$ = vertical velocity of node i

$\dot{v}_{i+1}$ = vertical velocity of node $i+1$

V_e = vertical distance between node i and node $i+1$

W_{ext} = external work done by load line

x = global horizontal coordinate

Δx_i = horizontal displacement of node i

y = global vertical coordinate

Δy_i = vertical displacement of node i

α = angle of incidence of impinging P-wave

β = angle of incidence of impinging S-wave

λ = wavelength of stress wave

μ_H = antihourglass coefficient

ν = Poisson's ratio

ρ = mass density

σ_{in} = incident stress

σ_n = normal viscous stress applied on boundary

σ_{ref} = reflected stress

σ_v = viscous stress applied on boundary

σ_x = horizontal component of viscous stress

σ_{xx} = normal stress in horizontal direction

σ_{xy} = shear stress

σ_{yy} = normal stress in vertical direction

τ = tangential viscous stress applied on boundary

Chapter 1

INTRODUCTION

In the computer analysis involving wave propagation within an infinite medium, a finite portion of the medium must be isolated so that it may be numerically modelled through the use of finite elements. This creates boundaries at the perimeter of the medium that can reflect the incident stress waves. These reflections can propagate back into the interior of the medium which is contradictory to the actual physical case. Therefore, it is appropriate to eliminate or significantly delay the reflection of these waves during a computer analysis. This can be accomplished in either of two ways. First, the dimensions of the discretized region, or mesh, can be extended with boundaries placed at a sufficient distance away from the area under consideration such that the required response is obtained before the reflections return and contaminate the solution. This necessitates the use of a large number of elements which engenders large storage requirements and computational time for the computer and may be unsatisfactory to the user. The second, which is the focus of this report, is the use of a nonreflecting boundary.

A nonreflecting boundary is also known as a transmitting, absorbing, or silent boundary. The purpose of the nonreflecting boundary is to effectively absorb the incident stress waves and, thus, simulate an infinite space. There are several advantages in using the nonreflecting boundary in comparison to the use of an extended or large mesh with a fixed/free boundary condition. First, the size of the mesh can be reduced which decreases the required amount of computer storage and computation time for

analyses. Along with the smaller mesh, there will be fewer input instructions that the user will need to prepare or modify. Finally, the solution can be performed for any length of time without the interruption of spurious reflections.

There are several beneficial characteristics a nonreflecting boundary should possess. In order for the nonreflecting boundary to serve its main purpose, it should not require an excessive amount of computer storage or central processing unit (CPU) time for it to function. Likewise, the necessary input instructions for the nonreflecting boundary should be minimal to save on user time. It is also advantageous for the boundary to be frequency independent. A frequency independent boundary allows nonlinear transient analyses to be easily performed in the time domain. In addition, a frequency- dependent boundary cannot be used in an explicit time solution because the natural frequencies of a system cannot be calculated. Versatility is another attractive property of the nonreflecting boundary. The nonreflecting boundary should be able to absorb both elastic and inelastic stress waves and be effective in an anisotropic medium. These become important factors when the medium is stratified and highly nonlinear, such as soil. Although not a stringent characteristic, the nonreflecting boundary should be relatively simple to incorporate into a computer code.

The Air Force Weapons Laboratory (AFWL) has a program called SAMSON2 which is used for analyses of large displacement, large strain, nonlinear problems with the capability for a user to model a structure/media interface. SAMSON2 is the second edition of the SMI (SAMSON) code that was developed at the Illinois Institute of Technology Research Institute (IITRI) in 1972-73. The SAMSON2 code has been subject to many changes since its introduction to the AFWL. There are intrinsic errors

that exist in the code which are continually being corrected. Also, the logic in certain sections of SAMSON2 has been created or modified to increase the efficiency of the code.

The personnel at the AFWL primarily use SAMSON2 to solve for the dynamic response of buried protective structures subject to blast and/or shock loads. In order to model this type of soil-structure interaction problem, an isolated portion of the surrounding soil in addition to the buried structure is discretized. Presently, the personnel at the AFWL need to generate a large mesh with boundaries far enough away from the structure to allow sufficient time for the analysis before the stress waves return from the boundary. A solution using a large mesh is not economical and requires a cumbersome input file. To allow the use of a smaller more efficient mesh, it was desirable to integrate into the SAMSON2 code a nonreflecting boundary.

The objective of this research was to implement into the SAMSON2 code a nonreflecting boundary that efficiently absorbs both linear and nonlinear stress waves in an anisotropic medium. It was also necessary for the boundary to be compatible with the SAMSON2 code. In other words, the nonreflecting boundary algorithm must be able to function within the framework of the SAMSON2 formulation.

This research effort began with a review of the various nonreflecting boundaries that exist in the literature. Of these boundaries, one needed to be selected that was best suited for the SAMSON2 code. If none of the boundaries were both efficient and compatible with SAMSON2, a new nonreflecting boundary had to be developed. Once the decision was made on a particular boundary, an algorithm for the nonreflecting boundary was to be written and implemented into the code. The major portion of

the research consisted of examining several sample problems, varying in complexity, that exhibit the versatility and reliability of the nonreflecting boundary. Though not originally part of the objectives of the research, any possible anomalies in the code that were discovered were to be noted with suggested corrections. This report is a compilation of the work completed and gives a summary of the capabilities and limitations of the nonreflecting boundary that was implemented into the SAMSON2 code .

Chapter 2

BACKGROUND

An overview of the SAMSON2 code is necessary in order to understand the type of nonreflecting boundary that could be used. The available nonreflecting boundaries that exist in the literature must be compatible with the code along with being efficient in the absorption of the radiant wave energy. The pertinent characteristics of the SAMSON2 code as they relate to a nonreflecting boundary are discussed in the first part of this chapter. The second part gives a brief summary of the nonreflecting boundaries that have been previously developed by various authors.

2.1 The SAMSON2 Code

There are several useful features within the SAMSON2 code. Those features that play an important role in the implementation of a nonreflecting boundary are presented.

The SAMSON2 code is an efficient two-dimensional dynamic finite element program. The code utilizes an explicit time integration scheme in its formulation. A central difference method is used to solve for the displacements and velocities of each node from their corresponding accelerations. The accelerations are simply computed from the equation of motion at each node during a specified time interval. Therefore, a system of equations does not have to be solved simultaneously during each time step. This implies that a stiffness matrix need not be generated in the calculations. The lack of a stiffness matrix means that one is unable to calculate the natural frequencies of a

system with SAMSON2. Without the frequencies, any nonreflecting boundary that is dependent on the frequencies of the system cannot be employed.

The use of explicit time integration can create an instability in the solution. The time step is restricted to a maximum length to maintain stability. This maximum time step is called the stability limit. The stability limit is approximately the time it takes for the fastest stress wave to travel the minimum length of any element divided by some constant factor usually greater than four.

Almost all of the arrays used in SAMSON2 are stored in a single large array, Q. Storage pointers or indices indicate the starting location of each major array within the Q array. A preprocessing phase of SAMSON2 reads the input parameters while the array storage pointers are saved. For a particular problem, the size of the Q array is adjusted before the actual solution phase is entered in order to reduce the storage required by the parameters. Also, this dynamic storage allocation allows the size of the individual arrays to be of any arbitrary length.

The SAMSON2 code possesses six material models in its formulation. In addition, there are three experimental models in the code that still require verification for the AFWL: an endochronic model, a viscoplastic model and a cap model developed by Weidlinger Associates. There are four elastic-plastic material laws and one purely elastic plane strain material law. The personnel at the AFWL primarily use an "engineering" material law in their soil-structure problems. The "engineering" model is defined by a segmented constitutive relationship between the hydrostatic pressure and the volumetric strain. Each linear segment has an associated bulk modulus and Poisson's ratio depending on whether the material is loading, unloading, or reloading. The

"engineering" model also contains a yield surface that correlates the hydrostatic pressure to the square root of the second invariant of the deviatoric stress tensor, $\sqrt{J_2'}$. If the current $\sqrt{J_2'}$ value calculated from the computed stresses exceeds the failure surface criterion, the elemental stresses are adjusted accordingly.

A unique capability of the SAMSON2 code is a slideline interface routine that allows sliding or separation of nodes along a specified line. The slideline interface is defined by master nodes and slave nodes that lie along the interface. The master nodes, generally, are nodes on the coarse side of the mesh while the slave node are on the fine side. The slideline interface is also useful in rigidly connecting nodes along a line that separates a fine mesh from a coarse mesh without the need for transitional elements. There are three frictional models available for the slideline interface. A discussion with Mr. Rudeen [12], however, revealed that the personnel at the AFWL are confident in the accuracy of only one of the frictional laws, the Coulombic sliding friction law. The other two, the impedence law and the shear wave transmission law, are not completely tested and verified.

Another unique feature of the SAMSON2 code is an ability to calculate a static solution using a technique called dynamic relaxation. Dynamic relaxation effectively dampens the lower frequency oscillations that occur in a dynamic solution. The lower frequency modes have the greatest effect on the response of a system. The amount of damping is controlled by a mass-proportional damping factor that is designated in the SAMSON2 input file.

The SAMSON2 finite element library is divided into three main categories: flexural, continuum, and miscellaneous elements. Of the three categories, the continuum

elements are the ones that have been considered in this study. The continuum elements can be further divided into triangular and quadrilateral elements. The purpose of the triangular element is to provide a transition between the quadrilateral elements and are seldom used solely in an analysis. Therefore, the triangular elements have not been examined extensively in this study. The remaining quadrilateral elements consist of the eight-node isoparametric element (8NQ) and four-node linear element (4NQ). The personnel at the AFWL are not completely confident in the results given by the 8NQ. Also, the mesh generation capabilities within SAMSON2 result in a more cumbersome input file for the 8NQ in comparison to the 4NQ. The 4NQ, besides being relatively easy to generate, is primarily used by the personnel at the AFWL and is trusted to give accurate results. Hence, the emphasis in this study has been on the 4NQ.

The disadvantage of the 4NQ element is the tendency for the element to exhibit hourglassing. Hourglassing is a mesh instability generated by an eigenvector displacement which results in no change in element forces, that can result in large fluctuations in the displacements of the nodes. These fluctuations can, in turn, make the element have a negative area, which will cease execution of SAMSON2. The instability arises from one-point quadrature used in the integration process within the element. Fortunately, an antihourglassing feature is used to dampen the effects of the instability. An hourglass damping coefficient, μ_H, is used to control the magnitude of the antihourglassing damping forces. At low levels, these damping forces will usually not affect the solution a great deal. Unless hourglassing poses a problem, μ_H is generally set to zero.

2.2 Review of the Literature

Various methods have been developed in attempts to model an infinite medium; all of which possess certain limitations. The objective in each case is to avoid little or no reflections while being efficient and practical.

Lysmer and Kuhlemeyer [7] developed a viscous boundary that absorbs the radiated wave energy by applying the following set of normal and tangential stresses to an otherwise free boundary:

$$\sigma_n = a\rho c_d \dot{u}_n \tag{2.1}$$

$$\tau = b\rho c_s \dot{u}_t \tag{2.2}$$

The wave energy will be absorbed if the applied viscous stresses are equal and opposite to the stresses caused by the incident wave. The surface stresses, σ_n and τ, would be proportional to the dilatational and shear impedences of the medium, ρc_d and ρc_s, the normal and tangential velocities on the boundary, $\dot{u}_n$ and $\dot{u}_t$, and dimensionless parameters a and b. The value for both of the dimensionless parameters that gave the best overall results was found to be one. The viscous boundary is a very good absorber of elastic dilatational (P) and elastic shear (S) waves. One of the best attributes of this boundary is that it is independent of the frequency of the transmitted wave and can be used within time domain solutions. Also, it would be suitable for both harmonic and transient analyses. Because of the simplicity of the viscous boundary scheme, it would be relatively easy to implement into a computer code. The viscous boundary is local in that it is based solely on the characteristic impedence and the normal and tangential velocities near the boundary. This local attribute becomes important in the analyses of

soil- structure interaction problems. The interior mesh can be highly nonlinear, which is a characteristic of soil, while the region away from the disturbance can remain linear. The authors limited the use of this viscous boundary to a plane isotropic medium.

A viscous boundary has been implemented into the explicit computer program FLEX by Weidlinger Associates [18,19]. FLEX has been used for several applications since its introduction. The applications include seismic wave propagation, electromagnetic wave propagation, earthquake engineering, and weapons effects. The formulation in FLEX contains a variety of features that are very similar to those used by SAMSON2.

It is a popularly held belief that one of the disadvantages of the viscous boundary is its inability to absorb surface waves; namely, Rayleigh waves and Love waves. Several authors have had varied results when applying the viscous boundary to surface waves. Lysmer and Kuhlemeyer [7] attempted to include the absorption of Rayleigh waves in their model. They suggested that the strength of the viscous surface stresses should also depend on the ratio of the depth from the free surface to the wavelength of the Rayleigh wave. This, however, makes the viscous boundary dependent on frequency and unsuitable for time domain solutions. The severity to which surface waves affect the solution is generally unknown. As the dilatational waves and shear waves propagate outward, they form surface waves as they strike the boundary at large angles of incidence. This may not necessarily be undesirable. If surface waves are generated, they will travel relatively slowly along the boundary without reflecting back into the interior of the medium.

If the directions of the incident stress waves were known, the viscous boundary would completely absorb the waves. Unfortunately, only in a one-dimensional wave propagation problem is the angle of incidence known. In two- or three-dimensional problems the angle of incidence varies between 0 degrees (wave impinging normal to the surface) and 90 degrees (wave travelling tangentially to the surface). The efficiency of the viscous boundary in absorbing the stress waves is dependent upon the angle of incidence of the incoming stress waves. At incident angles greater than about 60 degrees the efficiency of the viscous boundary begins to noticeably decrease. Usually, the wave energy that is not absorbed when the angle of incidence is large is of little concern for the following reasons. First, one can design a mesh such that the nonreflecting boundary is oriented normal to the wave source. Second, those waves that do impinge at large angles of incidence, usually strike one or more edges of the viscous boundary at lower angles of incidence, where they can be efficiently absorbed, before radiating back toward the source. Also, as previously mentioned, some of the wave energy that is not absorbed is transformed into surface waves. The surface waves travel along the boundary and, therefore, do not affect the interior of the mesh.

The efficiency of the viscous boundary is also dependent upon Poisson's ratio of the medium. Cohen and Jennings [3] noted that, as Poisson's ratio tends to its maximum value of 0.5, the absorption characteristics of the viscous boundary are generally less efficient. This is particularly noticeable when an incident S-wave reflects a P-wave. However, for normal values of Poisson's ratio, the effect on the efficiency is negligible.

White, Valliappan, and Lee [20] proposed to refine the Lysmer and Kuhlemeyer viscous boundary by making it more efficient and versatile. An iterative procedure

was developed to optimize the absorption qualities of the boundary. The stresses that are not initially absorbed by the viscous boundary are minimized with respect to the initial damping matrix. A new damping matrix is then calculated, and the procedure is repeated. For an isotropic medium, the optimized values of the dimensionless parameters, a and b, were found as functions of Poisson's ratio. Unfortunately, the use of the optimized parameters resulted in a very small increase in the efficiency of the boundary. The authors also stated that an anisotropic medium could be modelled by this iterative procedure. However, they have not concluded how efficient the new "unified" viscous boundary actually is for an anisotropic medium. In addition, the authors performed a study of an axisymmetric medium. They discovered that the efficiency of a viscous boundary parallel to the axis of symmetry is dependent upon the ratio of the distance away from the axis of symmetry (R) to the wavelength of the stress wave (λ). For R/λ values greater than 0.5, the axisymmetric coefficients are virtually the same as for the plane strain case. For a viscous boundary perpendicular to the axis of symmetry, there was a negligible decrease in the efficiency if plane strain coefficients were used instead of the axisymmetric coefficients regardless of the value of R/λ.

Lysmer and Waas [8] developed an excellent nonreflecting boundary for the transmission of shear waves within a layered medium. This boundary has been successfully used in the computer program FLUSH. Although the authors' work involved only Love waves, the application of this boundary into FLUSH has been extended to also transmit Rayleigh waves. The authors' theory is to incorporate the stiffness of the outer region into the equation of motion at the boundary. A "boundary stiffness" matrix is calculated from the wave numbers of the incident stress waves. The boundary

stresses that are applied to transmit the incident waves are then proportional to the displacements of the nodes on the boundary. Unfortunately, this boundary has several limitations. The primary limitation is that the boundary cannot transmit dilatational waves. Because the wavelength of the impinging wave must be known to calculate the boundary stiffness matrix, the boundary is frequency dependent. Therefore, the boundary is not applicable to time domain solutions and difficult to use in transient analyses. Another restriction of the boundary is that the interior region of the mesh must remain linear. Finally, the nonreflecting boundary can only be applied to the lateral sides of the mesh while the base must be fixed.

In order to eliminate all reflections from the boundary, the superposition of solutions that satisfy the Dirichlet and Neumann boundary conditions was suggested by Smith [16]. In two dimensions, the superposition boundary is analagous to a pair of regions in which boundaries of one region are fixed in the normal direction and free in the tangential while the boundaries for the other region are the opposite to the first region. The addition of the two solutions results in the cancellation of all reflections, including both body waves and surface waves. This method restricts the entire mesh to remain elastic so that the principle of superposition can be applied. The superposition boundary becomes exceedingly impractical for almost all cases. Each possible combination of reflections near the boundary surface must be accounted for by two solutions. In other words, for n nonreflective surfaces, the complete analysis requires 2^n solutions. The use of the superposition boundary becomes prohibitive even for a region that has only one or two nonreflecting surfaces.

Cundall, et al, [5] and Kunar and Rodriguez-Ovejero [6] developed an idea to eliminate the problem of the large number of solutions required by Smith's superposition boundary. The objective of their formulation was to have only a small area of the mesh require a superimposed solution. Two narrow boundary regions consisting of a depth of 3 or 4 elements would be connected to the interior mesh. Instead of fixed-free boundary conditions, the surfaces of the boundary regions would have constant *velocity-constant stress* similar to the scheme used by Smith. At every third or fourth time step the value for each variable in the two boundary regions is updated by averaging the corresponding values in both boundary regions. The stresses and velocities on the boundary surface are kept constant during the interim time steps. The distribution of the stresses and velocities near the boundary nearly behaves as if the attached boundary region extended to infinity. The major advantage of this boundary is the drastic reduction in the need for multiple solutions. Furthermore, only the boundary regions need to remain linear. The refined superposition boundary will cancel both body and surface waves regardless of the angles of incidence. The superposition boundary has been successfully used in the finite difference program DAMSEL. Perhaps the only disadvantages to this boundary are that it effectively adds a layer of 6 or 8 elements on the boundary of the mesh whose number may be significant in comparison to the number of elements in the interior mesh. Also, the variables within the boundary regions must be saved throughout the calculations.

Robinson [10] separated the dilatational waves and shear waves into their two respective potentials near the vicinity of the transmitting boundary. The author assumed that the body waves travel in both a plane and a cylindrical pattern. For the

plane-wave approximation, the transmitting boundary gave adequate results only at points away from the boundary. However, when the cylindrical wave approximation was used, the boundary yielded a very accurate solution for the entire region. The least accurate results in both cases appear at the junction of the axis of symmetry and the transmitting boundary. There is no restriction on the linearity of the interior mesh; only the region near the transmitting boundary needs to remain linear. The cylindrical-wave approximation becomes more accurate with an increase in the curvature of the wave. The need for a large curvature (or large radius) of the stress wave at the boundary implies that the transmitting boundary must not be placed too close to the wave source in order to obtain an accurate solution. Therefore, the size of the mesh, in some cases, may still be too large to allow the practical use of this nonreflecting boundary.

Cohen and Jennings [3] made improvements to a paraxial boundary developed from previous authors which they called the extended-paraxial boundary. A paraxial medium, which transmits waves in one direction only, is attached to the interior mesh. There were some obstacles to overcome before the extended-paraxial boundary could be effectively implemented. An interface element linking the paraxial boundary and the interior elastic mesh has to be used for a smooth wave transmission between the two regions. Because the paraxial boundary creates a nonsymmetrical boundary damping matrix, spurious oscillations will result in the solution. A numerical dissipative procedure is used to eliminate the undesired oscillations. Instabilities were observed when Poisson's ratio of the medium was greater than 1/3. This induced a negative term

in the stiffness matrix. For Poisson's ratio greater than 1/3, the authors equated this relatively insignificant negative term to zero which eliminated the instability.

A thorough study of the extended-paraxial boundary and the viscous boundary was made by Cohen and Jennings to compare the various characteristics of each boundary. It was noted that a viscous boundary is simply the first order paraxial boundary. The same advantages exist in both boundaries except that the extended-paraxial boundary is theoretically more accurate than the viscous boundary. However, in actual numerical results, this superiority is not significant. The authors showed that the extended-paraxial boundary is more efficient in transmitting Rayleigh waves than the viscous boundary. The viscous boundary, however, still performed adequately in the absorption of the Rayleigh waves. Similar to the work done by White, et al, Cohen and Jennings found that the viscous boundary parallel to the axis of symmetry does become less efficient for lower values of R/λ. Both the viscous and extended-paraxial boundaries did not absorb high frequency waves very effectively. The latter actually amplified the noise. These oscillations are easily eliminated by using some numerical damping that filters out only high frequency waves. A characteristic not pointed out by the previous authors concerning the viscous boundary is the insensitivity of the absorption efficiency to the parameters a and b. This implies that the viscous boundary may be able to absorb stress waves of varying velocities including slower travelling nonlinear waves. In the numerical application of the two nonreflecting boundaries, the authors noted that neither boundary had an adverse effect on the stability of the solution. Finally, the extended-paraxial boundary is slightly more costly to implement than the viscous boundary.

Of the several nonreflecting boundaries presented, only a few are not suitable for the SAMSON2 code. These include the boundaries that are frequency dependent, not compatible with the code, or do not allow the original size of the mesh to be reduced by an appreciable degree. The nonreflecting boundary that would be implemented into the SAMSON2 code would be chosen based on the boundary's efficiency of transmission versus the storage requirements and computation time for the computer and the ease of implementation into the SAMSON2 code.

Chapter 3

THE IMPLEMENTATION OF THE NONREFLECTING BOUNDARY

The viscous boundary scheme developed by Lysmer and Kuhlemeyer [2] was initially chosen to be implemented into the SAMSON2 code. Of the various nonreflecting boundaries that were investigated, the viscous boundary appeared to absorb the wave energy effectively and seemed to be particularly well suited for the code. The improvements made by White, et al, [6] had such a negligible effect on the efficiency of the viscous boundary that they were ignored in this study. The only other nonreflecting boundary considered in this study was the extended-paraxial boundary. The extended-paraxial boundary is slightly more costly to use than the viscous boundary and more difficult to implement. For these two reasons, the viscous boundary was the preliminary choice. If the viscous boundary did not perform to an acceptable level, the extended-paraxial boundary would then be implemented.

3.1 The Theory of the Viscous Boundary

The concept of the viscous boundary can be readily understood by examining the case of one-dimensional wave propagation in a bar. The governing differential equation for plane strain is

$$\rho \frac{d^2u}{dt^2} = E \frac{d^2u}{dx^2} \tag{3.1}$$

where, u = horizontal displacement variable

ρ = mass density

E = Young's modulus

The solution of Equation 3.1 is,

$$u = f(ct - x) + g(ct + x) \tag{3.2}$$

where,

$$c = \sqrt{\frac{E}{\rho}} \tag{3.3}$$

The arbitrary functions, f and g, represent two waves: one propagating in the positive direction and one propagating in the negative direction. The exact waveshapes are determined from the boundary conditions and the initial conditions of the problem. Assume that x is measured from the right end of a bar and that the right end is free to translate in the x-direction. For a wave travelling in the negative x-direction (to the right), the displacement function of the incident wave is given by the function g. The displacement function for the wave reflected from the free end is given by the function f. Therefore, the stress due to the incident wave is

$$\sigma_{in} = E\frac{dg}{dx} = Eg'(ct + x) \tag{3.4}$$

and the stress due to the reflected wave is

$$\sigma_{ref} = E\frac{df}{dx} = -Ef'(ct - x) \tag{3.5}$$

Assume a stress, σ_v, is applied to the free right end of the bar. The summation of the stresses at the right end must equal zero.

$$\sigma_{in} + \sigma_{ref} + \sigma_v = 0 \tag{3.6}$$

In order for the reflected wave stress in Equation 3.6 to be zero,

$$\sigma_{in} = -\sigma_v \tag{3.7}$$

Differentiating g with respect to time,

$$\frac{dg}{dt} = cg'(ct + z) \tag{3.8}$$

or

$$g'(ct + z) = \frac{1}{c}\frac{dg}{dt} \tag{3.9}$$

Substituting Equation 3.9 into Equation 3.4,

$$\sigma_{in} = \frac{E}{c}\frac{dg}{dt} \tag{3.10}$$

Therefore, the applied stress required to have no reflection from the free right end is

$$\sigma_v = -\frac{E}{c}\frac{dg}{dt} = -\rho c\frac{dg}{dt} \tag{3.11}$$

Because the applied stress σ_v is proportional to the velocity at the end of the bar, the stress is viscous and will dissipate the energy of the incident stress wave. The constant term, ρc, is called the characteristic impedence of the material. The negative sign implies that the viscous stress must be applied opposite in direction to the velocity at the boundary.

The simplicity of the one-dimensional wave propagation problem, unfortunately, does not exist in problems of two or more dimensions. Figure 3.1 shows an incident dilatational wave (P-wave) impinging on a boundary at an angle α. The P-wave will reflect as another P-wave at the same angle α and as a S-wave at an angle of β. The similar case of an incident S- wave is shown in Figure 3.2.

The viscous boundary scheme proposed by Lysmer and Kuhlemeyer equated the normal and tangential stresses of Equations 2.1 and 2.2 to the stresses at the boundary

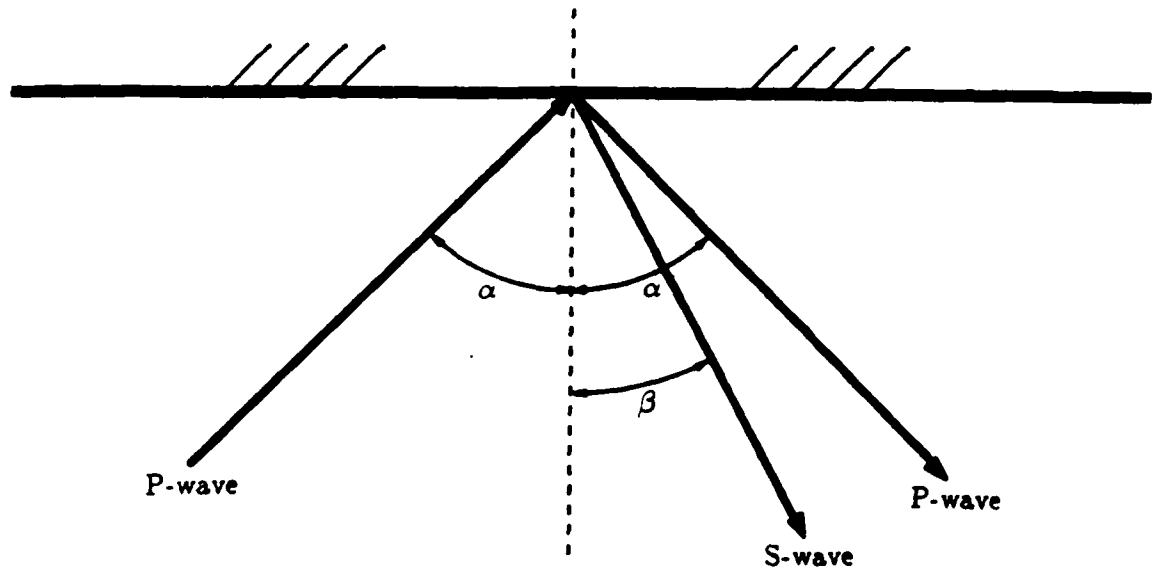

Figure 3.1 Incident P-wave

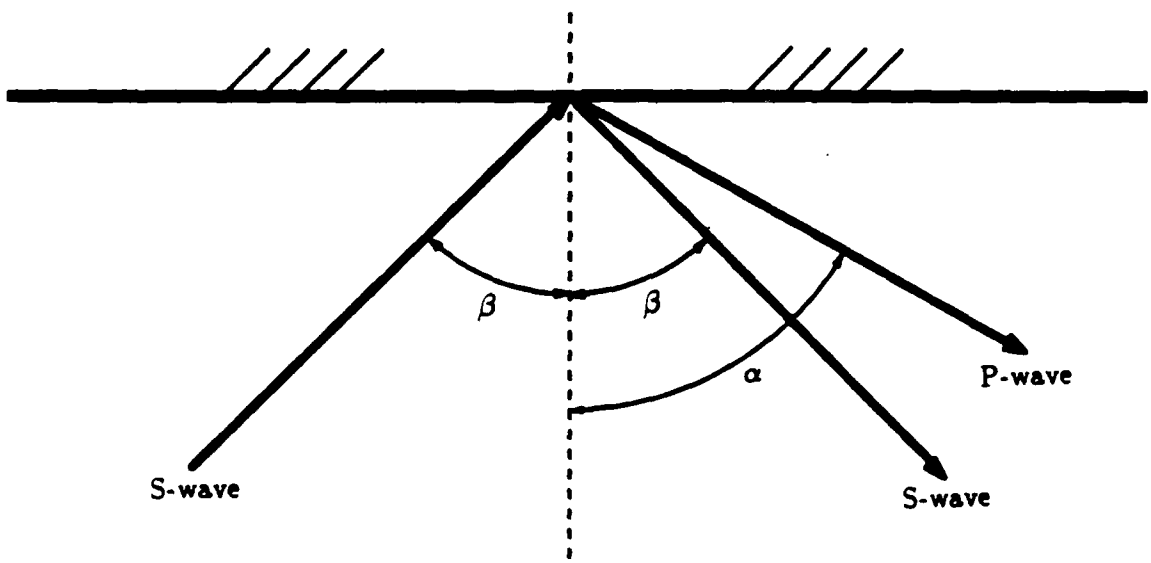

Figure 3.2 Incident S-wave

caused by the incidence of the P-wave and S-wave. The viscous stresses will perfectly absorb the incident stress waves if they impinge normal to the boundary. The efficiency of the viscous boundary, however, decreases as the angle of incidence of both waves increases from zero.

3.2 The Development of the Equations for the Nonreflecting Boundary

The wave speeds of the P-wave and S-wave and the mass density of the medium dictate the value of the dilatational and shear impedences. The relationship between the two impedences depends on the value of Poisson's ratio. The dilatational wave speed is given by

$$c_d = \sqrt{\frac{M}{\rho}} \tag{3.12}$$

where, M = constrained modulus

ρ = mass density

The shear wave speed is given by

$$c_s = \sqrt{\frac{G}{\rho}} \tag{3.13}$$

where, G = shear modulus

The modified formulation of the viscous boundary in the SAMSON2 code is based on Young's modulus. From the following two equations that relate the constrained modulus and shear modulus to Young's modulus by the Poisson's ratio, ν,

$$M = \frac{E(1-\nu)}{(1+\nu)(1-2\nu)} \tag{3.14}$$

$$G = \frac{E}{2(1+\nu)} \tag{3.15}$$

Equations 3.12 and 3.13 can be rewritten as

$$c_d = \sqrt{\frac{E(1-\nu)}{\rho(1+\nu)(1-2\nu)}} \tag{3.16}$$

$$c_s = \sqrt{\frac{E}{2\rho(1+\nu)}} \tag{3.17}$$

Therefore, the dilatational and shear impedences can be rewritten as

$$\rho c_d = \sqrt{\frac{\rho E(1-\nu)}{(1+\nu)(1-2\nu)}} \tag{3.18}$$

$$\rho c_s = \sqrt{\frac{\rho E}{2(1+\nu)}} \tag{3.19}$$

The impedence terms on the right side of equations 3.18 and 3.19 are the ones used in the modified formulation in SAMSON2.

From the impedences of the elements near the boundary, the viscous forces at the boundary can be calculated. Figure 3.3 shows a typical element (in this case, a four-node quadrilateral element) adjacent to a nonreflecting boundary. The nodes i and $i+1$ are nodes that define a segment along the nonreflecting boundary. The horizontal and vertical velocities of the nodes are represented as $\dot{u}$ and $\dot{v}$, respectively. H_e is the horizontal projection and V_e is the vertical projection of the line connecting nodes i and $i+1$ to the global x and y axes.

The normal and tangential stresses applied on the boundary can be transformed into their respective horizontal and vertical components. The horizontal and vertical viscous stresses applied at the nodes, therefore, are both dependent on the contributing effects of the impinging S-waves and P-waves. For simplicity, the case of an incident plane P-wave is examined. The horizontal component of the normal viscous stress is

$$\sigma_x = -\rho c_d \dot{u}_x \tag{3.20}$$

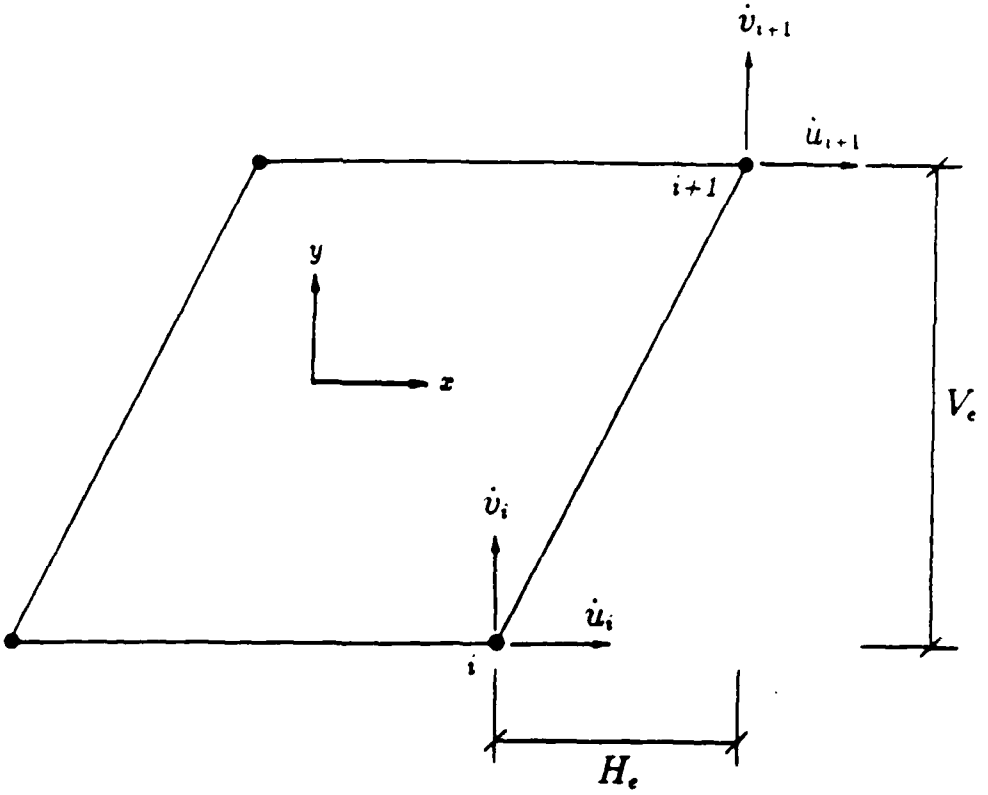

Figure 3.3 Typical Element adjacent to a Nonreflecting Boundary

where, $\dot{u}_x$ is the horizontal component of the normal velocity.

$$\dot{u}_x = N_i(y)\dot{u}_i + N_{i+1}(y)\dot{u}_{i+1} \tag{3.21}$$

where $N_i(y)$ and $N_{i+1}(y)$ are the linear interpolation functions of the horizontal component of the normal velocity whose origin is at node i

$$N_i(y) = 1 - \frac{y}{V_e} \tag{3.22}$$

$$N_{i+1}(y) = \frac{y}{V_e} \tag{3.23}$$

The horizontal forces at the nodes can be calculated using the linear interpolation functions of Equations 3.22 and 3.23

$$F_{x_i} = -\int_0^{V_e} N_i(y)\sigma_x t dy \tag{3.24}$$

$$F_{x_{i+1}} = -\int_0^{V_e} N_{i+1}(y)\sigma_x t dy \tag{3.25}$$

where, t = thickness of the element normal to the plane of the element

Substituting Equations 3.20 and 3.21 into Equations 3.24 and 3.25

$$F_{x_i} = -\int_0^{V_e} \rho c_d N_i(y)[N_i(y)\dot{u}_i + N_{i+1}(y)\dot{u}_{i+1}] \tag{3.26}$$

$$F_{x_{i+1}} = -\int_0^{V_e} \rho c_d N_{i+1}(y)[N_i(y)\dot{u}_i + N_{i+1}(y)\dot{u}_{i+1}] \tag{3.27}$$

Integrating and putting into matrix form,

$$\begin{Bmatrix} F_{x_i} \\ F_{x_{i+1}} \end{Bmatrix} = -\rho c_d t V_e \begin{bmatrix} 2/6 & 1/6 \\ 1/6 & 2/6 \end{bmatrix} \begin{Bmatrix} \dot{u}_i \\ \dot{u}_{i+1} \end{Bmatrix} \tag{3.28}$$

By a similar argument, the horizontal nodal forces caused by an incident plane S-wave can be found. In this case, the linear interpolation functions for the horizontal component of the tangential velocity must now be used.

$$N_i(x) = 1 - \frac{x}{H_e} \tag{3.29}$$

$$N_{i+1}(x) = \frac{x}{H_e} \tag{3.30}$$

Resulting in the equation

$$\begin{Bmatrix} F_{x_i} \\ F_{x_{i+1}} \end{Bmatrix} = -\rho c_s t H_e \begin{bmatrix} 2/6 & 1/6 \\ 1/6 & 2/6 \end{bmatrix} \begin{Bmatrix} \dot{u}_i \\ \dot{u}_{i+1} \end{Bmatrix} \tag{3.31}$$

Combining the total horizontal forces from the incident P-wave and the incident S-wave,

$$\begin{Bmatrix} F_{x_i} \\ F_{x_{i+1}} \end{Bmatrix} = -\rho c_d t V_e \begin{bmatrix} 2/6 & 1/6 \\ 1/6 & 2/6 \end{bmatrix} \begin{Bmatrix} \dot{u}_i \\ \dot{u}_{i+1} \end{Bmatrix} - \rho c_s t H_e \begin{bmatrix} 2/6 & 1/6 \\ 1/6 & 2/6 \end{bmatrix} \begin{Bmatrix} \dot{u}_i \\ \dot{u}_{i+1} \end{Bmatrix} \tag{3.32}$$

Expanding this procedure further, the total vertical forces at the two nodes are

$$\begin{Bmatrix} F_{y_i} \\ F_{y_{i+1}} \end{Bmatrix} = -\rho c_d t H_e \begin{bmatrix} 2/6 & 1/6 \\ 1/6 & 2/6 \end{bmatrix} \begin{Bmatrix} \dot{v}_i \\ \dot{v}_{i+1} \end{Bmatrix} - \rho c_s t V_e \begin{bmatrix} 2/6 & 1/6 \\ 1/6 & 2/6 \end{bmatrix} \begin{Bmatrix} \dot{v}_i \\ \dot{v}_{i+1} \end{Bmatrix} \quad (3.33)$$

Equations 3.32 and 3.33 are the final versions of the equations that are implemented into the SAMSON2 code. The horizontal viscous force vector including F_{x_i} and $F_{x_{i+1}}$ is represented by FX1 and FX2 in the code. Likewise, the vertical viscous force vector is represented by FY1 and FY2. Also, the vertical distance and the horizontal distance, V_e and H_e, are expressed as CC and SS respectively. The variable name THICK is the thickness t.

The preceding equations assumed planar stress waves. For the axisymmetric case, all of the forces are multiplied by the distance the midpoint of the segment joining nodes i and $i+1$ is from the axis of symmetry.

3.3 The Formulation of the Nonreflecting Boundary in the SAMSON2 Code

The viscous boundary, as originally developed, is limited to an isotropic plane medium. Also, the region near the boundary must remain elastic. The features within the SAMSON2 code provided the means to extend the capability of the viscous boundary. The wave energy propagating in an anisotropic, axisymmetric medium could also be absorbed by using the modified formulation within the SAMSON2 code. The effectiveness of the viscous boundary in absorbing inelastic waves, however, was unknown. Cohen and Jennings [3] stated that the viscous boundary could be applied for inelastic problems due to the insensitivity of the viscous stresses to the dimensionless parameters a and b. However, they did not solve any problems that had nonlinear behavior.

Several problems were run in this study to test the effectiveness of the viscous boundary in an inelastic medium. The results will be discussed in Chapter 4.

The principle material law used by the AFWL is the "engineering" material model. During each time step, the "engineering" material model subroutine updates the stiffness within each element (i.e., a nonlinear material law). This implies that the characteristic impedence for each element can also be updated at each time step. For an element located on the boundary, the strengths of the viscous stresses applied at its boundary are dictated by its current impedences. Consequently, the viscous boundary should be able to absorb the radiating wave energy in an inelastic, anisotropic medium. Unfortunately, when the logic was programmed into the SAMSON2 code and several test runs were made, the results were less accurate than those that were based on a purely elastic viscous boundary.

The strategy for implementing the nonreflecting boundary into SAMSON2 was to create as few additional executable lines of code as possible. Fewer lines would limit the amount of CPU time required for the operation of the nonreflecting boundary. Thus, there was no incorporation of an additional subroutine in the code. The existing subroutines were to be modified to provide the means to implement a nonreflecting boundary.

Within the subroutine FREEF2, the external forces of the system are calculated and located in the array FORCD. FREEF2 mainly uses input information from the load line data cards to calculate these external forces. Among the arguments passed to FREEF2 are the velocity array, V, and the load line information arrays: IVOL, KPRES and PT. IVOL contains the load line master control data, KPRES lists the

node numbers along the load line, and PT contains either time function pairs or the initial velocity data. The nonreflecting boundary can be interpreted as externally applied forces that depend on the velocity of the nodes on the boundary and the local impedences of the medium near the boundary. The nonreflecting boundary, therefore, can be treated as a load line. Thus, the main formulation of the nonreflecting boundary was located in the subroutine FREEF2. The velocity array is already available to the subroutine in the original SAMSON2 code (passed to FREEF2 as array V). Only an array of the impedences of the material near the boundary needed to be added to the list of arrays that are passed to FREEF2.

The subroutine READPV is used to read the load line input information. The modifications made to READPV by the authors would entail two objectives. First, the subroutine must allow the input instructions for the nonreflecting boundary to be read. Second, the impedences of the medium near the boundary would be calculated and stored in an array. The new modified version of READPV is listed in Appendix C.

The subroutine READPV is called NPRES times by the subroutine PREPROC, where NPRES is the total number of load lines in a problem. In the original SAMSON2 code, the arguments passed to READPV are the load line information arrays and the variables THICK and LADD. THICK is the thickness of a planar problem pressure line, and LADD is the extra storage requirement for the load line information. In the modified version, four additional arrays are passed to READPV: E, INDXE, IX and BIMP. E contains the element group data. The E array is split into three different "subarrays" for each material group. The three subarrays are the element-group master

control array, the element parameter array and the material law parameter array. The storage pointers that list the starting locations of the three subarrays for each element group are stored in array INDXE. The material law parameter subarray is the only one that is utilized in READPV. IX contains the element connectivity data. BIMP is a new array that stores the dilatational and shear impedences for each element along the nonreflecting boundary. When the arrays KPRES, PT, and BIMP are passed to READPV from PREPROC, they are all indexed from the same storage pointer. The call statement passes these three arrays as Q(L+6).

At the beginning of subroutine READPV, the load line control data on card 10A are initially read. This procedure has not been changed by the authors. The next step is an IF- THEN-ELSE block that reads time function pairs (if IVOL(1) equals -2, -1, 1, or 2) or the initial velocity data (if IVOL(1) equals 0) of card 10B. The values are stored in the array PT. An additional ELSEIF statement has been included in this block. If IVOL(1) equals 3 or 4 (the load line is a nonreflecting boundary), the number of time function pairs is zero and the value is stored in IVOL(5). The node numbers along the load line are then read and stored in the array KPRES. Because PT and KPRES were indexed at the same location when they were passed to READPV, the values of KPRES are stored beginning at location 2*NPT+1. This procedure has also not been changed from the original code. The remainder of the subroutine is the addition of a double DO loop block that finds the element numbers along a nonreflecting boundary, calculates the dilatational and shear impedences for each element and stores the values in the array BIMP.

The first DO loop is incremented from the starting location of the array KPRES to the second from last location of KPRES. The purpose of the DO loop is to retrieve two successive node numbers along the boundary at a time. Each pair of successive node numbers define a segment on the boundary and an edge of a particular element. The second DO loop then checks each element in the mesh and finds which element has an edge that corresponds to the current pair of node numbers on the boundary. At the beginning of the DO loop, the type of each element is found (i.e., the number of nodes of an element). Depending on the type of the element, all of the edges of the element (two adjacent nodes on the element) will be compared to the current pair of node numbers on the boundary. The nodes numbers are checked in a counterclockwise sense. In other words, the element will be to the left of the line connecting the first node to the second node. If none of the edges of the element match the current segment on the boundary, the next element is checked. If an edge of the element matches the current segment, the second DO loop is exited. The dilatational and shear impedences of the element are then calculated and stored.

The element group number of the element is used to find the storage pointer of the material law parameter array. From this array, the density, Young's modulus and Poisson's ratio within the element are found. The dilatational and shear impedences of the element are calculated using Equations 3.18 and 3.19 and stored in the array BIMP. Similar to KPRES, BIMP was passed to READPV indexed at the same location as PT. As previously mentioned, the first DO loop begins from the storage pointer, 2*NPT+1, where the array KPRES is indexed. The element impedences must be stored starting from the location immediately after KPRES. Therefore, the storage pointer

for the array BIMP is NDNOD greater than the storage pointer for KPRES, where NDNOD is the number of nodes on the load line. An additional counter is used to allow for the storage of two variables for each pass of the first DO loop. The dilatational impedence is stored first and the shear impedence second. After the impedences have been calculated and stored for a segment on the boundary, the next pair of node numbers is examined, and the procedure is repeated until all of the nodes on the load line have been accounted for. The last step of the subroutine is to adjust the value of LADD for the additional storage requirement for the array BIMP. For a series of nodes along a load line, the number of elements will be one less than the number of nodes. Thus, the variable LADD must be increased by NDNOD-1 for a nonreflecting boundary.

The subroutine SOLVE controls the main solution phase of SAMSON2. SOLVE begins by calling the subroutine FREEFD that calculates the initial boundary conditions of a problem. The main time integration loop is then entered. Within the loop, the external forces of the problem are computed by the subroutine FREEF2, the internal forces by the subroutine FRCIN and the slideline forces by the subroutine SLIDER. With these forces, the displacements, velocities and accelerations of the nodes are found using the equations of motion by calling the subroutine MOTION. There have only been two modifications made by the authors to the subroutine SOLVE. The two modifications are to the call statements for FREEFD and FREEF2. In the modified code, the array BIMP is also passed to these two subroutines. The array is passed as PR(L3). In the subroutine SOLVE, all of the load line arrays are stored in the array PR. The

variable L3 is the storage pointer for the array KPRES. The reason for the modification to the call statement to subroutine FREEFD is that FREEFD later calls the subroutine FREEF2.

The changes to subroutine FREEFD were made solely to allow for the call to FREEF2. The array BIMP has been added to the argument list of the first line of FREEFD. Correspondingly, the size of the array must be declared to be one in the dimension statement. The last modification is the addition of the array BIMP to the arguments passed in the call statement to FREEF2.

The new modified subroutine FREEF2 is listed in Appendix C. Only two lines in the subroutine have been changed; all other modifications have been only the addition of new lines. The argument list in the first line of FREEF2 now lists an additional array called BIMP. Recall that BIMP contains the boundary impedences of the elements along a particular nonreflecting boundary that were calculated in the subroutine READPV. The second line modification is the dimension statement where the size of the array BIMP is declared to be one.

Upon entering subroutine FREEF2, several variables are initialized. The subroutine then branches using an IF-THEN-ELSEIF block that calculates the values for the arrays FORCD and STRS depending on the value of IVOL(1). The procedure in calculating the external forces for a nonreflecting boundary is similar to that used for a pressure line. The primary difference is that the velocity-dependent viscous stresses (or pressures) of the nonreflecting boundary are continually changing during the solution, while the pressures of the pressure load line are dictated by the input information. For each successive pair of node numbers, or segments, along the boundary, the viscous

forces are computed from the horizontal and vertical velocities of the two nodes and the dilatational and shear impedences of the adjacent element within a DO loop. At the beginning of the DO loop, the horizontal and vertical distances (SS and CC) between the current two nodes are calculated. The positive sign convention is shown in Figure 3.3. The horizontal and vertical velocities of the two nodes are retrieved from the array V. Because the array BIMP was passed to FREEF2 from the same location as KPRES, the index of BIMP is increased by NDNOD, the number of nodes on the load line. Equations 3.32 and 3.33 are used to solve for the viscous forces. If the non-reflecting boundary is for an axisymmetric problem, the viscous forces are multiplied by the average distance the two nodes are from the axis of symmetry. The resulting viscous forces are finally stored in the appropriate locations in the external force array FORCD.

The equations for computing two of the global variables for a load line have been modified by the authors. The external work done by the viscous forces is incrementally added for each segment along the load line.

$$W_{ext} = \sum_{i=1}^{NDNOD} F_{x_i} \Delta x_i + F_{y_i} \Delta y_i \tag{3.34}$$

where, Δx = displacement in the x-direction during a a time step

Δy = displacement in the y-direction during a a time step

The equation for the change in impulse on the load line is

$$\Delta I = \delta t \sqrt{\sum_{i=1}^{NDNOD} F_{x_i}^2 + F_{y_i}^2} \tag{3.35}$$

where, δt = the time step

3.4 Revised Input Instructions for SAMSON2

The nonreflecting boundary is treated as another load line in the input instructions. The new updated load line control data card (card 10A) is given in Appendix A. Card 10A is the only card in the SAMSON2 input instructions that has been modified. The only modifications to the load line card are the extra two options for the load line type (IVOL(1)). For a nonreflecting boundary in a axisymmetric problem, IVOL(1) must equal three; and for an plane problem, IVOL(1) must equal four. The only requirement for the use of the nonreflecting boundary is that the nodes on the nonreflecting boundary must be inputted in a counterclockwise fashion. An example is seen in Figure 3.4. Assume the surface along the left and bottom edges of the figure are to be nonreflective. The nodes would be inputted as 3, 4, 5, ..., 80, 90. Also, the node generation option is still applicable for the nonreflecting boundary if the difference between successive node numbers is constant.

Example input files utilizing the nonreflecting boundary are located in Appendix D. The nonreflecting boundary input instructions are the last lines in all of the input files. The first set of load line instructions (load line 1) is the actual pressure or displacement function applied to the system.

For 4NQ element problems involving the AFWL "engineering" material model, Young's modulus is used only for the antihourglassing damping forces. The Poisson's ratio on card 5C-1 is not used at all. The values of Young's modulus and Poisson's ratio should be such that they predict the approximate dilatational and shear wave speeds of the medium during a solution. In the following chapter, the results show that the best overall approximations for Young's modulus and Poisson's ratio correspond to

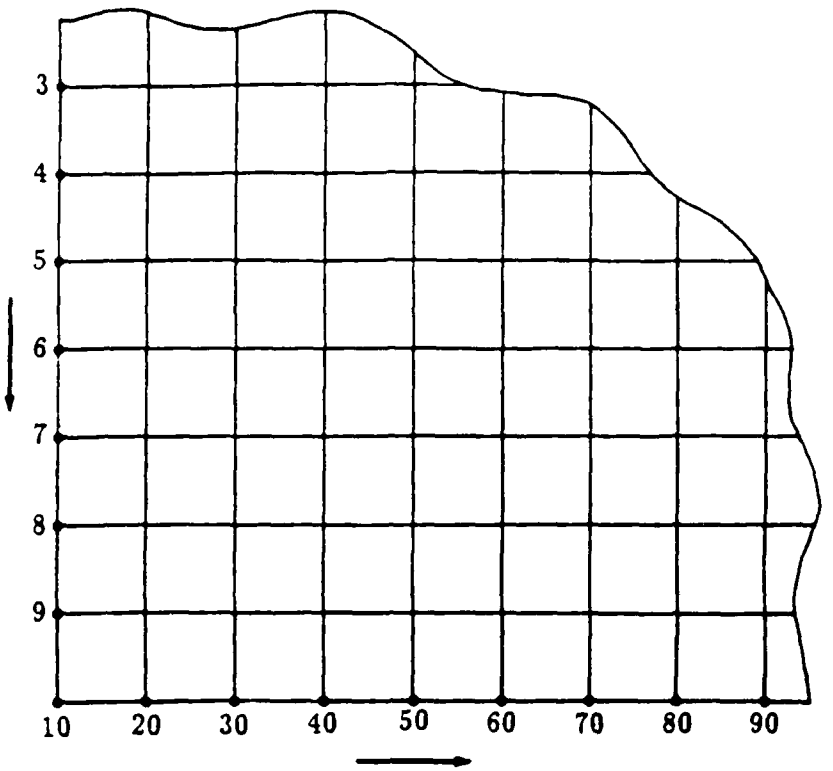

Figure 3.4 Order of Nodes Along a Nonreflecting Boundary

the values of the bulk modulus and Poisson's ratio for the first loading segment. The antihourglass damping coefficient, μ_H, should be used to regulate the magnitude of the antihourglass damping forces for a given Young's modulus.

Chapter 4

THE EVALUATION OF THE NONREFLECTING BOUNDARY

Once the algorithm for the nonreflecting boundary was implemented into the SAMSON2 code, a series of tests was performed to check the effectiveness of the boundary. Each individual test consisted of three solutions. The first solution was obtained for a large, or extended, mesh. The large mesh solution would simulate an infinite medium. A small portion of the large mesh surrounding the loading area was then isolated and analyzed under two different sets of boundary conditions. The boundary conditions were defined along the line that truncated the larger mesh. The second solution was the response of the small, or truncated, mesh with the nonreflecting boundary active along this line. The comparison of these two solutions would demonstrate if the nonreflecting boundary were absorbing the radiant wave energy and, thus, simulating an infinite medium. The third or final solution was the analysis for the same small mesh but with a fixed/free boundary condition. The small mesh solution without the nonreflecting boundary gave a qualitative measure of the effectiveness of the nonreflecting boundary and showed what can occur when the reflections of the stress waves are allowed to return and contaminate the analysis in the interior of the mesh. The total solution time for all three solutions was limited to the approximate time the first stress wave reflection from the boundary of the large mesh returned to the analysis area for the three tests. This time would determine when the large mesh solution would cease to behave as an infinite medium.

The three solutions obtained for each test may be inaccurate due to the probable existence of logical errors in the SAMSON2 code. This inaccuracy, however, is unlikely to pose problems in the evaluation of the nonreflecting boundary. The objective for each test is to compare the results of three solutions. Since the nonreflecting boundary depends solely upon parameters near the boundary, it does not affect the behavior of the interior of the mesh. The same errors that may be generated in one solution will be consistently repeated in the other two. Therefore, the effectiveness of the nonreflecting boundary will be independent of the potential errors generated in the three solutions.

There are four possible results that can occur in each test. The following are conclusions which can be obtained from each result:

1. If all three of the solutions are similar;

   the radiating stress waves in the small mesh without the nonreflecting boundary have not had time to propagate to the boundary and return to the point under analysis. Therefore, the total solution time should be extended to allow sufficient time for the reflections to return.

2. If all three of the solutions are not similar;

   the nonreflecting boundary is only partially effective in the absorption of the stress waves. This is an unsatisfactory condition.

3. If only the small mesh solutions with and without the nonreflecting boundary are similar;

the nonreflecting boundary is completely ineffective. This is the worst possible result that can occur.

4. If only the solution of the small mesh with the nonreflecting boundary and the large mesh solution are similar;

   the nonreflecting boundary is satisfactorily absorbing the radiating stress waves. The test is successful.

One other result might occur that is unrelated to the calculations within the SAMSON2 code. If all three solutions do not coincide up to a certain point, then an error exists in one or more of the input files. This was a check to verify that each input file was correct. If all three of the input files were correct, the files are said to be compatible.

The evaluation of the nonreflecting boundary is separated into two categories of problems. First, a simple one-dimensional wave propagation problem is thoroughly investigated. Many facets of the SAMSON2 code, including both material and element properties, were varied for a bar subjected to a dilatational wave and a shear wave. This study provided simple tests for the effectiveness of the nonreflecting boundary for several parameters. Also, the various tests in the one-dimensional wave propagation study was used to check the formulation of the nonreflecting boundary within the SAMSON2 code. Once the nonreflecting boundary appeared to be functioning correctly, a much more realistic and complex problem was analyzed. The second part of the evaluation involved a two-dimensional axisymmetric problem that provided tests

to check the effectiveness of the nonreflecting boundary subject to stress waves with varying angles of incidence and material properties.

The original scope of the research was to include the solution of a typical soil-structure interaction (SSI) problem that has been analyzed by the personnel at the AFWL. Unfortunately, the slideline interface routine within the authors' version of SAMSON2 did not function properly. The time to correct the errors in the slideline routine would not justify the need to include a slideline interface in the test problems. The nonreflecting boundary is independent of the interior properties of the mesh. Therefore, the slideline interface would not affect the effectiveness of the nonreflecting boundary and, thus, its inclusion in the two-dimensional problems would not be essential in this study.

4.1 One-Dimensional Wave Propagation

The initial tests involving the nonreflecting boundary consisted of examining various sample problems that were modifications of the one-dimensional wave propagation problem in Appendix A of the SAMSON2 user's manual [12]. The purposes of utilizing this particular problem are twofold. The computer solutions that exist in the user's manual provided the opportunity to check that the present version of SAMSON2, transferred to the Washington State University's IBM 3090, performs correctly. Second, a comparison of the original SAMSON2 solutions in the users manual to the modified version of SAMSON2 solutions affirmed that the implementation of the nonreflecting boundary into the code did not affect the correct results.

Two bars were used exclusively throughout the one-dimensional study. A long bar, which will be referred to as a large mesh, was 40-cm long by 4-cm high with a thickness of 1-cm. The right end of the long bar was free to translate. A short bar, accordingly referred to as a small mesh, had the same cross-sectional dimensions as the long bar while the length was shortened to 6-cm. In one case, the nonreflecting boundary was applied to the right end of the short bar; in the other case, the right end was free. Each bar is perfectly elastic and has no internal damping. Poisson's ratio is zero except when noted and Young's modulus and the mass density are each assigned the value of one.

For all the wave propagation tests, a displacement history function described in Figure 4.1 was applied to the left end of each of the bars. When a bar is subjected to a dilatational wave, all nodes are free to translate in both the horizontal and vertical direction relative to the longest axis of the bar. The displacement function is then applied normal to the nodes on the left face of the bar. When a bar is subjected to a shear wave, all nodes are free to translate in the vertical direction but are fixed in the horizontal direction. This restricts the bar to deform only in shear and greatly reduces the flexural deformation. The displacement function is then applied tangentially to the nodes on the left face of the bar.

All of the various continuum elements in the SAMSON2 library were tested. However, only the four-node quadrilateral (4NQ) and the eight-node quadrilateral (8NQ) element results are presented. The 4NQ and 8NQ are the principal elements used by the personnel at the AFWL. The remaining triangular elements are mostly used

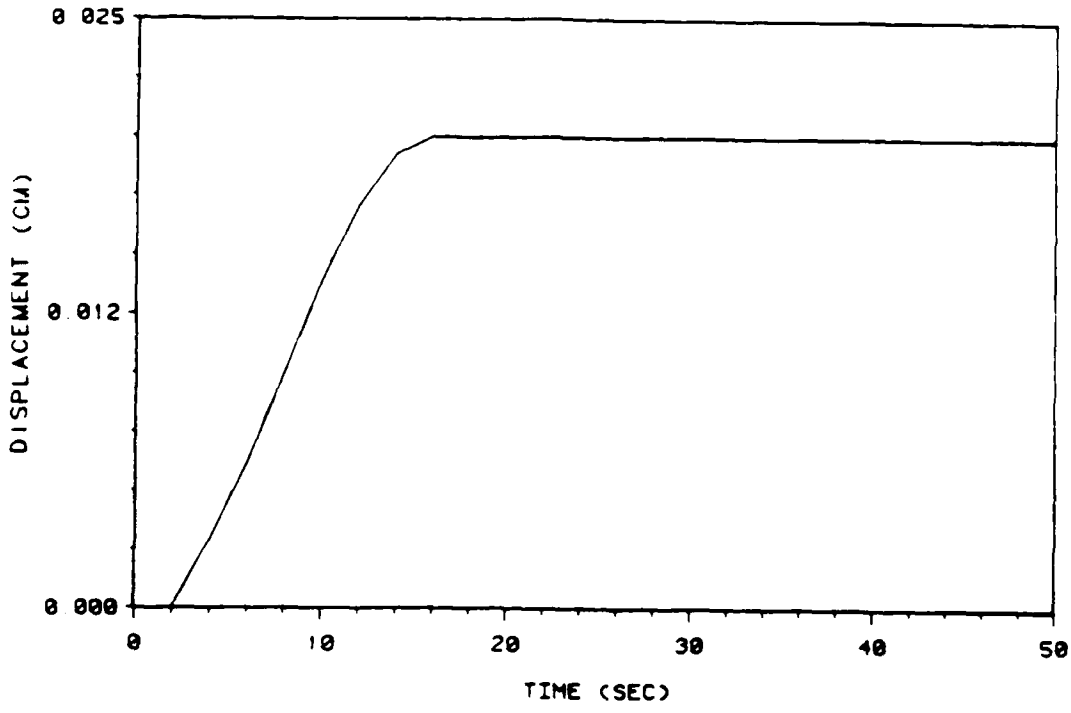

Figure 4.1 Displacement Function

in a transition between the quadrilateral elements and were not considered to be important in this study. The results of the one-dimensional problem using the triangular elements were similar - but slightly less accurate - to the results using the quadrilateral elements. The SAMSON2 input files for a selected number of wave propagation tests are listed in Appendix D.

The tests that involved the 4NQ element used the two discretized meshes shown in figure 4.2. The large mesh consists of 63 nodes and 40 elements. The small mesh has 12 nodes and 6 elements. Each element is 2-cm by 2-cm with a thickness of 1-cm. The horizontal and vertical displacement of a node located 2-cm from the left and 2-cm from the bottom of the bar (x = 2-cm, y = 2- cm) are compared in the three solutions. The normal and shear stresses are also evaluated at the center of an element

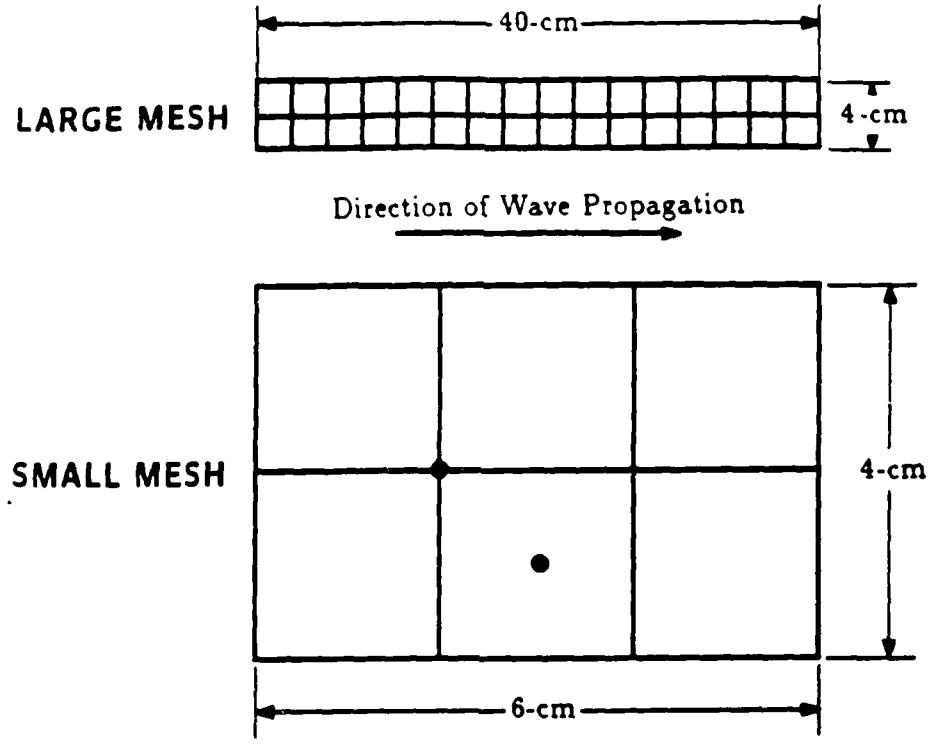

Figure 4.2 4NQ Discretization of One-Dimensional Bars

at a point 3-cm from the left and 1-cm from the bottom of the bar (x = 3-cm, y = 1-cm). The positions of both points in the two discretized bars are marked as dots in the figure.

The first test was a bar consisting of 4NQ plane continuum elements subjected to a dilatational stress wave. The graphical results for the displacement and the normal stress versus time are shown in Figures 4.3 and 4.4. The large mesh solution, simulating an infinitely long bar, is plotted as a solid line. The short dashed line represents the small mesh solution with the nonreflecting boundary applied at the right end of the bar. If the nonreflecting boundary is working properly, the solid line and the short-dashed line should be superimposed. Finally, the long-dashed line represents the small mesh with a free right end and demonstrates the effective absorption of the nonreflecting

boundary. Note that all three curves coincide up to a time of about 8-sec indicating that the input files are compatible. The two figures show that there is almost complete absorption of the dilatational stress wave.

The next test was similar to the previous test except that the bars are now subjected to a shear wave instead of a dilatational wave. The graphical results are presented in Figures 4.5 and 4.6. Once again, there is nearly perfect absorption of the shear wave. The slight discrepancy in the shear wave solutions can be accounted for by small amounts of flexural deformations that occur in the bars.

At this point in the testing, several conclusions could be made. The algorithm of the nonreflecting boundary implemented into the subroutine FREEF2 is correct for all plane continuum elements. The procedure for finding the elements along the nonreflecting boundary for the 4NQ continuum element and the equations for the dilatational and shear impedences written into the subroutine READPV are correct. There were no errors in the passage of the various arrays added to the argument lists of the modified subroutines which suggest that the storage pointers for the arrays have been correctly indexed.

To insure the complete accuracy for the algorithm of the nonreflecting boundary in the subroutine FREEF2, tests were conducted with the 4NQ axisymmetric continuum element. Bars parallel and perpendicular to the axis of symmetry were again subjected to a dilatational and a shear wave. For the bars parallel to the axis of symmmetry, identical solutions to those calculated in the previous plane case were observed.

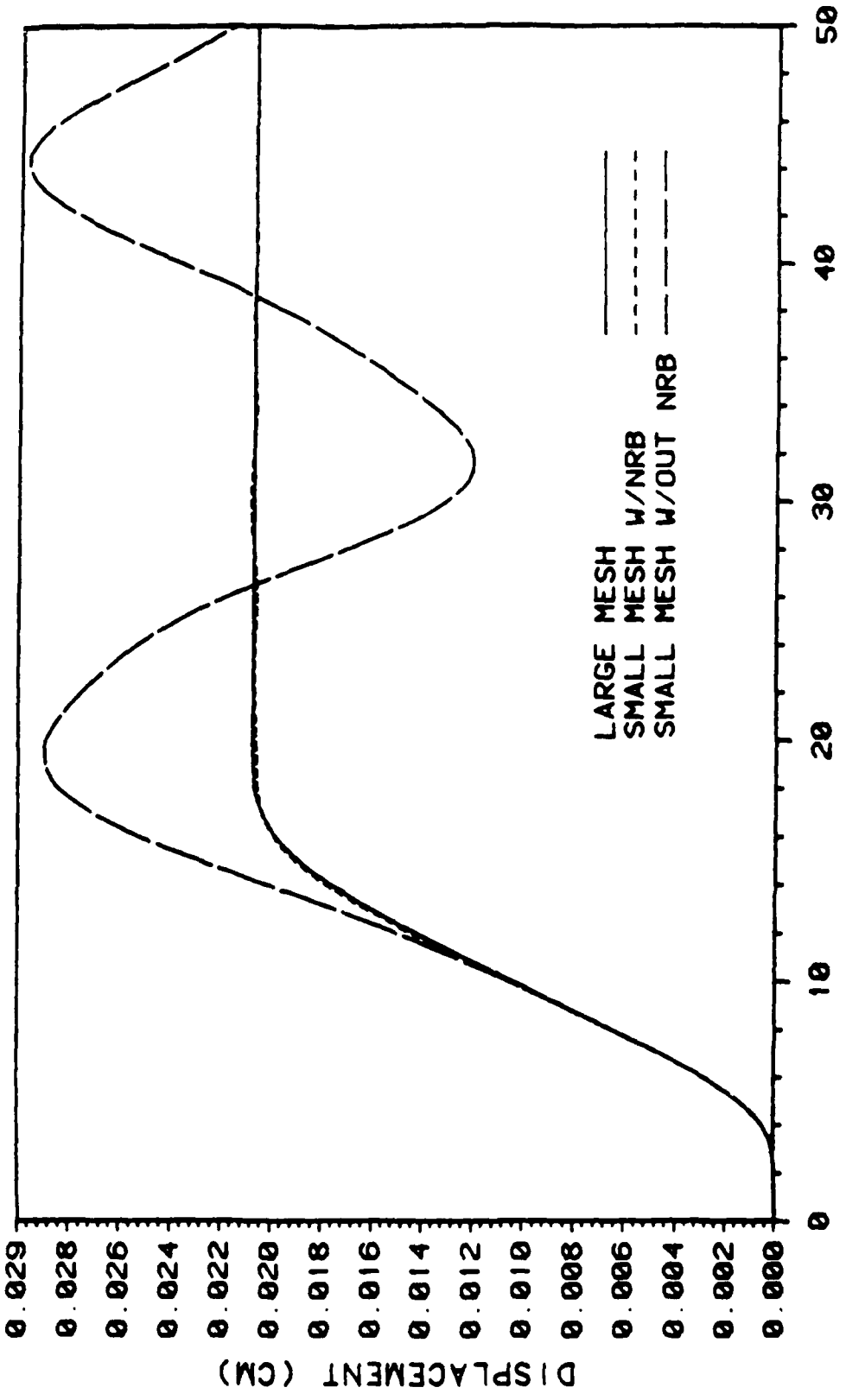

Figure 4.3 Horisontal Displacement vs. Time at $x = 2$-cm, $y = 2$-cm

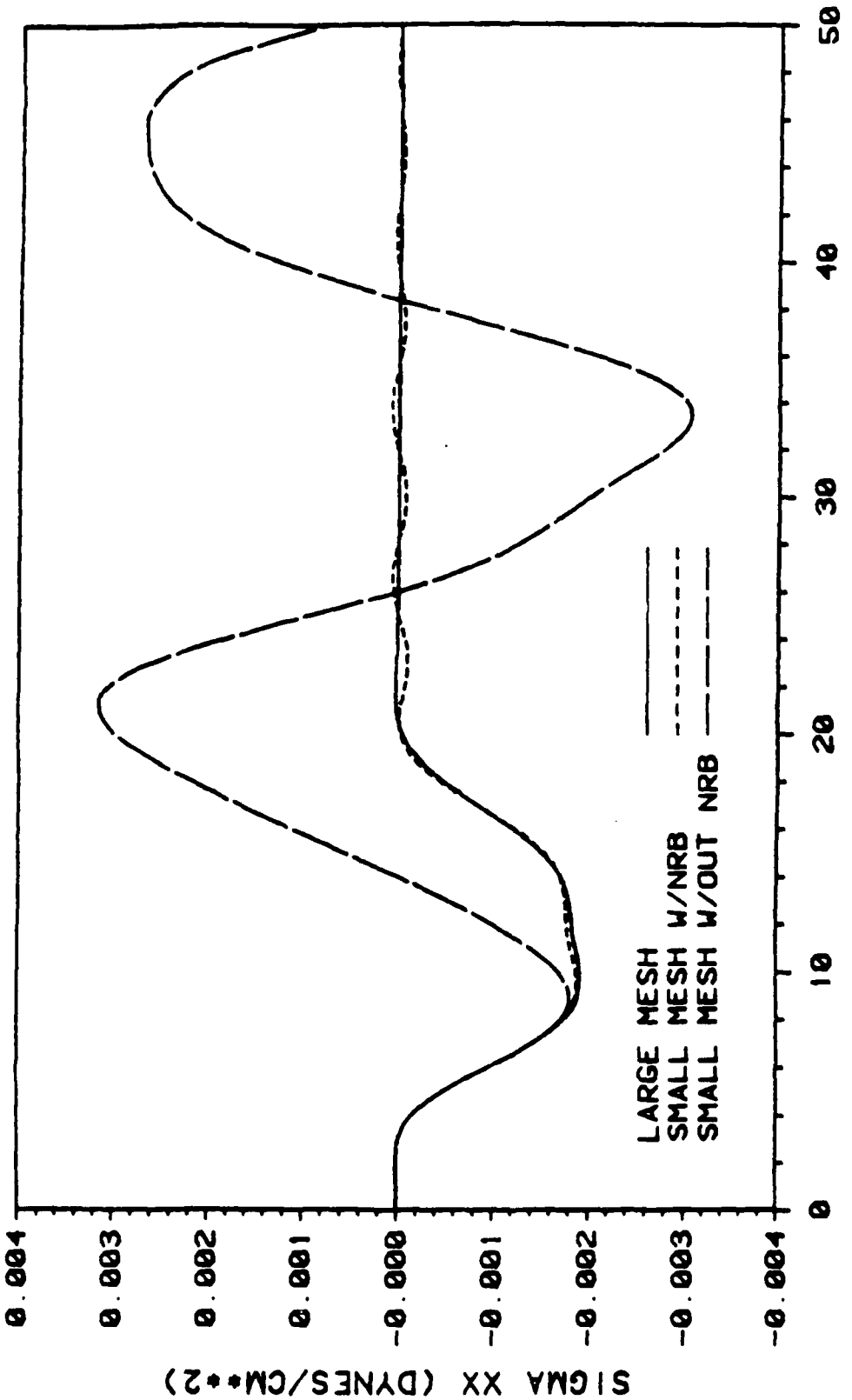

Figure 4.4 σ_{xx} vs. Time at x = 3-cm, y = 1-cm

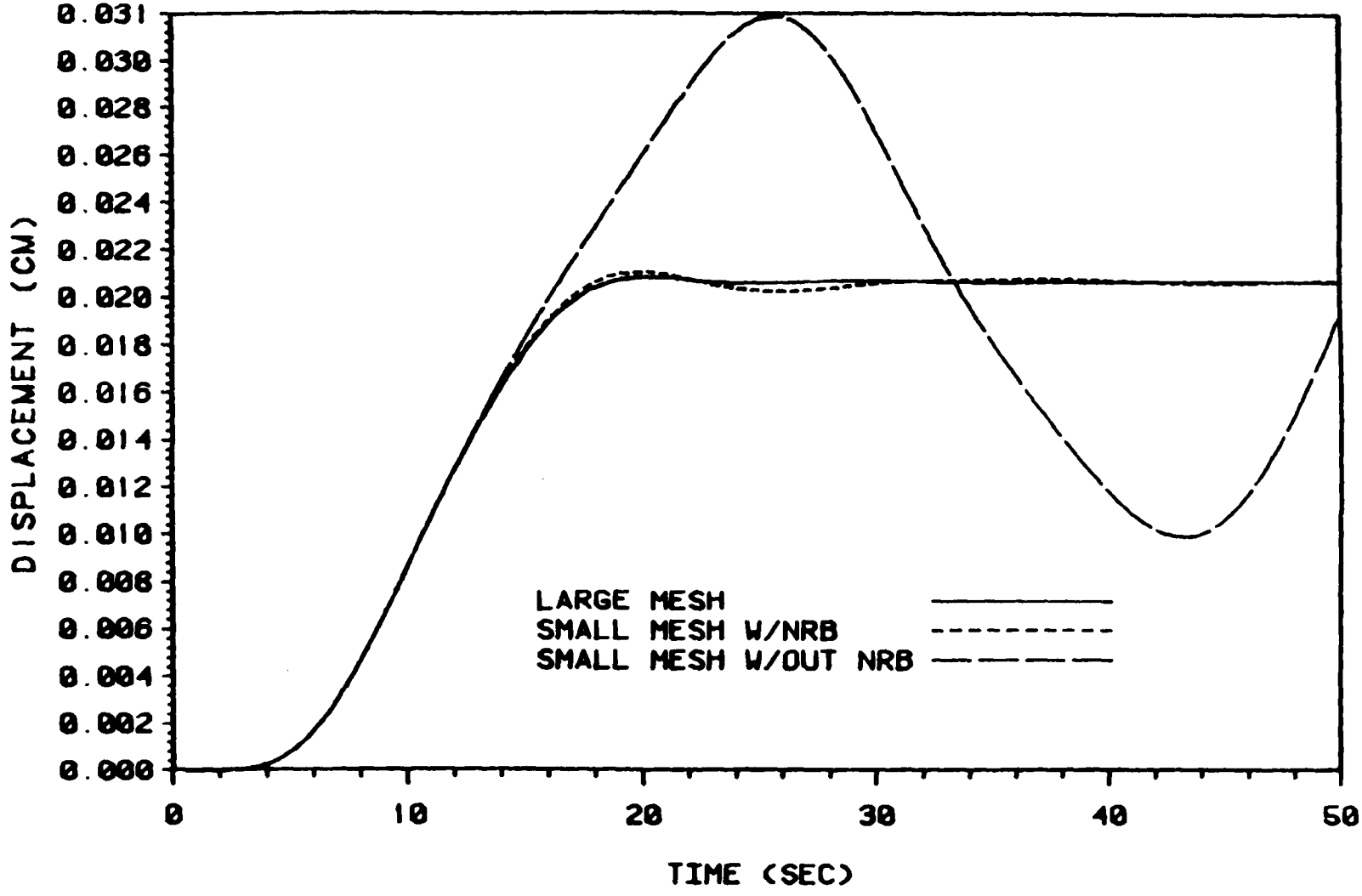

Figure 4.5 Vertical Displacement vs. Time at x = 2-cm, y = 2-cm

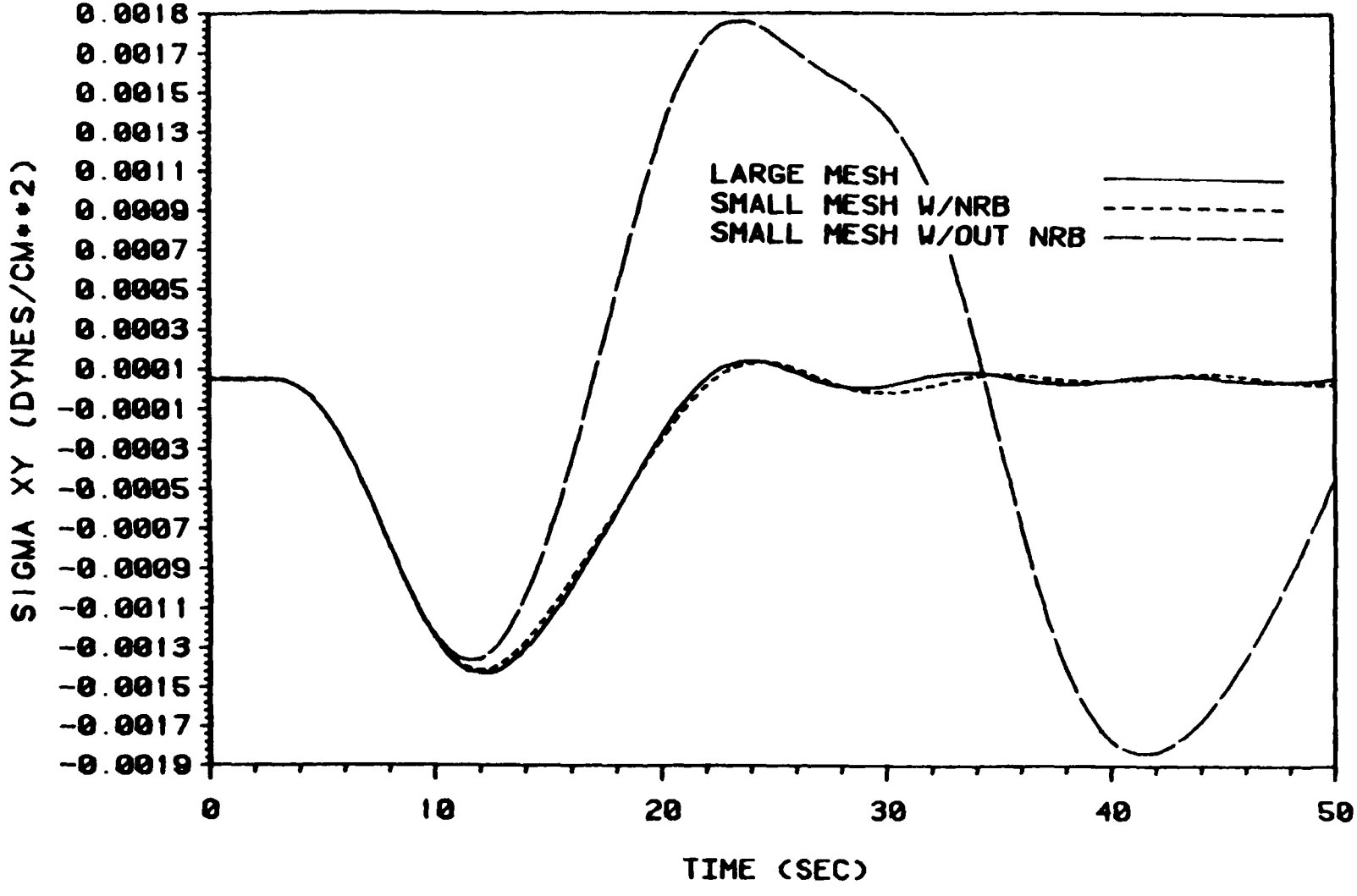

Figure 4.6 σ_{xy} vs. Time at x = 3-cm, y = 1-cm

For the bars perpendicular to the axis of symmetry, the geometry of the axisymmetric problem had to be altered. White, Valliappan, and Lee [20] stated that the efficiency of the viscous nonreflecting boundary was dependent upon the ratio of the distance the boundary was from the axis of symmetry to the wavelength of the incident stress wave. Recall that for an R/λ ratio greater than 0.5, the nonreflecting boundary should be effective. The sinusoidal displacement function applied to the left end of the bar has an angular frequency of 0.1963 rad/sec (f = 0.0312 Hz). The wave speed of the dilatational wave through the bar is 1.0 cm/sec. It can be easily proven that the wavelength of the dilatational wave is 32 cm. Two tests were conducted using R/λ values of 0.5 and 2.0, respectively. For an R/λ value of 0.5, the two bars were placed such that the left ends of the bars were 10-cm from the axis of symmetry. The right end of the short bar would then be 16-cm from the axis of symmetry. Similarly for an R/λ value of 2.0, the left ends of the bars are located at x = 58-cm. Only the dilatational wave graphical results, shown in Figures 4.7 - 4.10, are given for the two values of R/λ. Consistent with reference [20], as the ratio of R/λ is increased, the efficiency of the nonreflecting boundary does, in fact, increase. Note that for R/λ = 0.5, the results do not correspond as well as those for $R/\lambda = 2.0$. Therefore, to insure adequate results, the limiting R/λ value of 0.5, should be increased to 2.0.

With the successful completion of the axisymmetric problem, the formulation of the nonreflecting boundary within the subroutine FREEF2 was determined to be error-free. The only remaining untested portion of the code is the procedure in subroutine READPV that retrieves the element numbers along the nonreflecting boundary. The

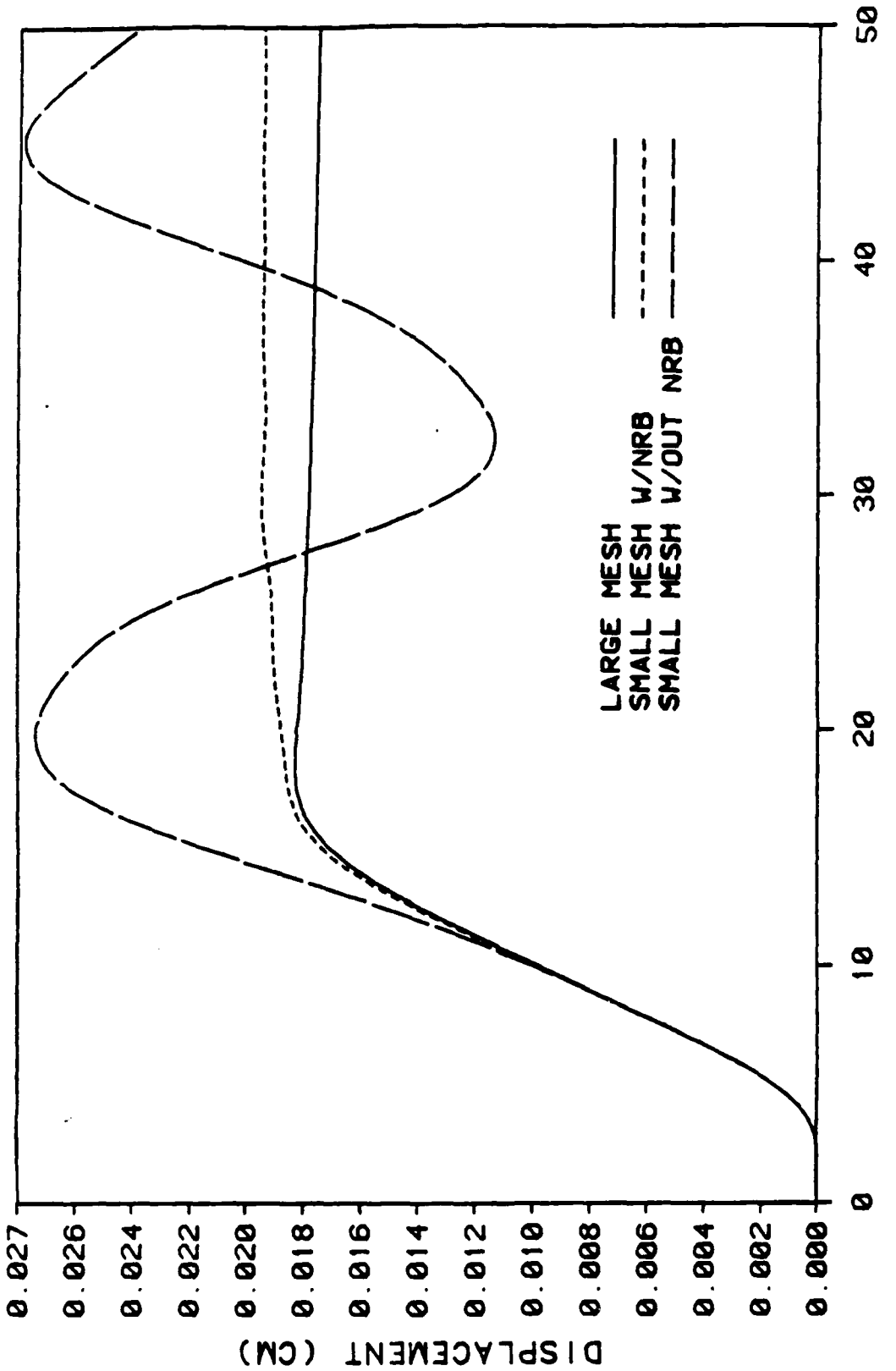

Figure 4.7 Horizontal Displacement vs. Time at $x = 12$-cm, $y = 2$-cm for $R/\lambda = 0.5$

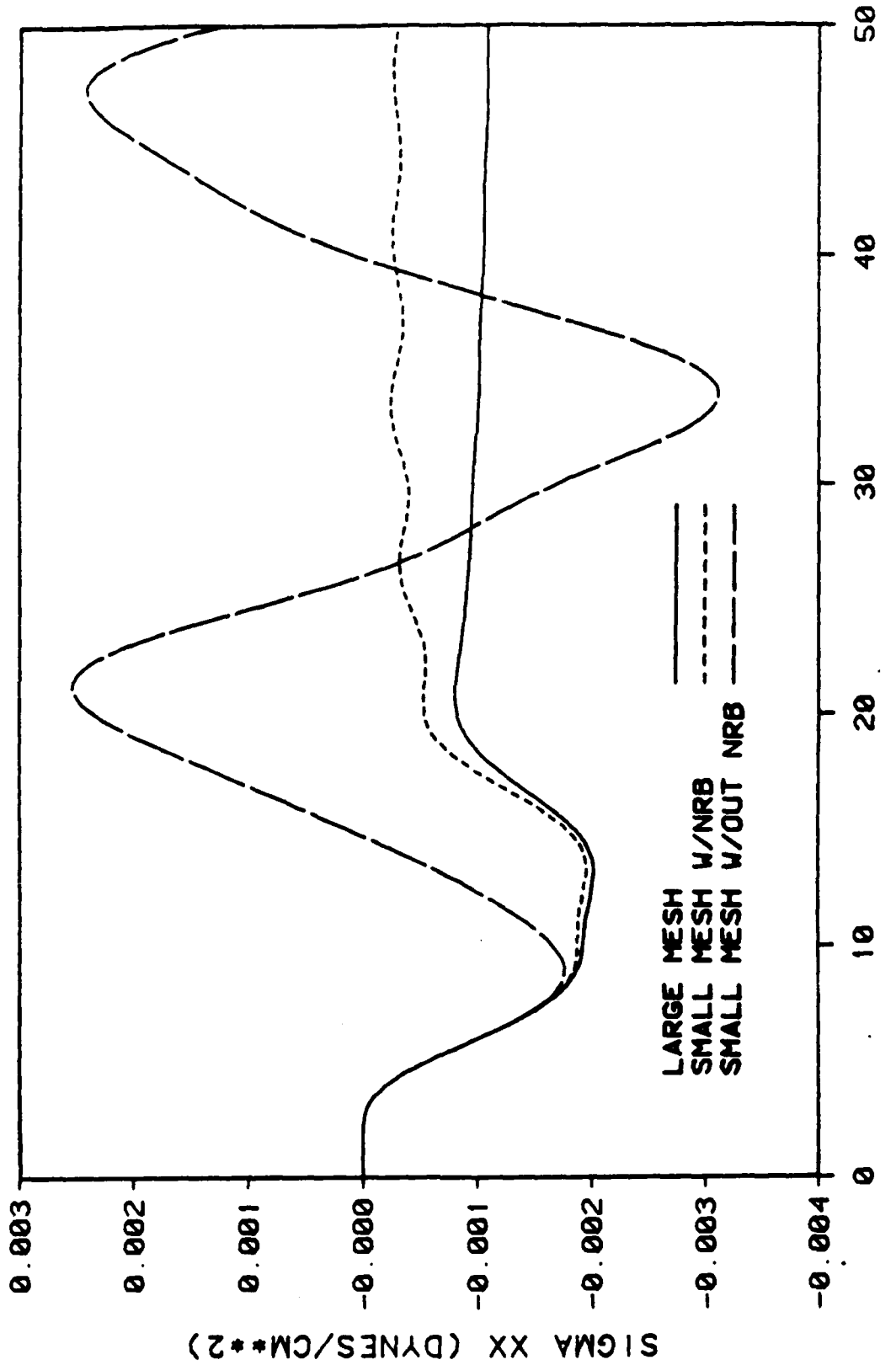

Figure 4.8 σ_{xx} vs. Time at x = 13-cm, y = 1-cm for $R/\lambda = 0.5$

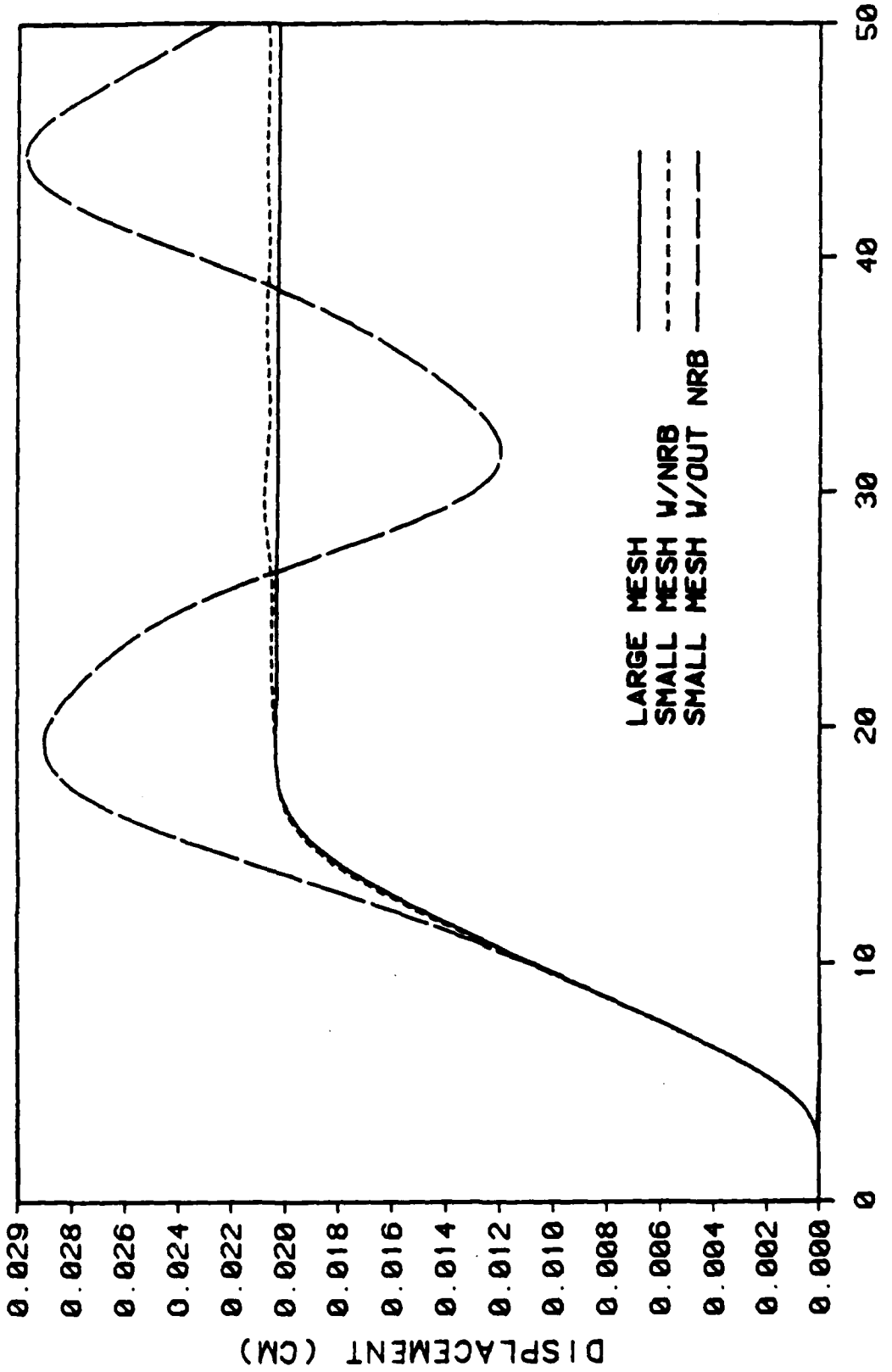

Figure 4.9 Horizontal Displacement vs. Time at $x = 60$-cm, $y = 2$-cm for $R/\lambda = 2.0$

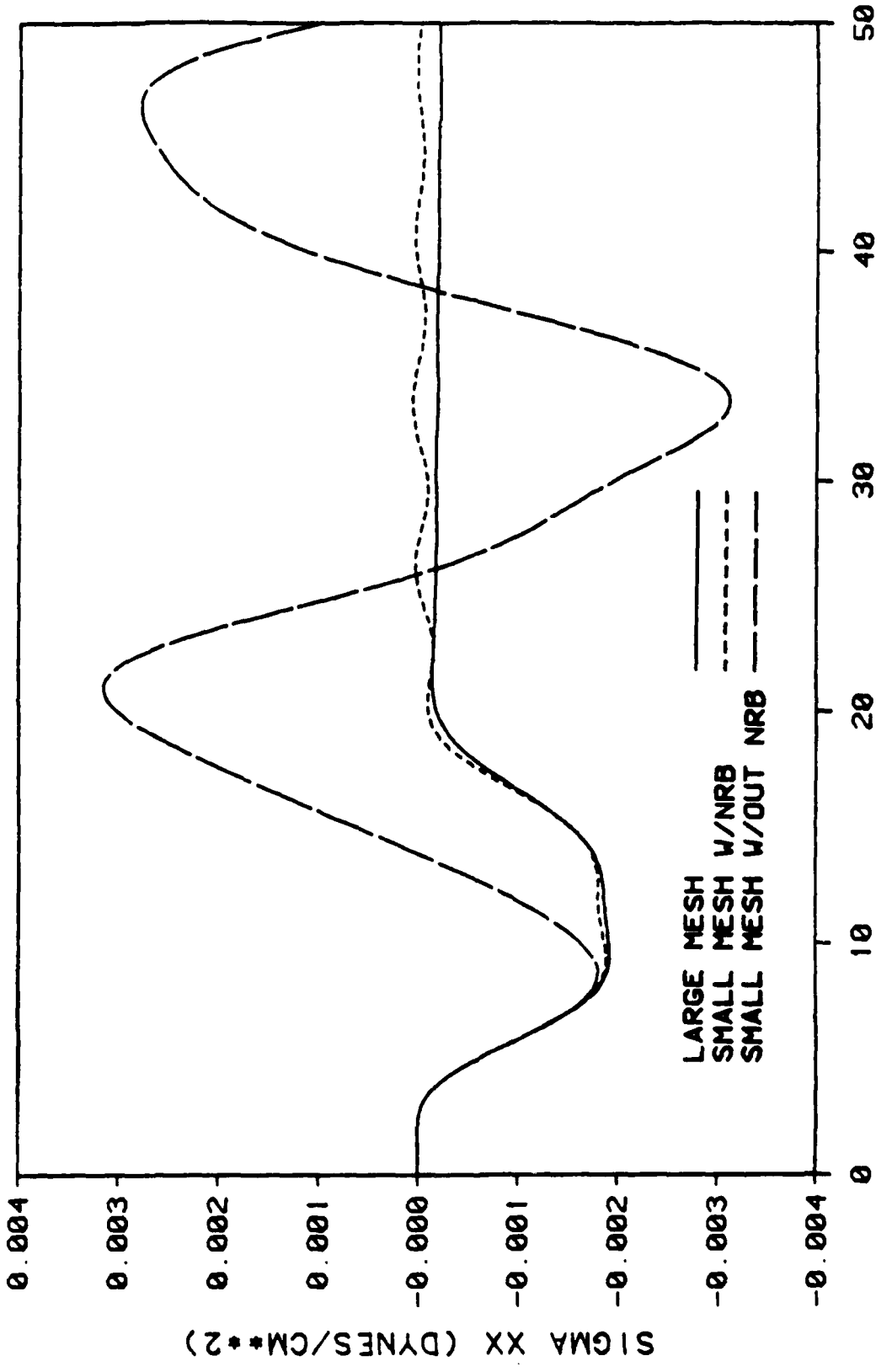

Figure 4.10 σ_{zz} vs. Time at x = 61-cm, y = 1-cm for $R/\lambda = 2.0$

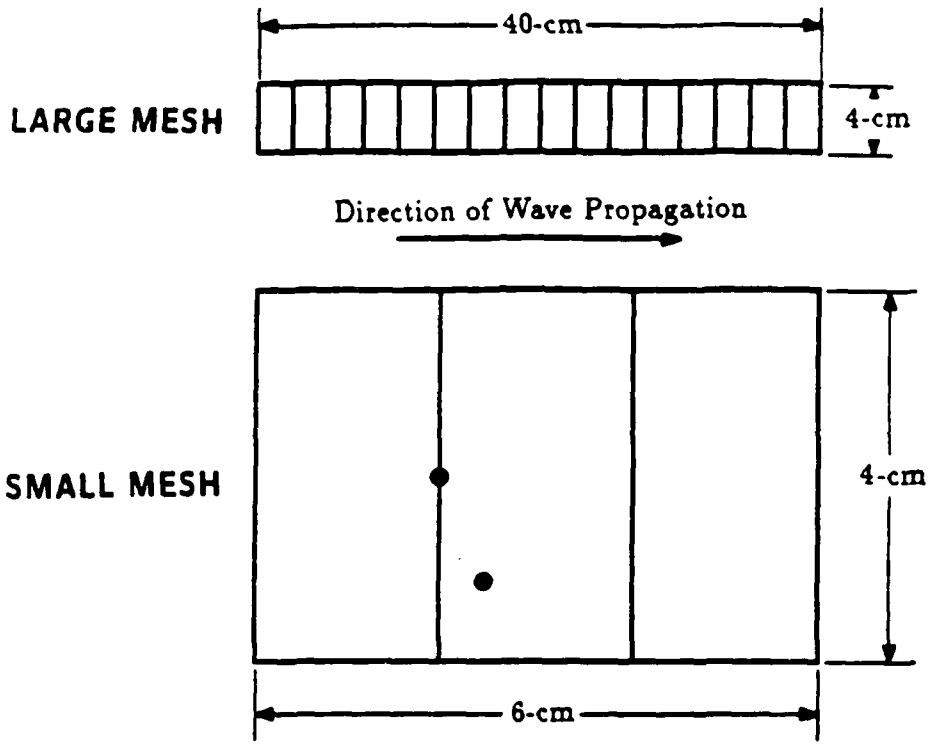

Figure 4.11 8NQ Discretization of One-Dimensional Bars

triangular elements and the eight-node quadrilateral elements still required verification. For each of these elements, only a dilatational stress wave test was used.

The 40-cm bar and 6-cm bar were now discretized using 2-cm by 4-cm 8NQ plane isoparametric elements. The meshes are shown in Figure 4.11. The long bar consists of 20 elements and 103 nodes while the short bar has 3 elements and 18 nodes. All of the material properties remain unchanged. The integration order of the 8NQ elements was two. Figures 4.12 and 4.13 give the graphical results of the dilatational stress wave tests. The displacement versus time graph for the plane 8NQ is very similar to that of the plane 4NQ element. The graph showing the normal stress versus time, although exhibiting very good results, is more erratic in comparison to the corresponding graph of the plane 4NQ element.

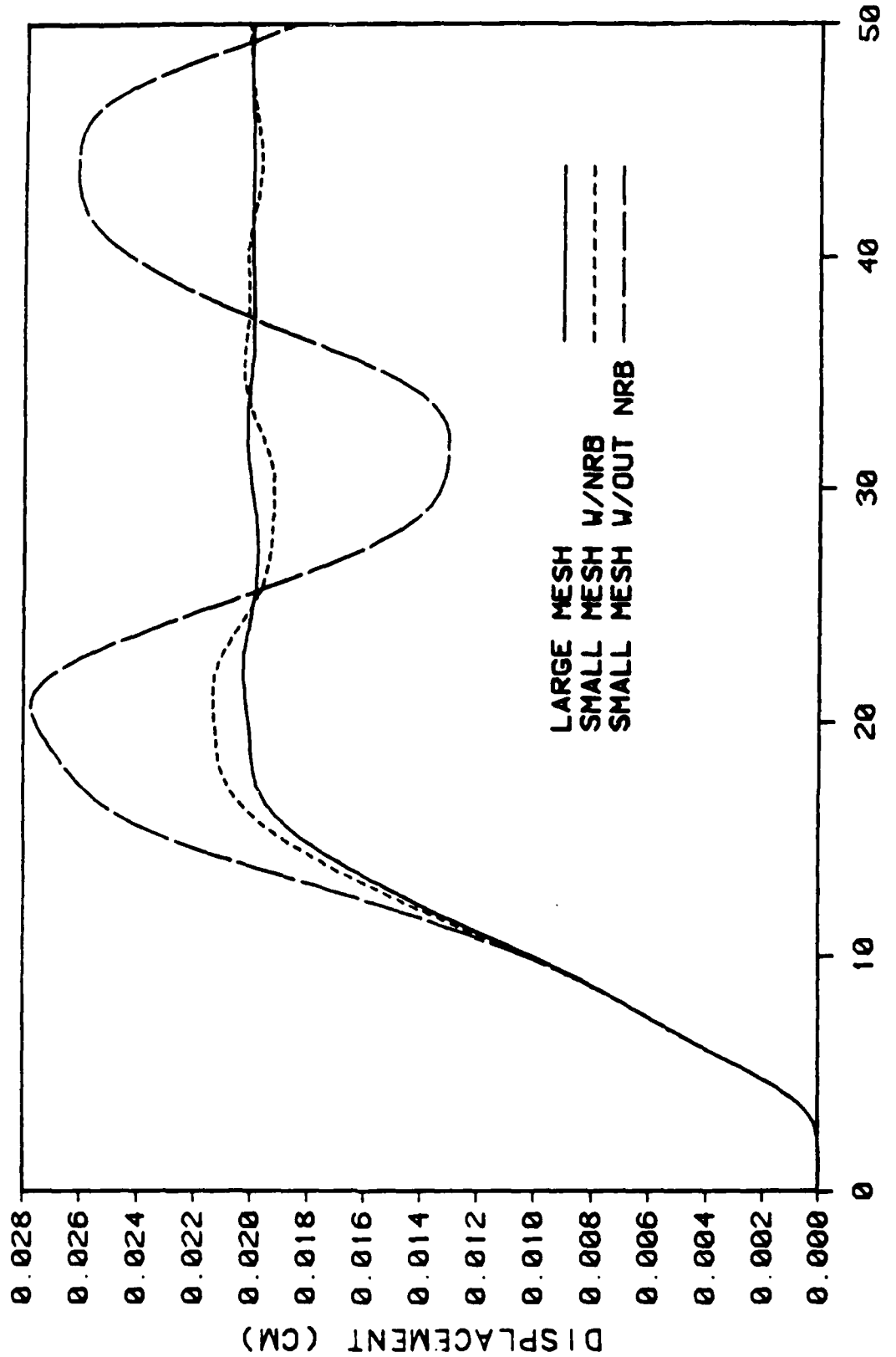

Figure 4.12 Horizontal Displacement vs. Time at $x = 2$-cm, $y = 2$-cm

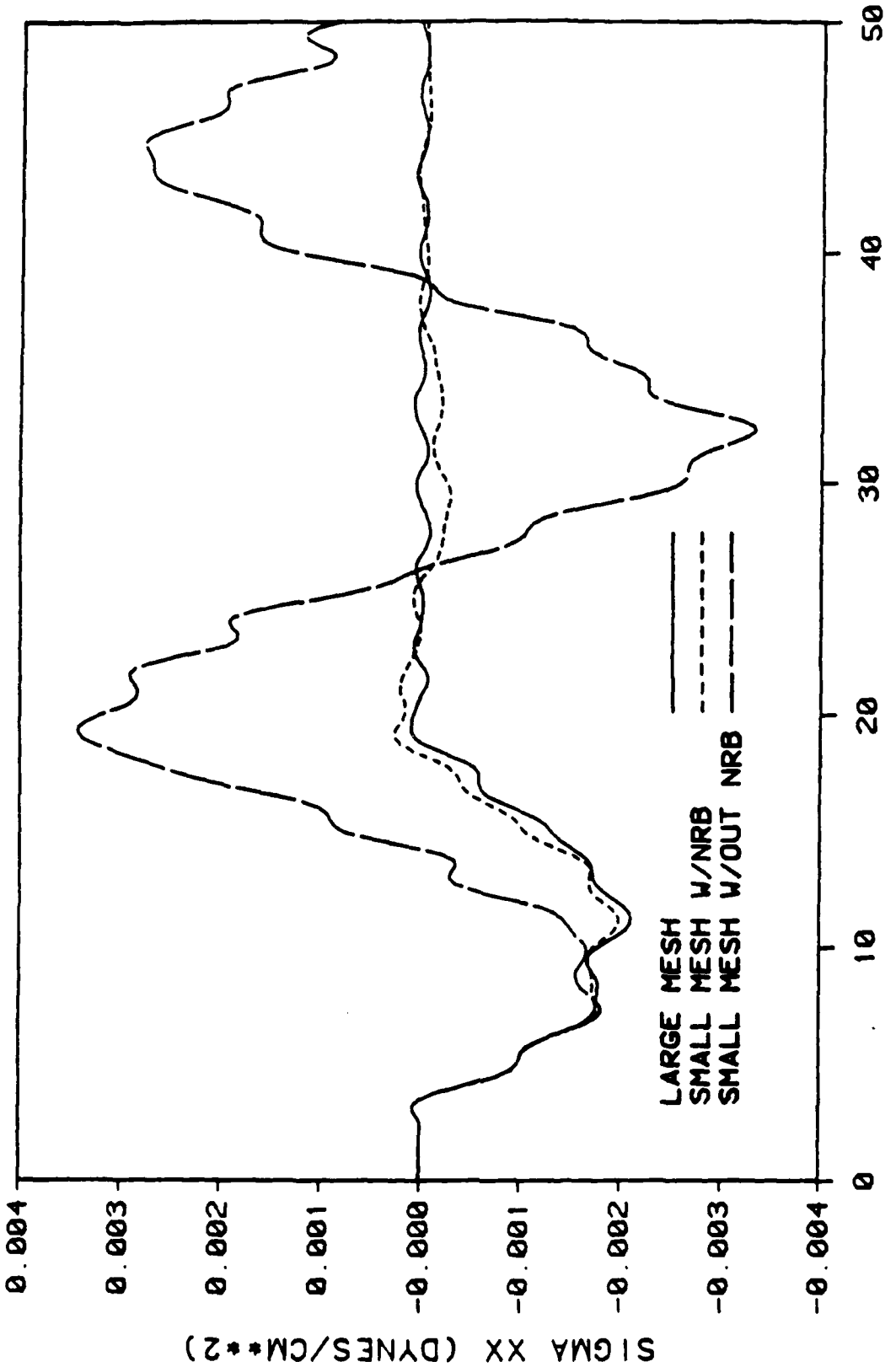

Figure 4.13 σ_{zz} vs. Time at x = 2.423 cm, y = 0.423 cm

Similar tests were conducted for the three-node, five-node and six-node plane triangular elements. Although the results have not been included in this report, all three triangular elements displayed the same behavior as the 4NQ and 8NQ elements except for slightly less accuracy. At the conclusion of these tests, all of the modifications to the SAMSON2 code were believed to be correct.

The purpose of the remaining tests in this research was to assess the versatility of the nonreflecting boundary under varying material properties. Poisson's ratio, ν, of the medium is known to affect the effectiveness of the nonreflecting boundary. Two tests were conducted employing the plane 4NQ discretized bars for two different values of Poisson's ratio: $\nu = 0.20$ and $\nu = 0.45$. A value of 0.45 would be an extreme value of Poisson's ratio ($\nu = 0.5$ would imply an incompressible material). The bars were again subjected to a dilatational wave and a shear wave, respectively. Figures 4.14 - 4.17 show the solutions associated with $\nu = 0.2$. There is a small deviation in the graphs shown in the four figures between the large mesh solution and the nonreflecting boundary solution. This deviation becomes greater for $\nu = 0.45$ as is evident by the graphs shown in Figures 4.18 - 4.21. The results from these tests support the evidence of Cohen and Jennings [3] that the efficiency of the nonreflecting boundary decreases as Poisson's ratio increases. Furthermore, the degree of error demonstrated in the two tests is appreciable only when Poisson's ratio tends to its maximum value of 0.5. For Poisson's ratio in the range of 0 to 0.4, the nonreflecting boundary performed satisfactorily.

The final test of the nonreflecting boundary involving one-dimensional wave propagation used the plane 4NQ discretized bar consisting of two different materials

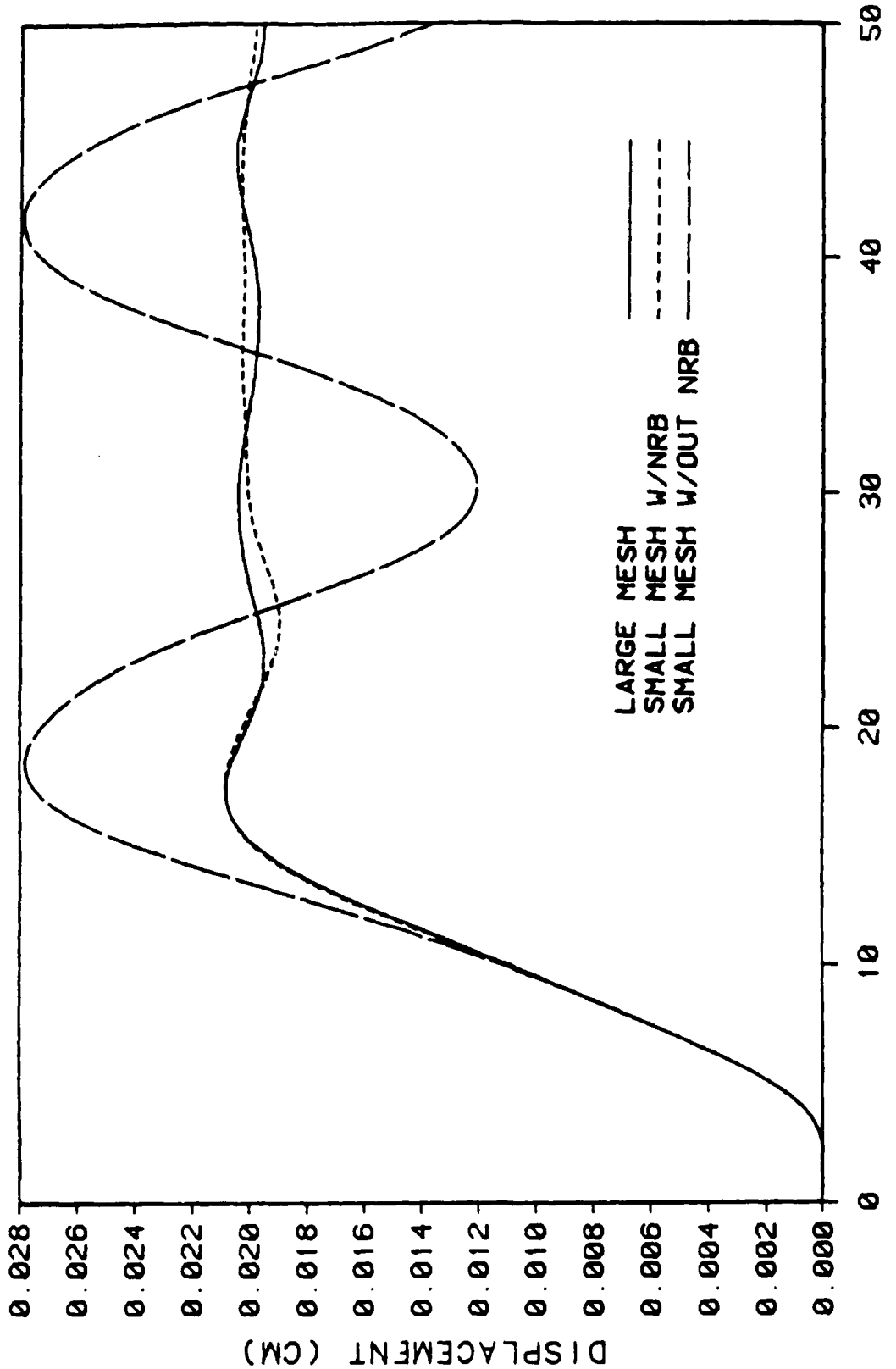

Figure 4.14 Horizontal Displacement vs. Time at x = 2-cm, y = 2-cm for ν = 0.20

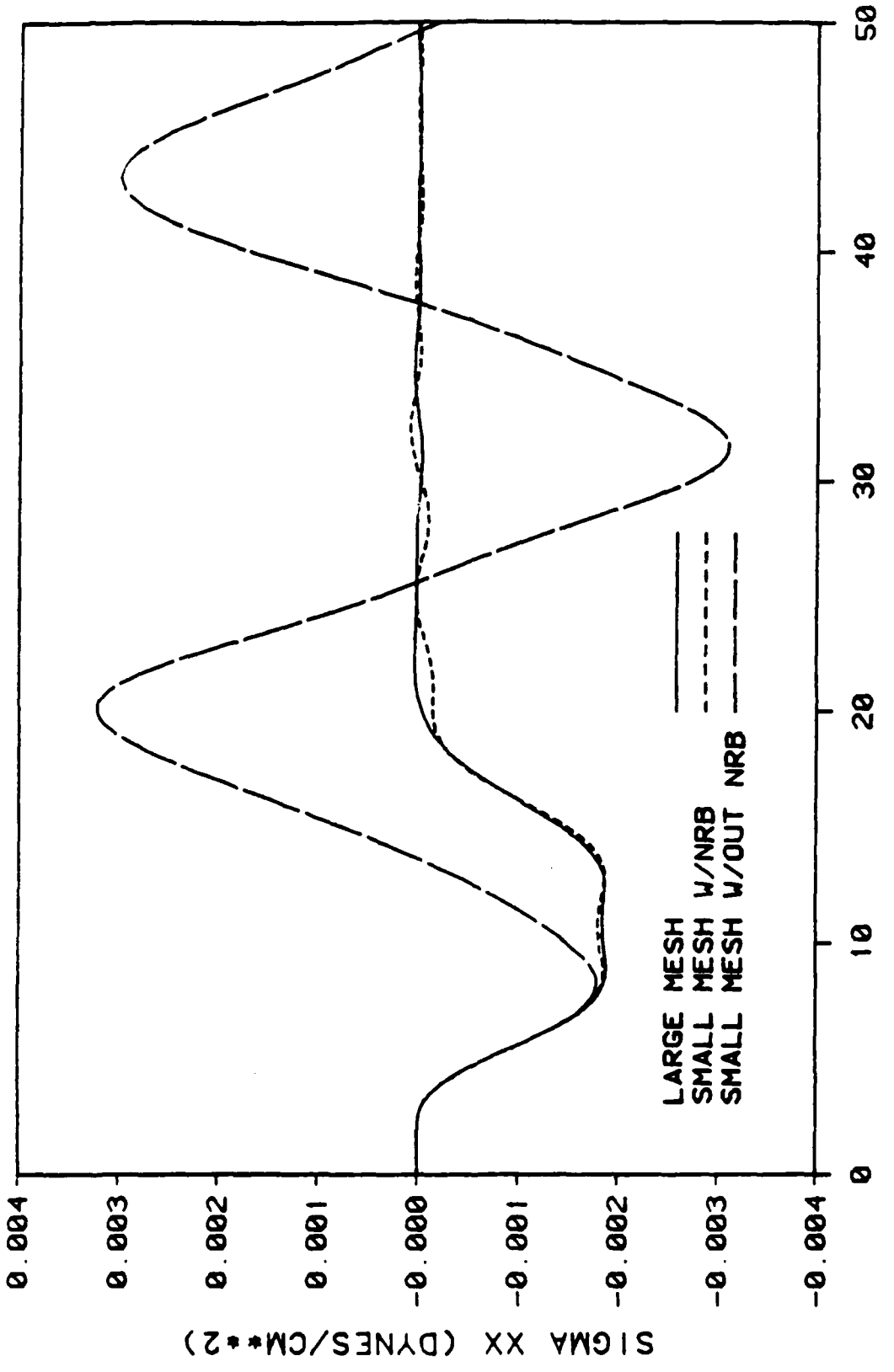

Figure 4.15 σ_{zz} vs. Time at $x = 3$-cm, $y = 1$-cm for $\nu = 0.20$

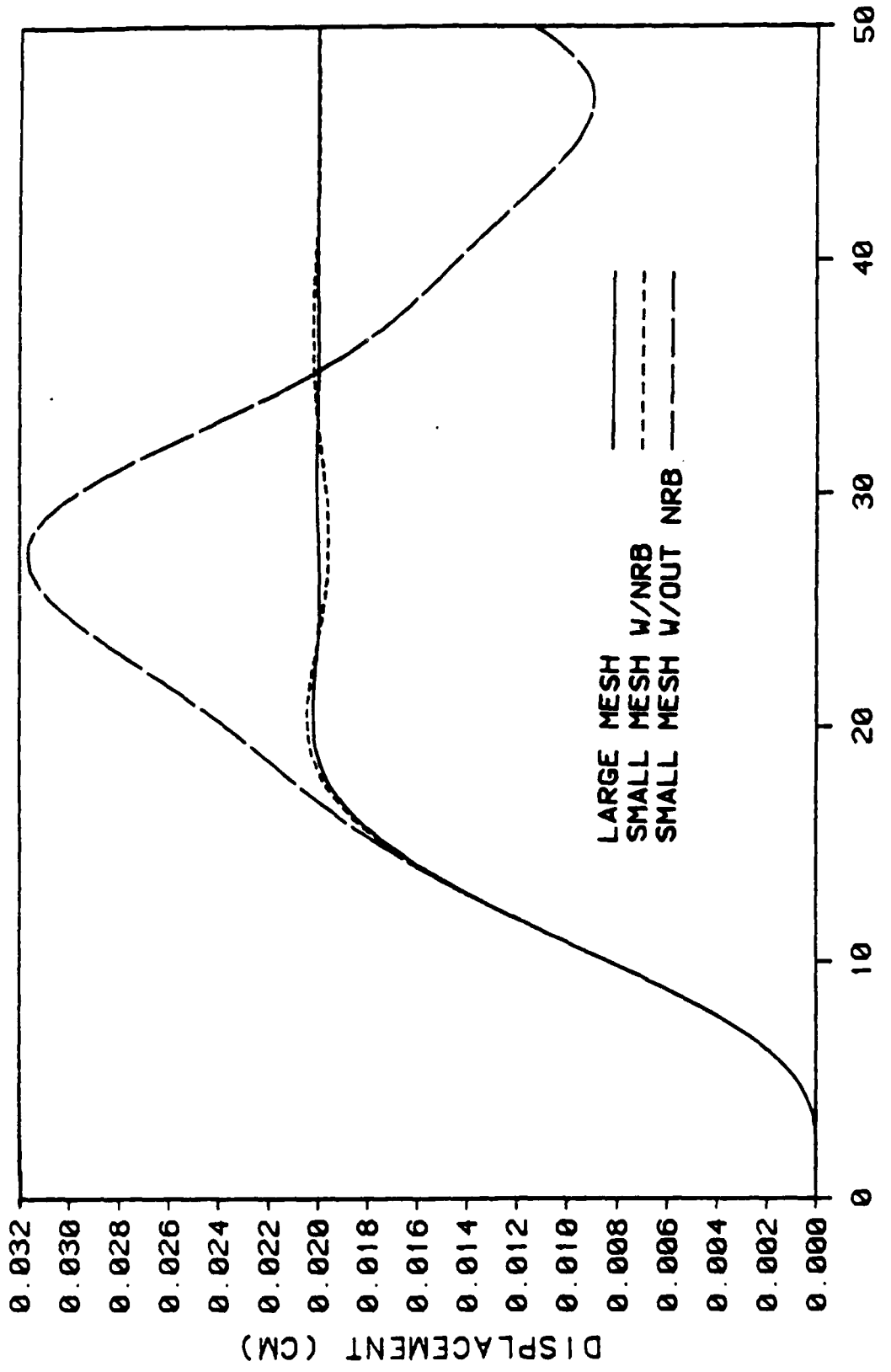

Figure 4.16 Vertical Displacement vs. Time at $x = 2$-cm, $y = 2$-cm for $\nu = 0.20$

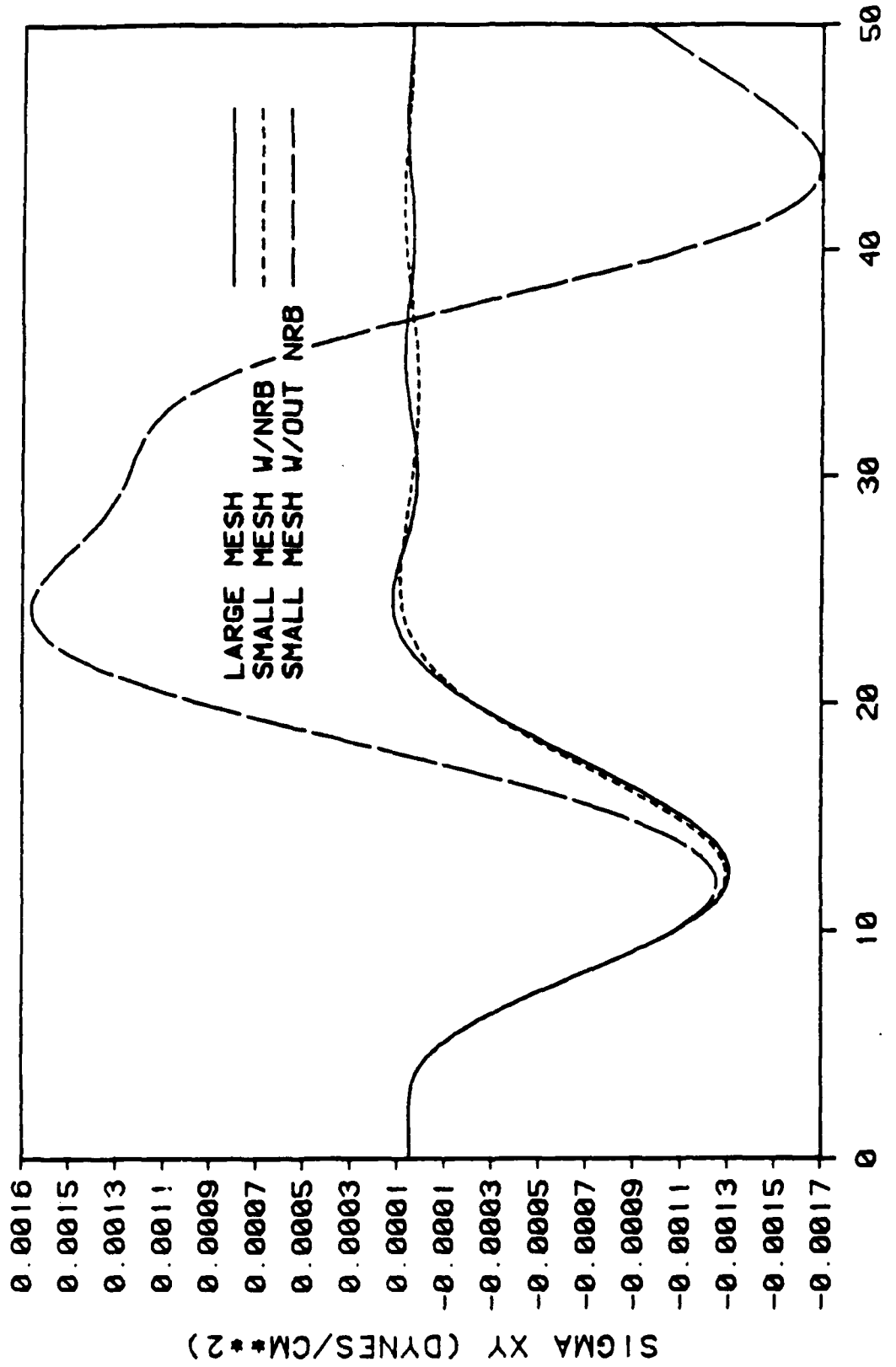

Figure 4.17 σ_{xy} **vs. Time at** $x = 3$**-cm,** $y = 1$**-cm for** $\nu = 0.20$

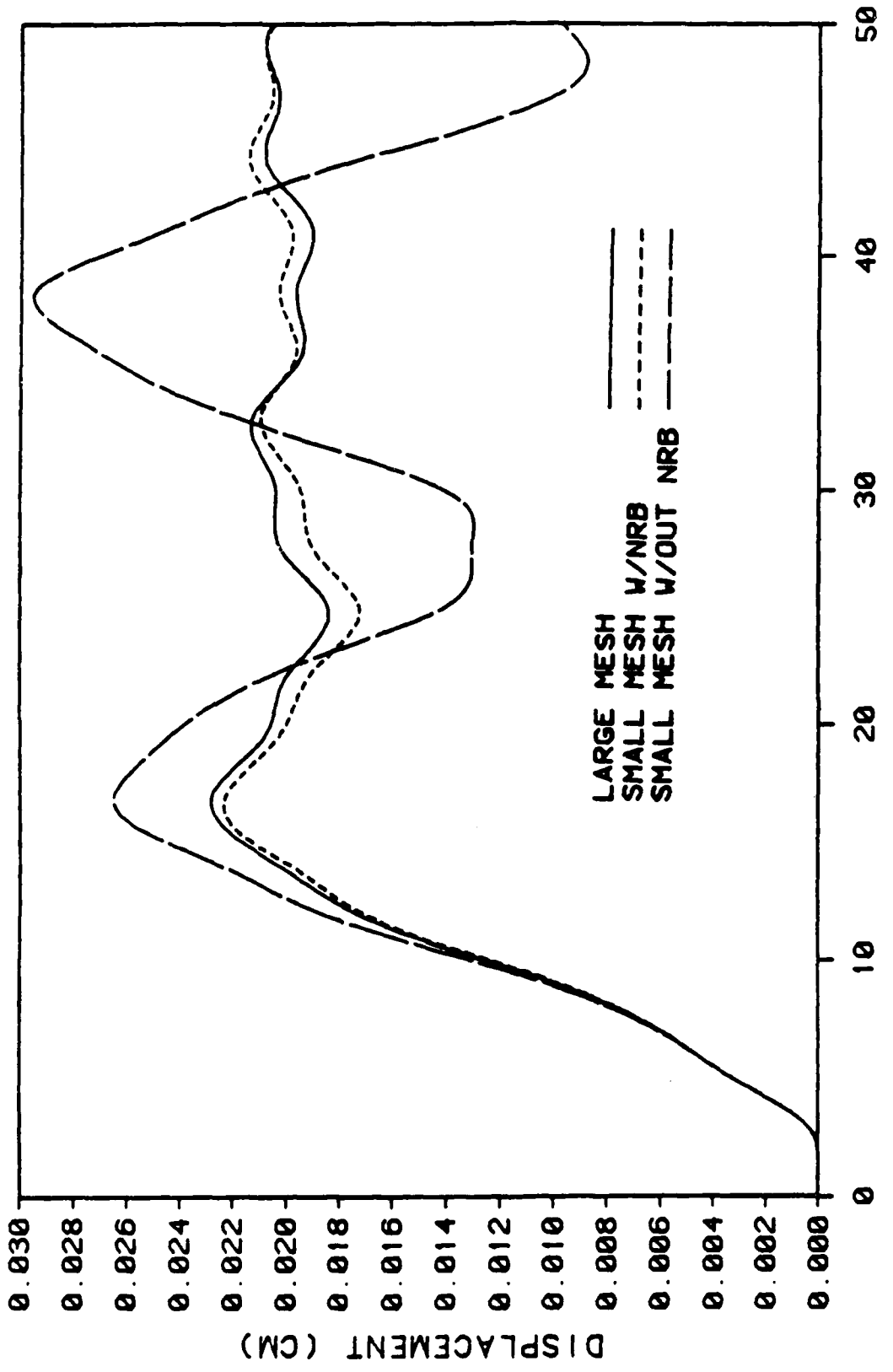

Figure 4.18 Horizontal Displacement vs. Time at x = 2-cm, y = 2-cm for $\nu = 0.45$

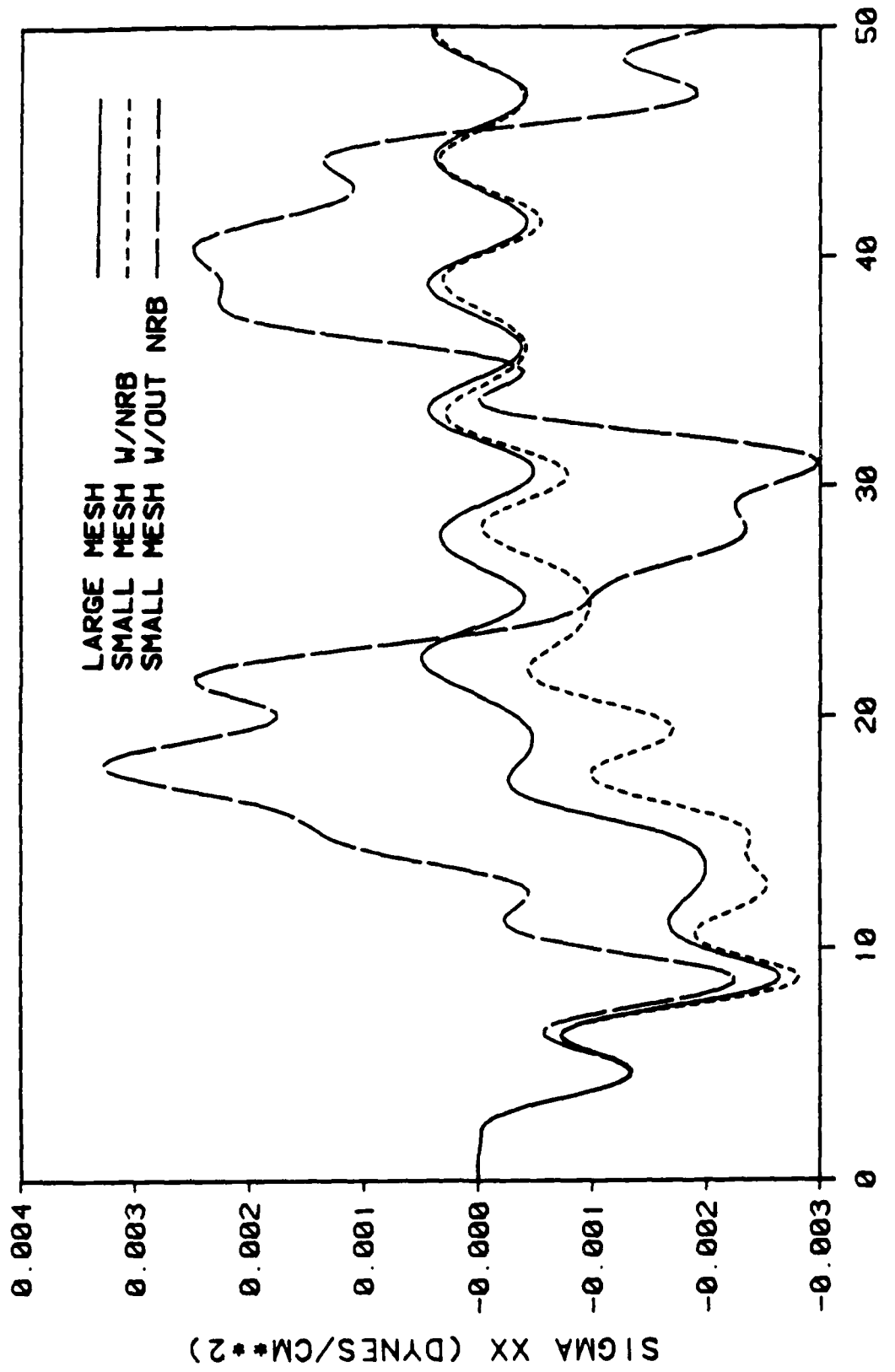

Figure 4.19 σ_{xx} vs. Time at $x = 3$-cm, $y = 1$-cm for $\nu = 0.45$

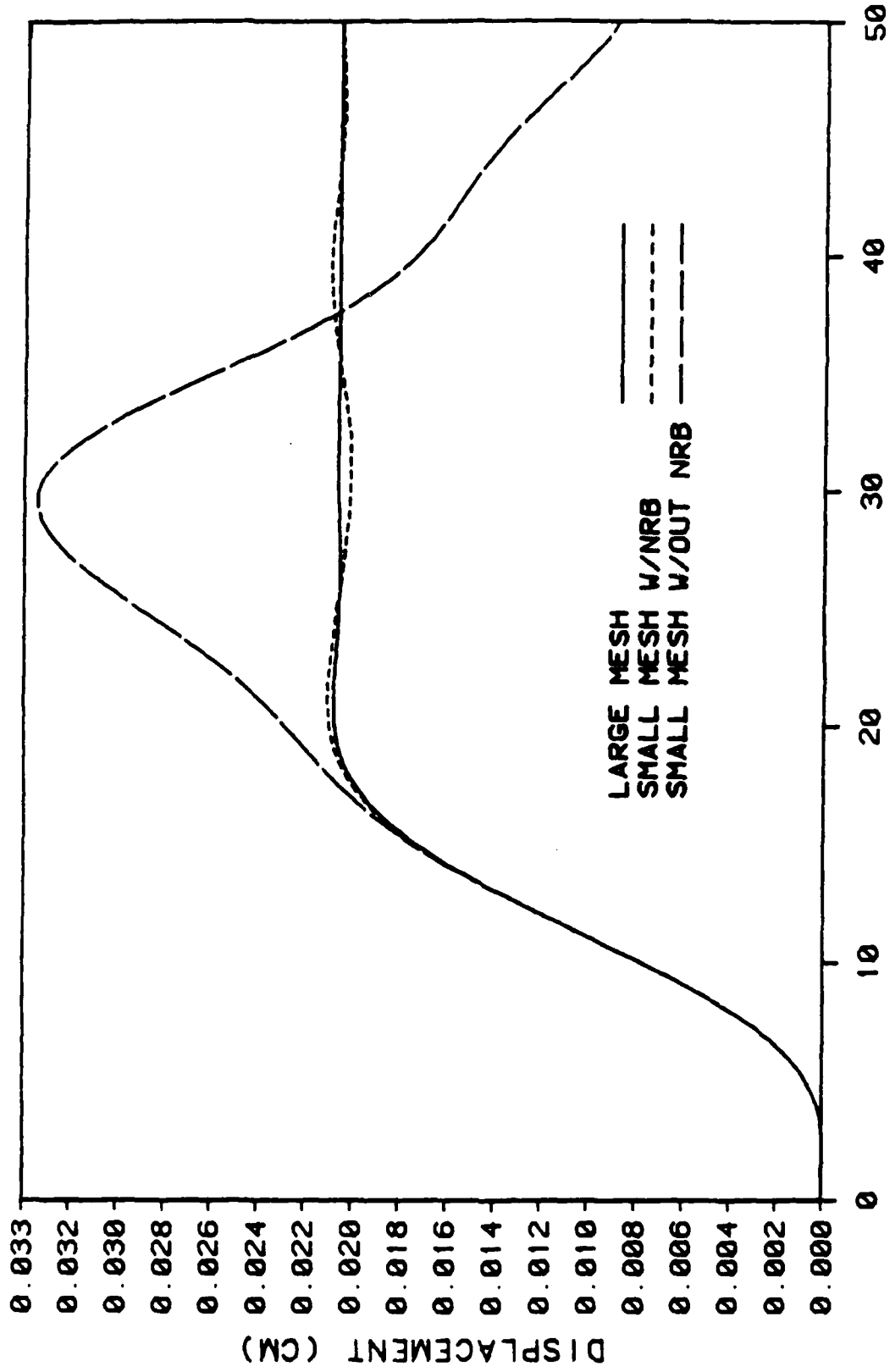

Figure 4.20 Vertical Displacement *vs.* Time at $x = 2$-cm, $y = 2$-cm for $\nu = 0.45$

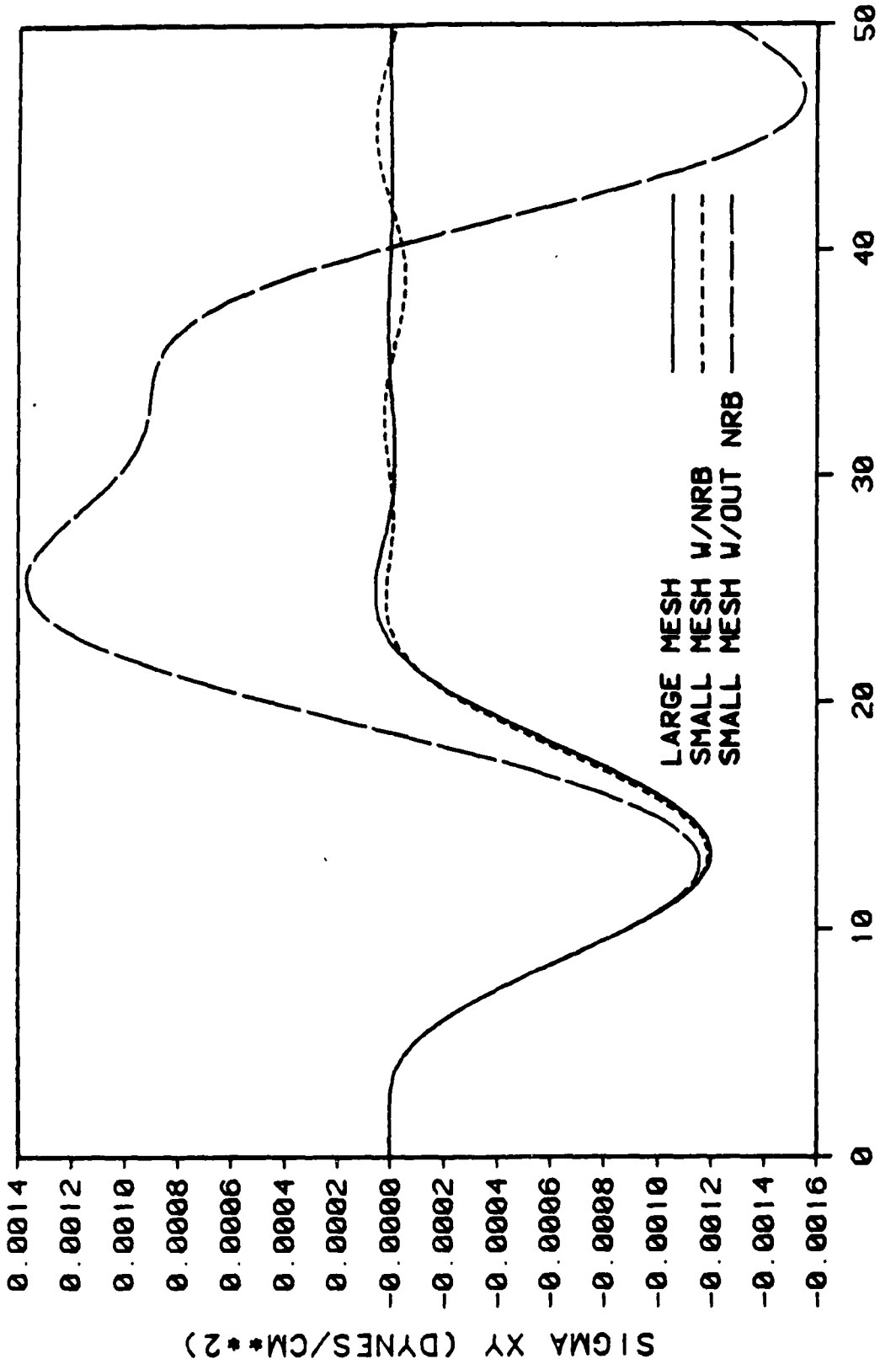

Figure 4.21 σ_{xy} vs. Time at x = 3-cm, y = 1-cm for $\nu = 0.45$

(i.e., an anisotropic medium). The lower half of both bars had the same material properties as before with $\nu = 0.0$. Only Young's modulus for the upper halves of the bars differed from the lower halves of the bars. Young's modulus for the upper halves of the bars was 4.0 dyne/cm^2. Therefore, the dilatational wave speed and the shear wave speed for the upper half is double that for the lower half. The bars were again subjected to a dilatational wave and a shear wave. Figures 4.22 - 4.25 show the graphical results for these tests. The nonreflecting boundary absorbed both stress waves very effectively. Although this test may be oversimplified to conclude that the nonreflecting boundary can adequately absorb stress waves in a two-dimensional space, it does, however, give an indication of its capability.

4.2 Two-Dimensional Wave Propagation

The second category of the evaluation of the nonreflecting boundary entails the use of a two-dimensional half-space. Within a two-dimensional half-space the dilatational waves and the shear waves can impinge simultaneously on the nonreflecting boundary at different angles of incidence. The angles of incidence of the stress waves are unknown during the analysis of the system. The stress and displacement distributions in a mesh are results of the combined effects of both the dilatational wave and the shear wave. It is difficult to distinguish the contribution of an individual stress wave. The response of the system due to these radiant stress waves can become quite complicated. In the evaluation of the nonreflecting boundary, therefore, the emphasis is not on the actual response of the system (unless, of course, the results are obviously incorrect) but on the comparison of the three solutions during each test.

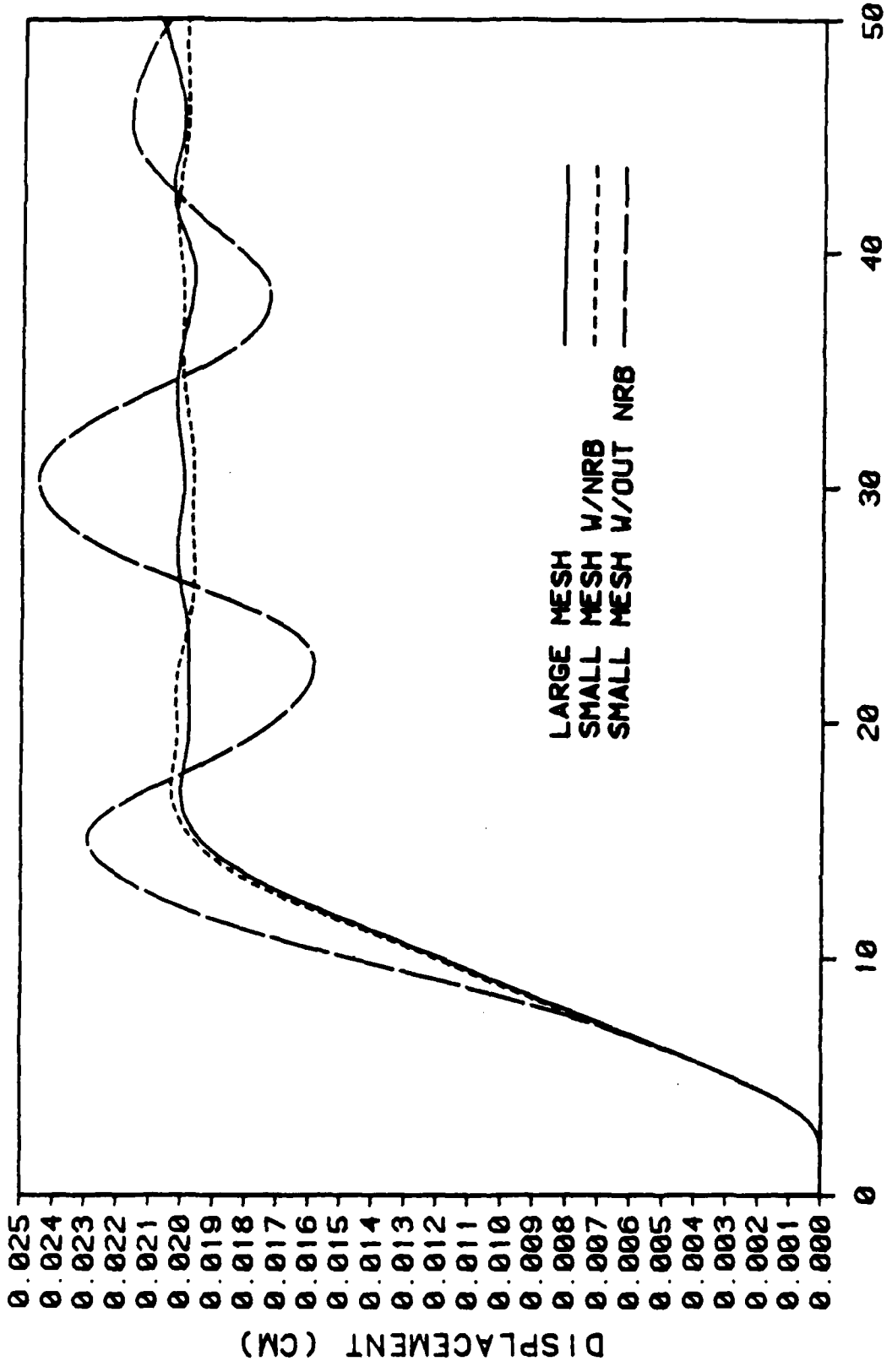

Figure 4.22 Horisontal Displacement vs. Time at x = 2-cm, y = 2-cm

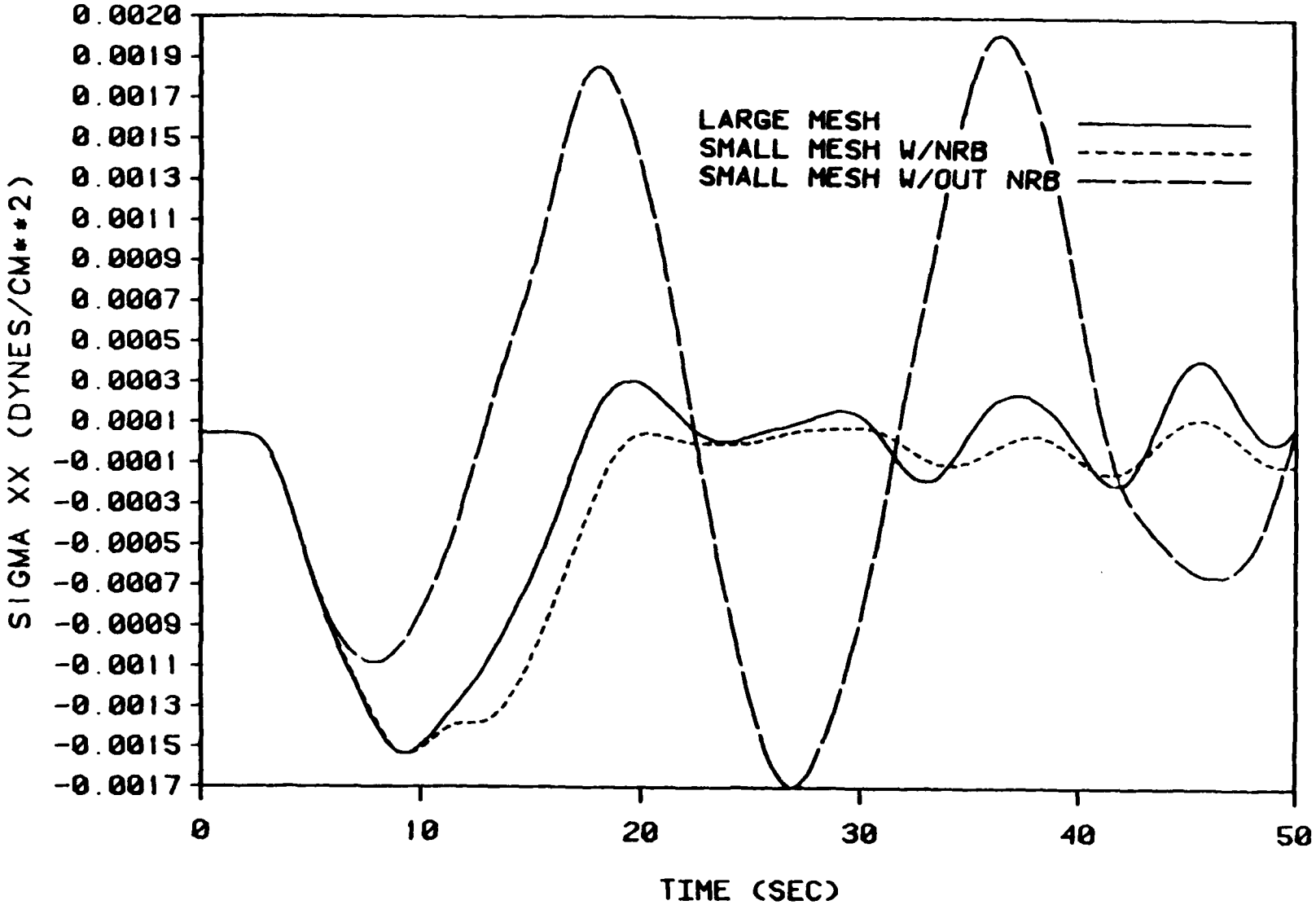

Figure 4.23 σ_{xx} vs. Time at x = 3-cm, y = 1-cm

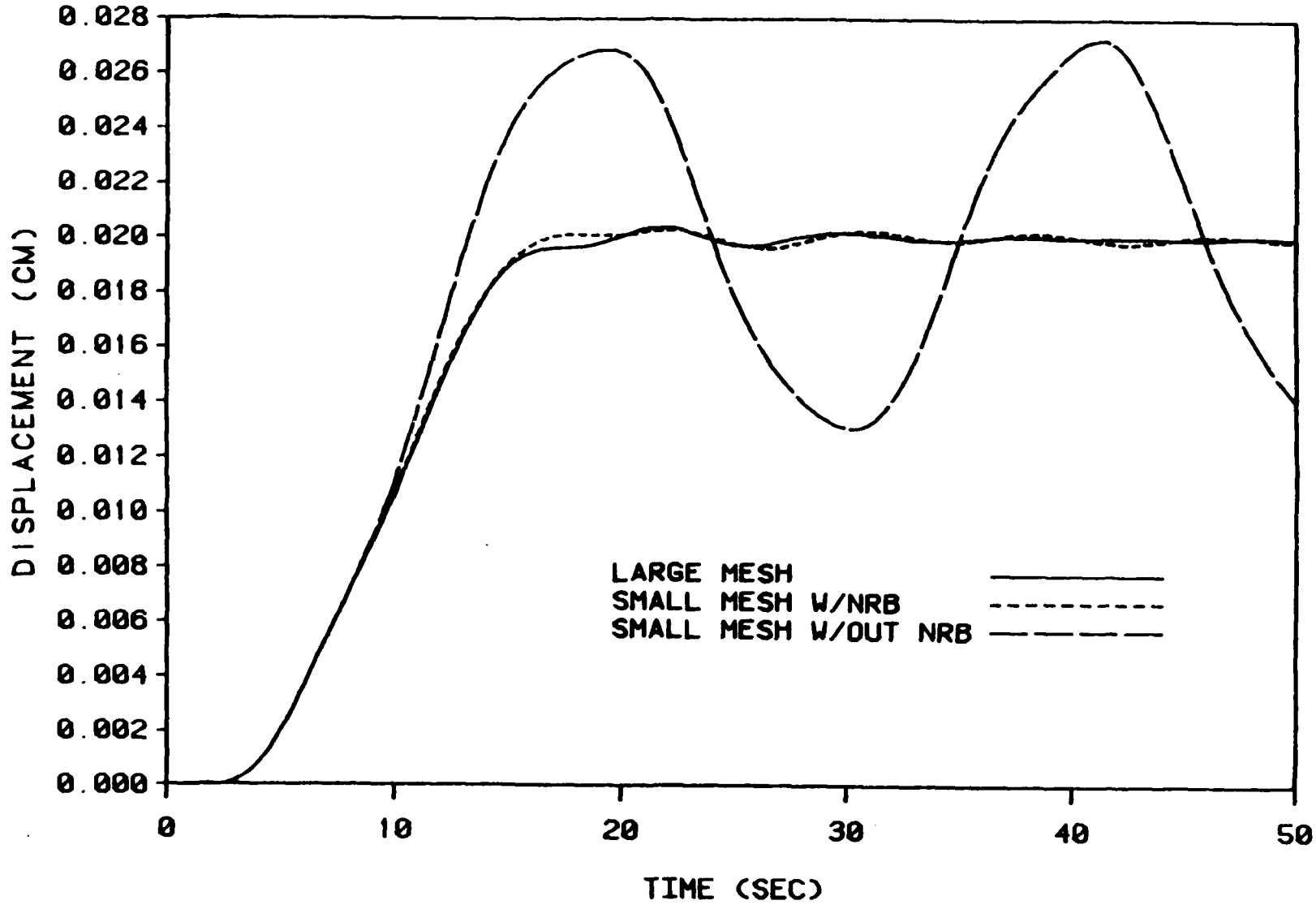

Figure 4.24 Vertical Displacement vs. Time at x = 2-cm, y = 2-cm

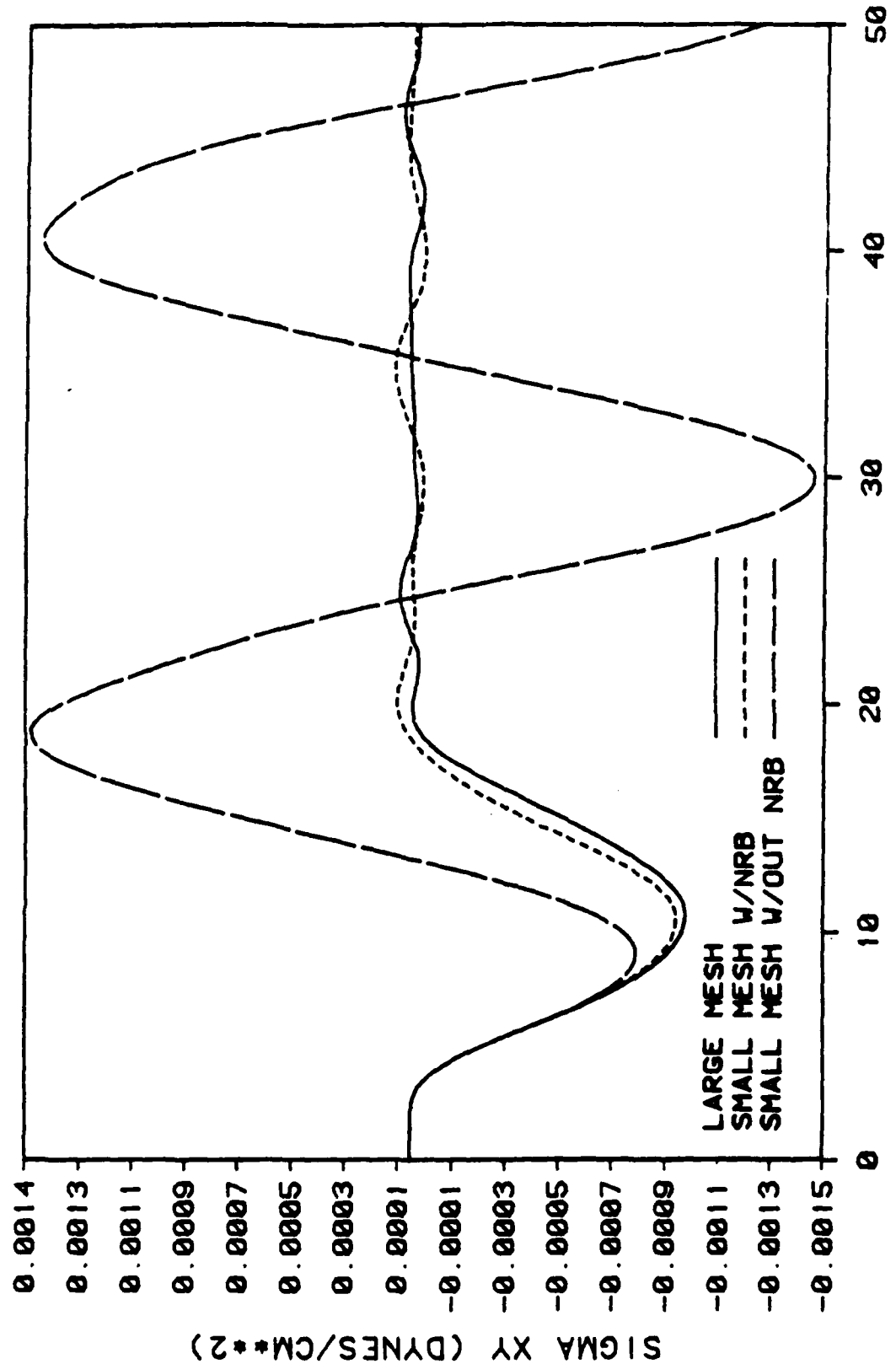

Figure 4.25 σ_{xy} vs. Time at x = 3-cm, y = 1-cm

The large mesh that will be used in the two-dimensional study is shown in Figure 4.26. It is composed of 6-in by 6-in 4NQ axisymmetric continuum elements. The dimensions of the large mesh are 90-in by 90-in. The left edge and the right edge are fixed in the horizontal direction and free in the vertical direction. For an axisymmetric case, the left edge will lie along the axis of symmetry. The base is fixed in the vertical direction and free in the horizontal. The fixity conditions of the three edges result in the bottom two corner nodes being fixed in both directions. The loading will be applied to the top edge of the mesh. The dotted line in the upper left section of the mesh marks the truncation line that defines the boundary of the corresponding small mesh. The small mesh is shown in Figure 4.27. For one solution, the nonreflecting boundary is applied along this truncation line. For the next solution, the small mesh has the exact fixity conditions as that of the large mesh.

Each two-dimensional wave propagation test involves three field variables versus time at a certain point: the displacement of a node located 12-in from the left edge and 24-in from the top edge and the normal stress, σ_{yy}, and the shear stress, σ_{xy}, at a point 15-in from the left edge and 21-in from the top edge. The locations of these two points are shown in Figure 4.27. However, the results from these tests can be misleading. The analysis of these field variables are indicative of the response of the mesh only in the vicinity of these points of observation. While the graphical results may show that the nonreflecting boundary is effective, areas further away from these observed points may show that the nonreflecting boundary is completely ineffective. Instead of checking each point in the mesh over time to prove conclusively that the

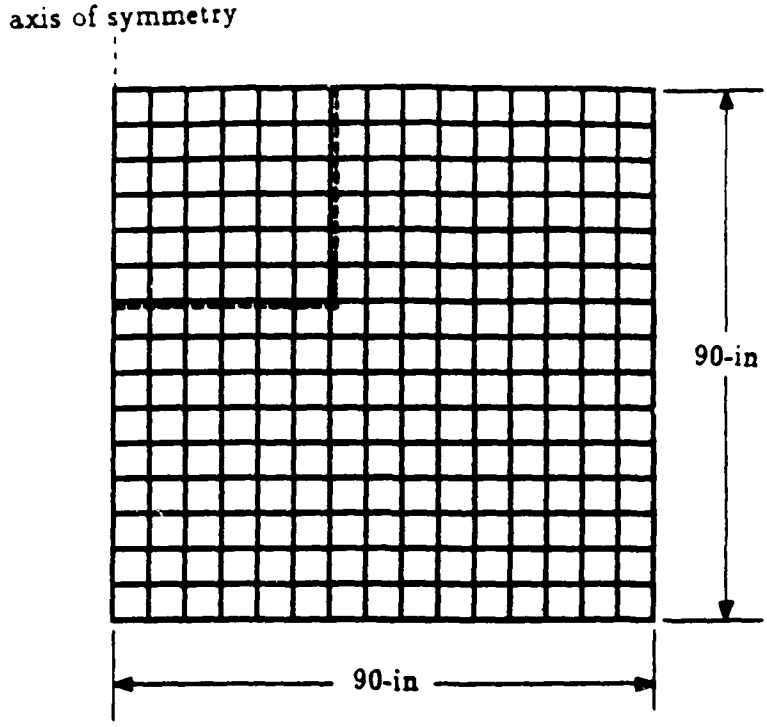

Figure 4.26 Two-Dimensional Large Mesh

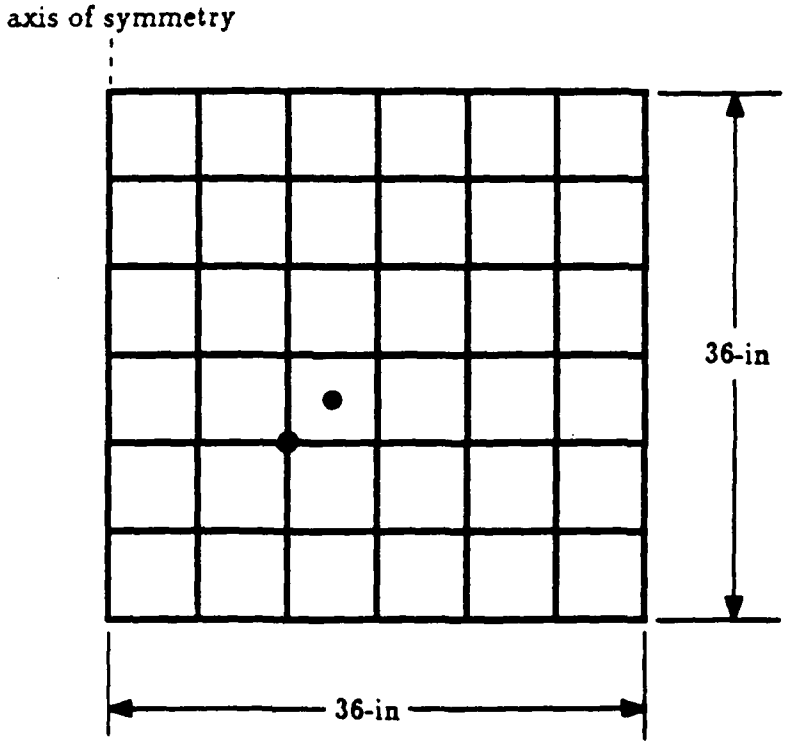

Figure 4.27 Two-Dimensional Small Mesh

nonreflecting boundary was performing well, the vertical displacement of each node in the mesh was examined at a certain time for each solution.

Of the three field variables, the displacement plots are relatively unimportant in comparison to the normal stress and shear stress plots. There will be a "residual" displacement at the completion of a problem utilizing a nonreflecting boundary. The displacement of the nodes in the two meshes are given simply to provide a general indication of the effectiveness of the nonreflecting boundary.

The limiting solution time for the three field variables was the approximate time the reflections returned from the boundary of the large mesh. Unfortunately, it was impossible to tell when these reflections actually did return. The distance from the point of excitation to the boundary of the large mesh back to the location of the field variables was roughly three times the distance for the same route in the small mesh. Assuming that the stress waves travelled at the same speed in both meshes, the time for the stress wave to return from the boundary of the large mesh would be three times the time for the stress wave to return from the boundary of the small mesh. Therefore, from the time the three solutions began to diverge (the time the reflections have returned from the boundary of the small mesh), the limiting solution time was computed to be three times the time at this divergent point.

The material law used exclusively for the two-dimensional problems was the AFWL "engineering" model. Two different materials were modelled: Yuma soil and fiber reinforced concrete. The material parameters of the Yuma soil are listed in Figure 4.28 along with the hydrostatic pressure versus volumetric strain curve and the yield surface curve. The same items are shown in Figure 4.29 for fiber reinforced concrete.

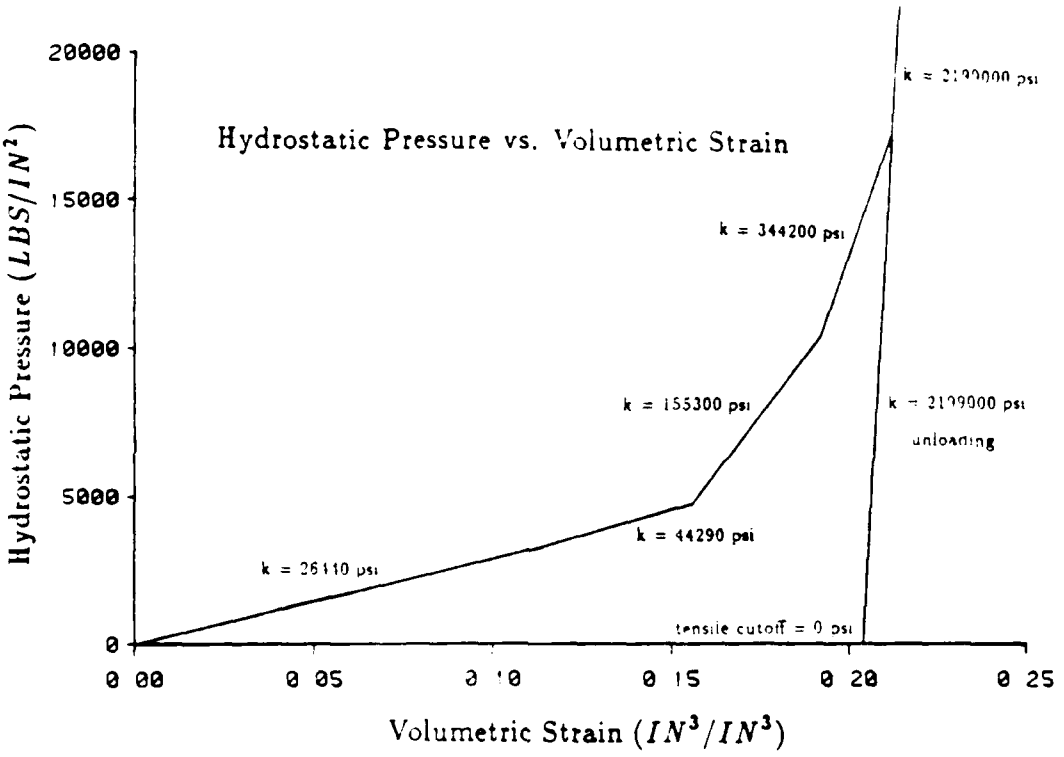

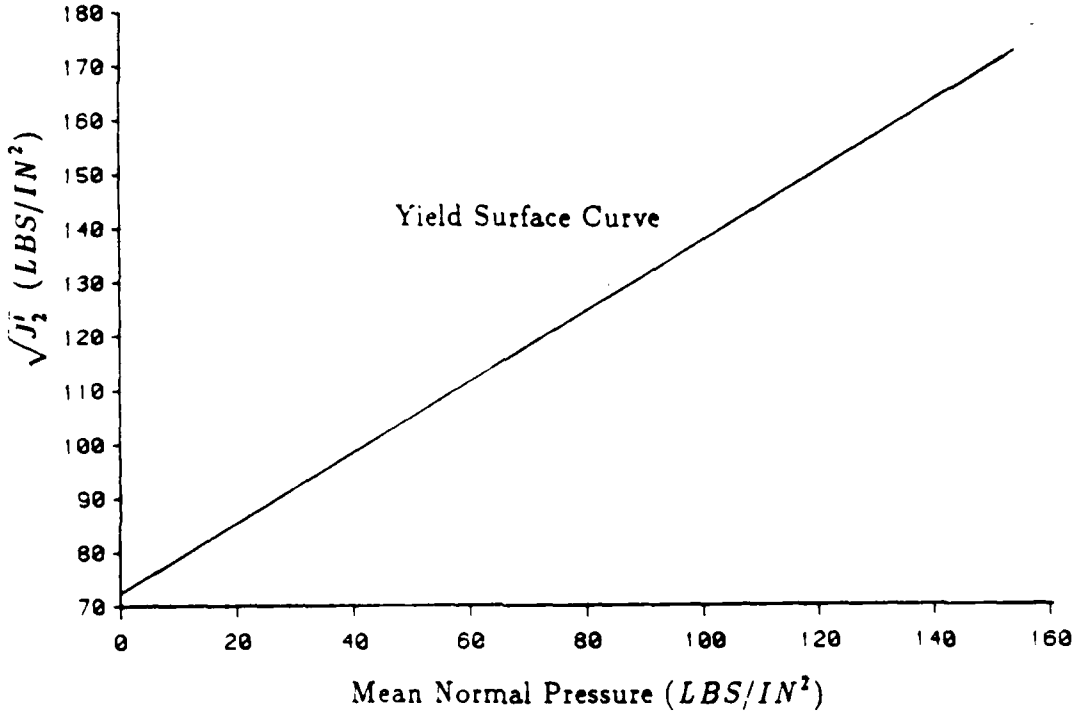

Mass Density = 0.173E-3 $lbs \cdot sec^2/in^4$ Poisson's Ratio = 0.38
Young's Modulus = 0.1904E5 lbs/sec^2 Fraction of Critical Damping = 0.01

Figure 4.28 Material Properties of Yuma Soil

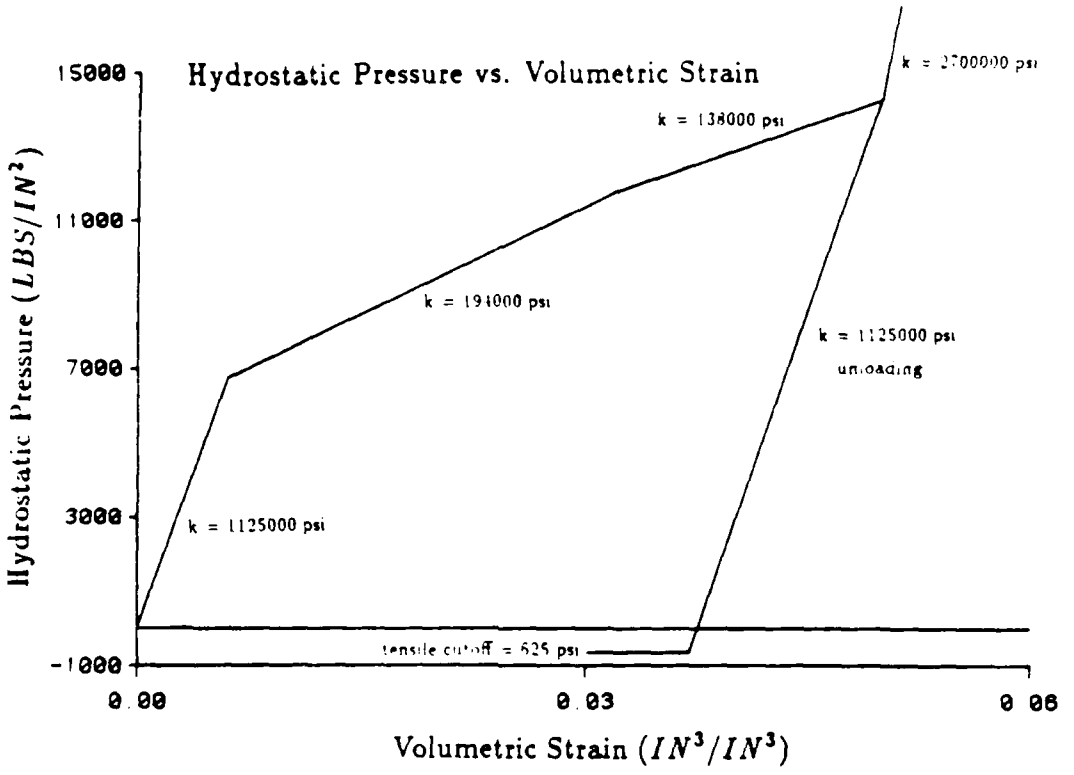

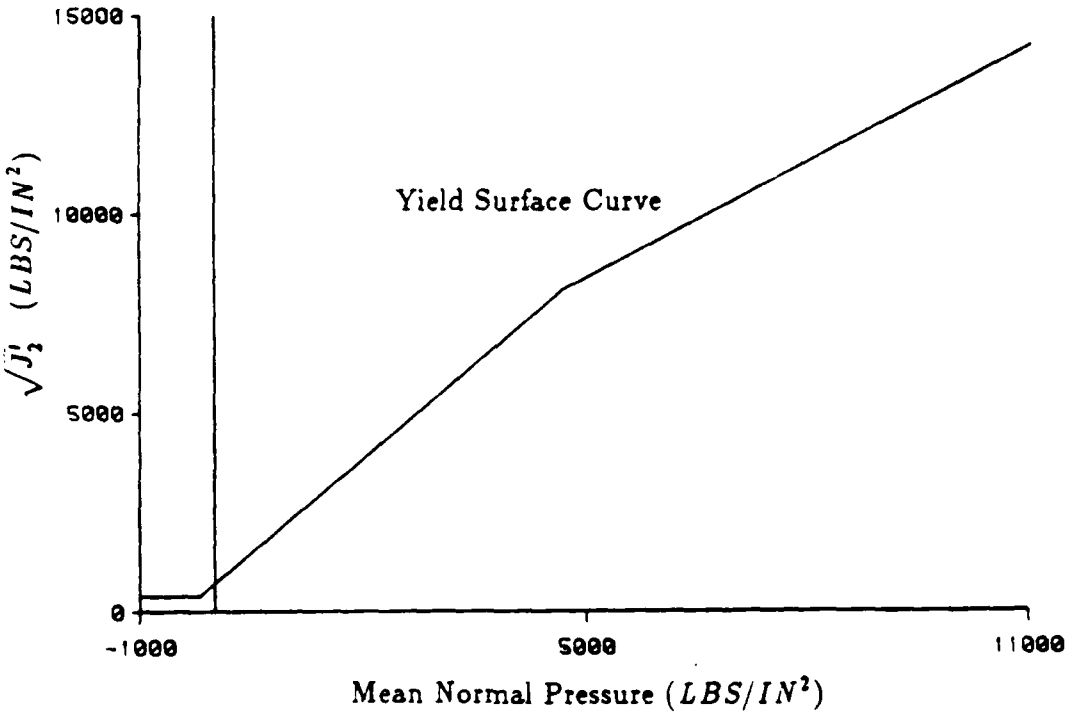

Mass Density = 0.2516E-3 $lbs \cdot sec^2/in^4$ Poisson's Ratio = 0.24
Young's Modulus = 0.1755E7 lbs/sec^2 Fraction of Critical Damping = 0.01

Figure 4.29 Material Properties of Fiber-Reinforced Concrete

Note that the values of Young's modulus and Poisson's ratio, which determine the dilatational and shear impedences of the material, correspond to the bulk modulus and Poisson's ratio of the first loading segment for both materials.

For all of the two-dimensional wave propagation problems, the large mesh and the small mesh were isotropic. It was impractical to analyze an anisotropic medium. If the large mesh were anisotropic, the radiating stress waves would both refract and reflect at the interface for a change in material properties. The stress wave reflections from this interface may return to the area under analysis prematurely. The large mesh would then cease to behave as an infinite medium. Therefore, it would not be applicable to compare the nonreflecting boundary solution to the large mesh solution, and the test would be invalid.

Several tests were initially conducted employing Yuma soil. The performance of the nonreflecting boundary was analyzed under a variety of test conditions. Unless specified otherwise, the loading function used will be a Brode nuclear airblast curve with a peak pressure of 50 ksi. The airblast curve is shown in Figure 4.30. Also, the two meshes will consist of 4NQ axisymmetric elements for which the axis of symmetry will lie along the left edge of the mesh.

For both Yuma soil and concrete, the parameters of the AFWL "engineering" material law describe a very nonlinear material. Together with the large magnitude loading condition, the test cases examined in this two-dimensional study are extreme tests of the nonreflecting boundary. The effective limit of the nonreflecting boundary

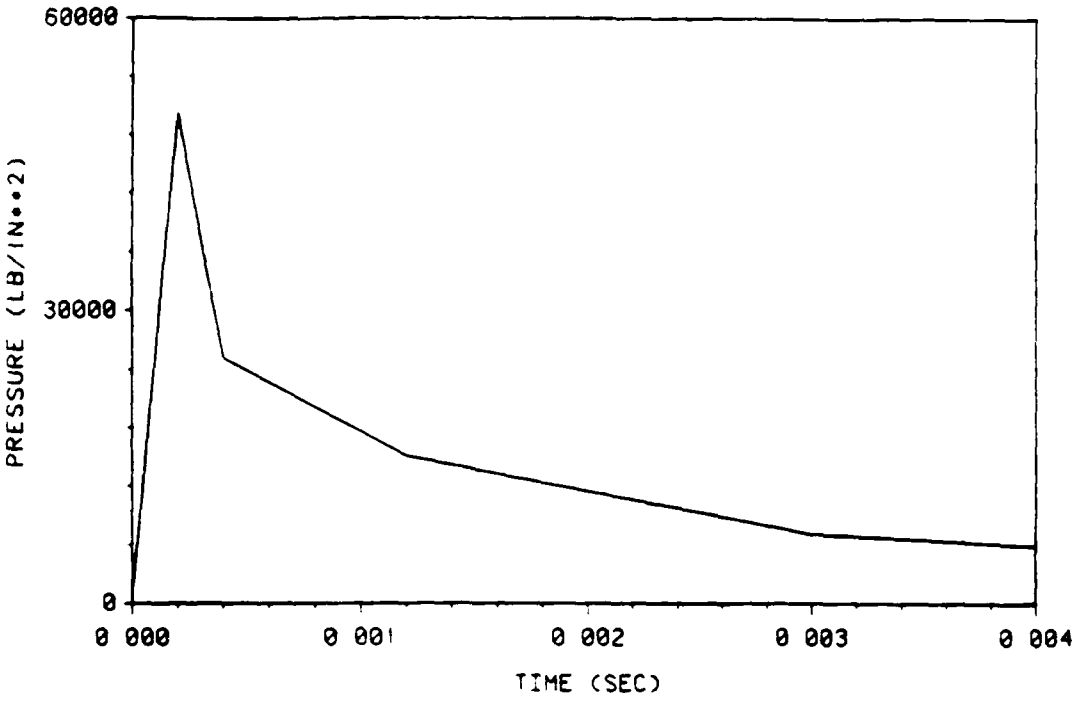

Figure 4.30 Brode Nuclear Airblast Curve

was sought. For problems that involved an elastic or near elastic material, the nonreflecting boundary performed very well regardless of the type of material law. However, the results have been omitted in this report.

The purpose of the first two tests involving two-dimensional wave propagation was to examine the effect of loading applied tangentially along the nonreflecting boundary line. For the first test, the airblast load was applied vertically downward along the top line of the small mesh from the axis of symmetry to the top right node of the small mesh. Thus, the right end of this load line is in contact with the nonreflecting boundary. Because the load line length for both meshes must be equal, the airblast load was applied from the axis of symmetry of the large mesh to the node located 36-in to the right.

The graphical results are presented in Figures 4.31 - 4.33. Note that the time of divergence of the three solutions is approximately 0.0015 sec. The termination time for the solutions is 0.004 sec. Because the point of divergence is greater than 1/3 the termination time, the large mesh simulates an infinite medium during the entire solution period. The displacement versus time and normal stress versus time graphs show a good correlation between the large mesh solution and the nonreflecting boundary solution. However, the plot of the shear stress versus time exhibits more discrepancy than the previous two graphs.

The second test was identical to the previous test except that the length of the airblast load line was shortened. For both meshes, the load line now extends from the axis of symmetry for a distance of 18-in. The same three parameters versus time, as were analyzed in the first test, are examined. The graphical results of the test are shown in Figures 4.34 - 4.36. In all three cases, the nonreflecting boundary solution was very comparable with the large mesh solution.

In order to investigate the response of the entire mesh, the vertical displacement distribution of all nodes were plotted at time = 0.004 sec. Figure 4.37 shows the vertical displacement of the nodes in the upper left section of the large mesh. Likewise, Figures 4.38 and 4.39 show the vertical displacement of all the nodes in the small mesh. To clarify the orientation of the plots in the figures, the bottom left corner of the plot corresponds to the bottom left corner of the small mesh. The vertical displacements are projected upward from each node in the mesh. The large mesh displacement distribution is bounded by 28.77-in. while the nonreflecting boundary displacement distribution is bounded by 28.10-in. The surfaces described by the displacements in

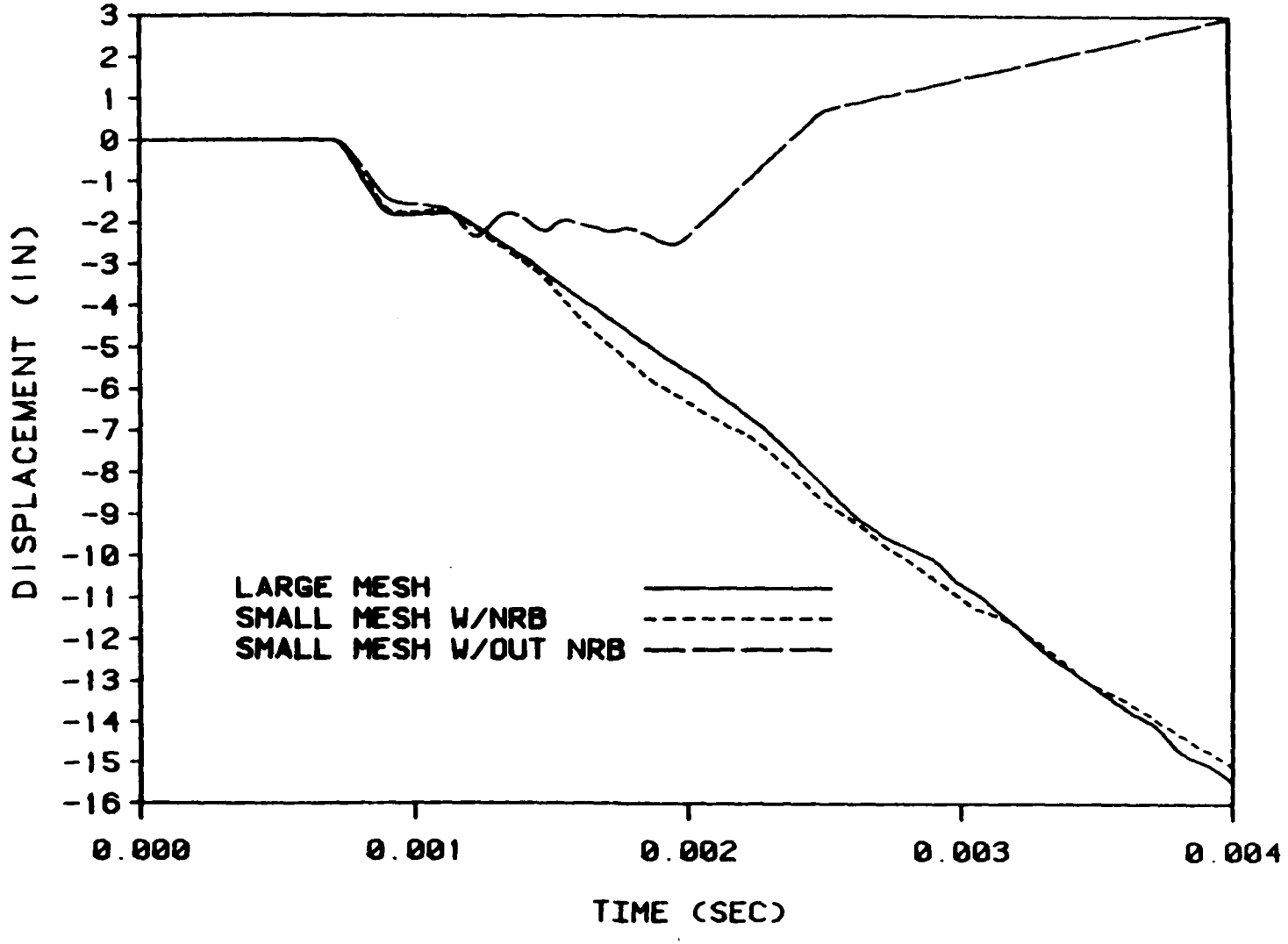

Figure 4.31 Vertical Displacement vs. Time. Extended Load Line

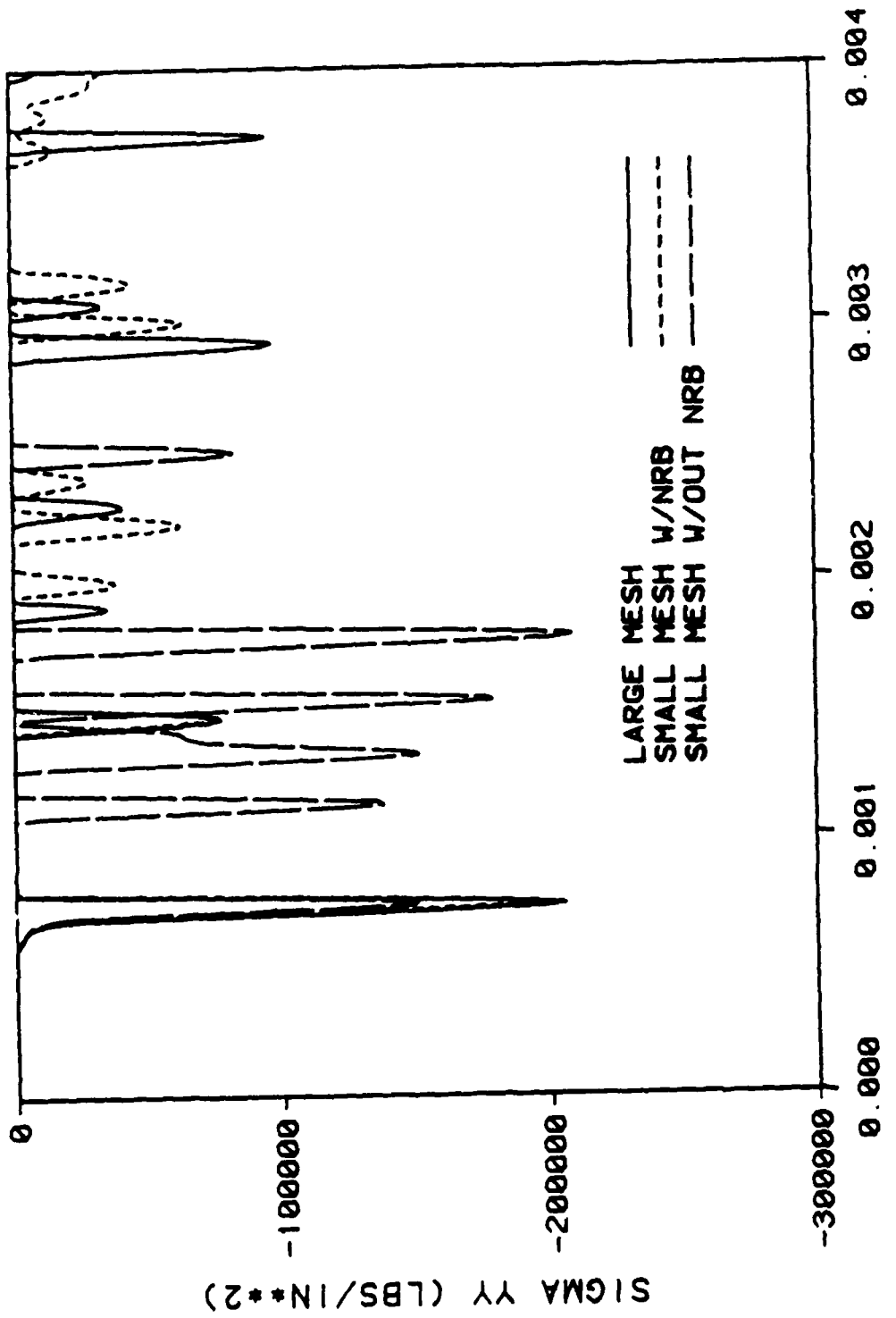

Figure 4.32 Normal Stress, σ_{yy} vs. Time. Extended Load Line

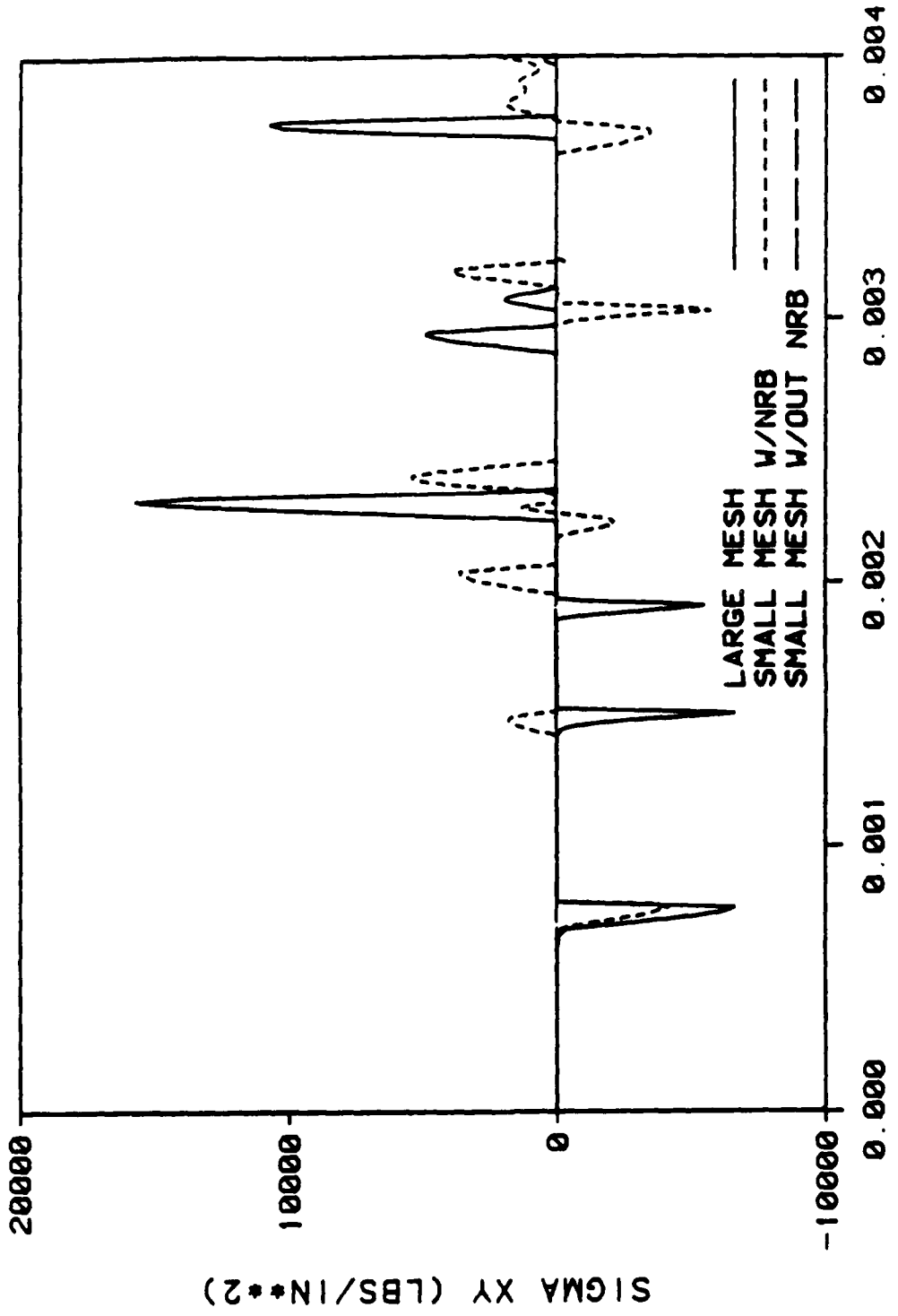

Figure 4.33 Shear Stress, σ_{xy} vs. Time. Extended Load Line

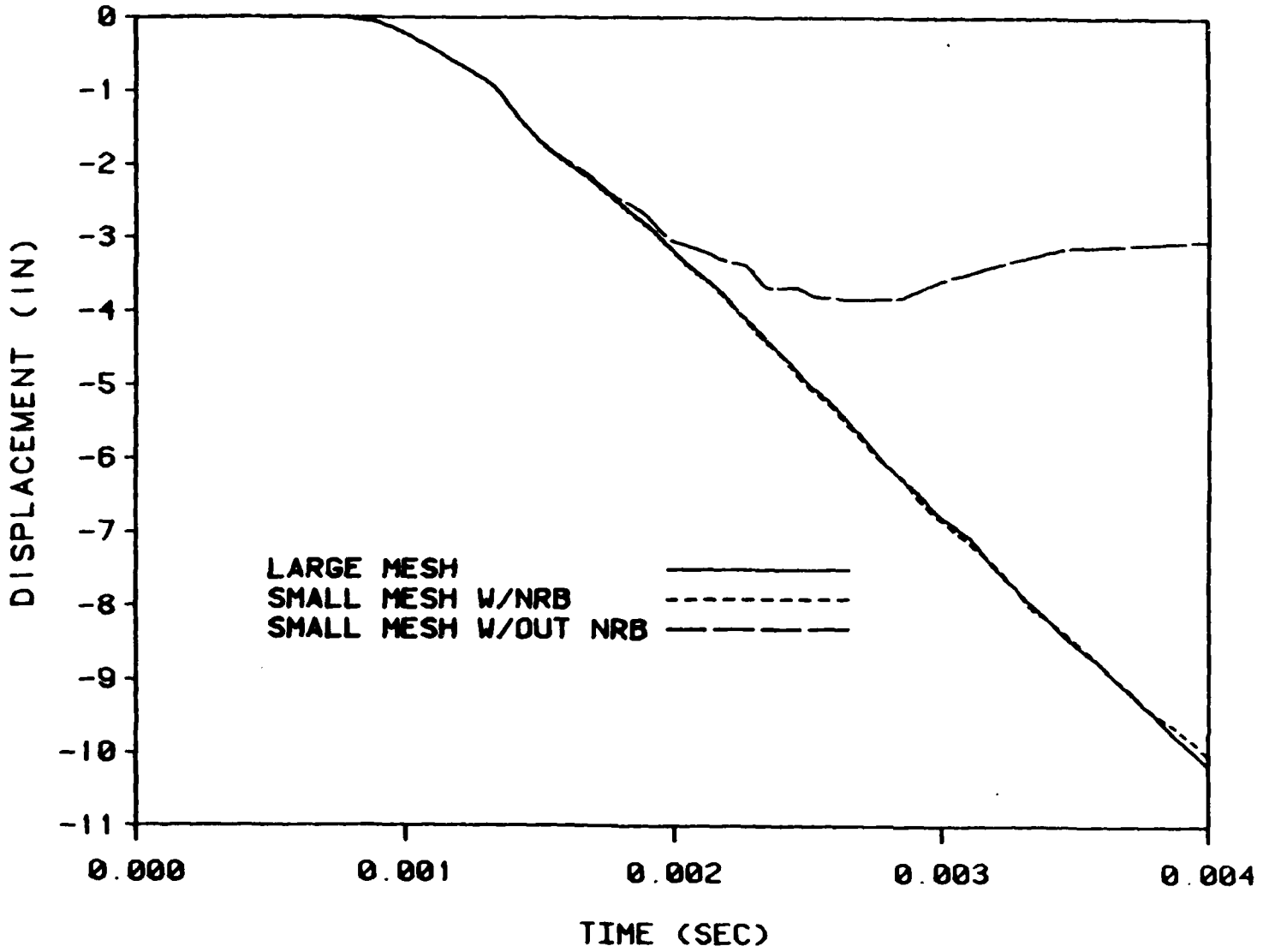

Figure 4.34 Vertical Displacement vs. Time Shortened Load Line

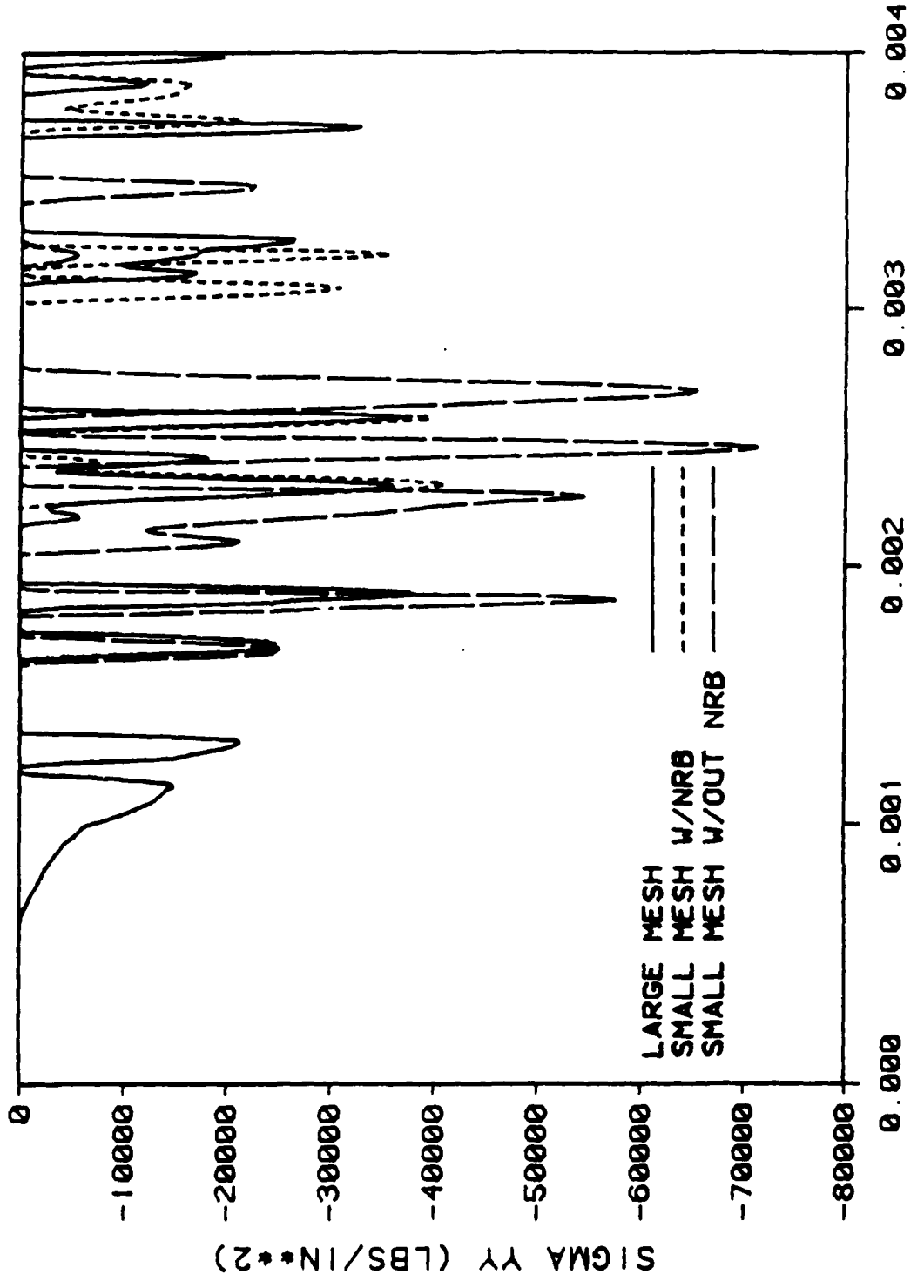

Figure 4.35 Normal Stress, σ_{yy} vs. Time Shortened Load Line

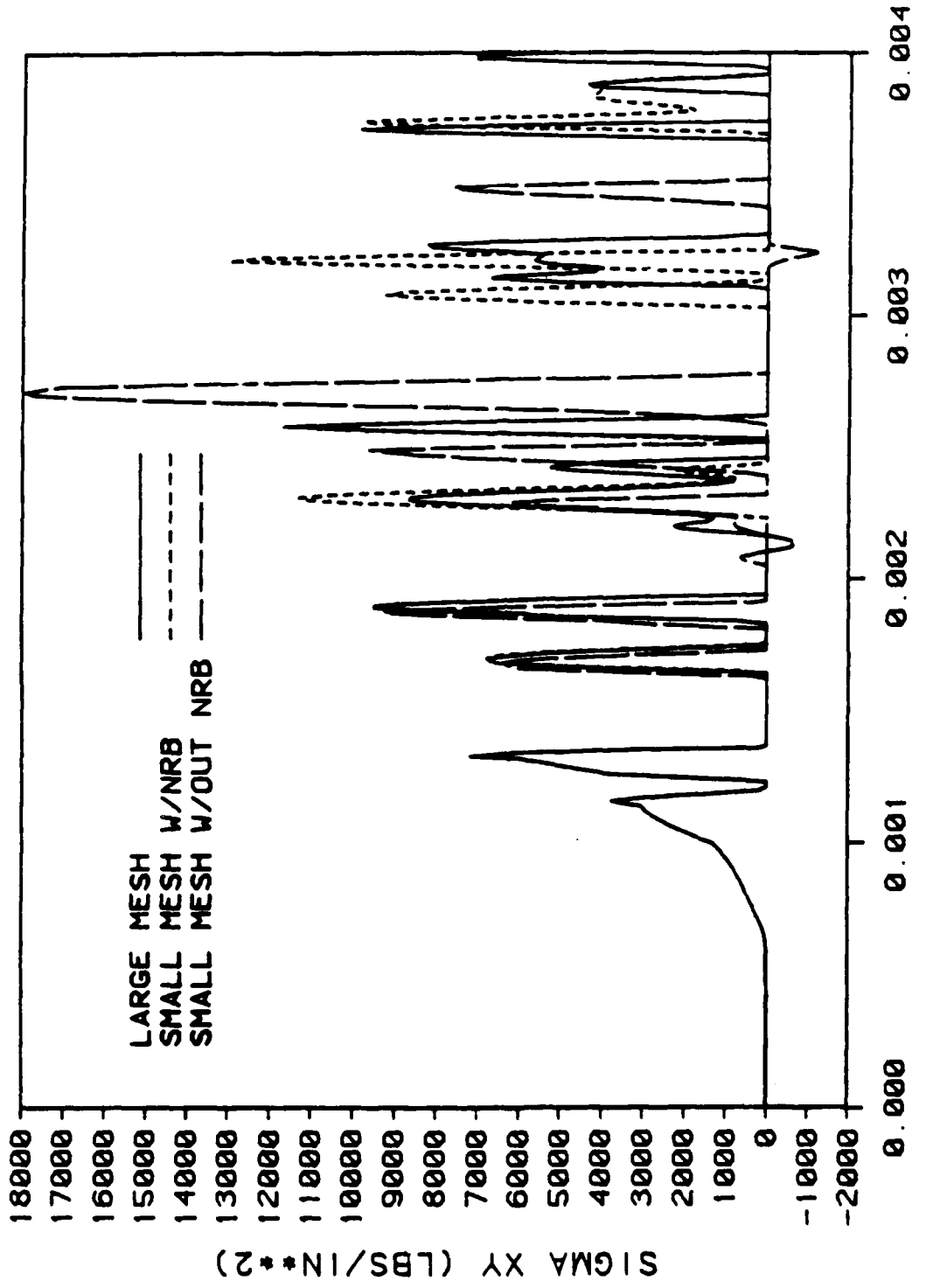

Figure 4.36 Shear Stress, σ_{xy} vs. Time Shortened Load Line

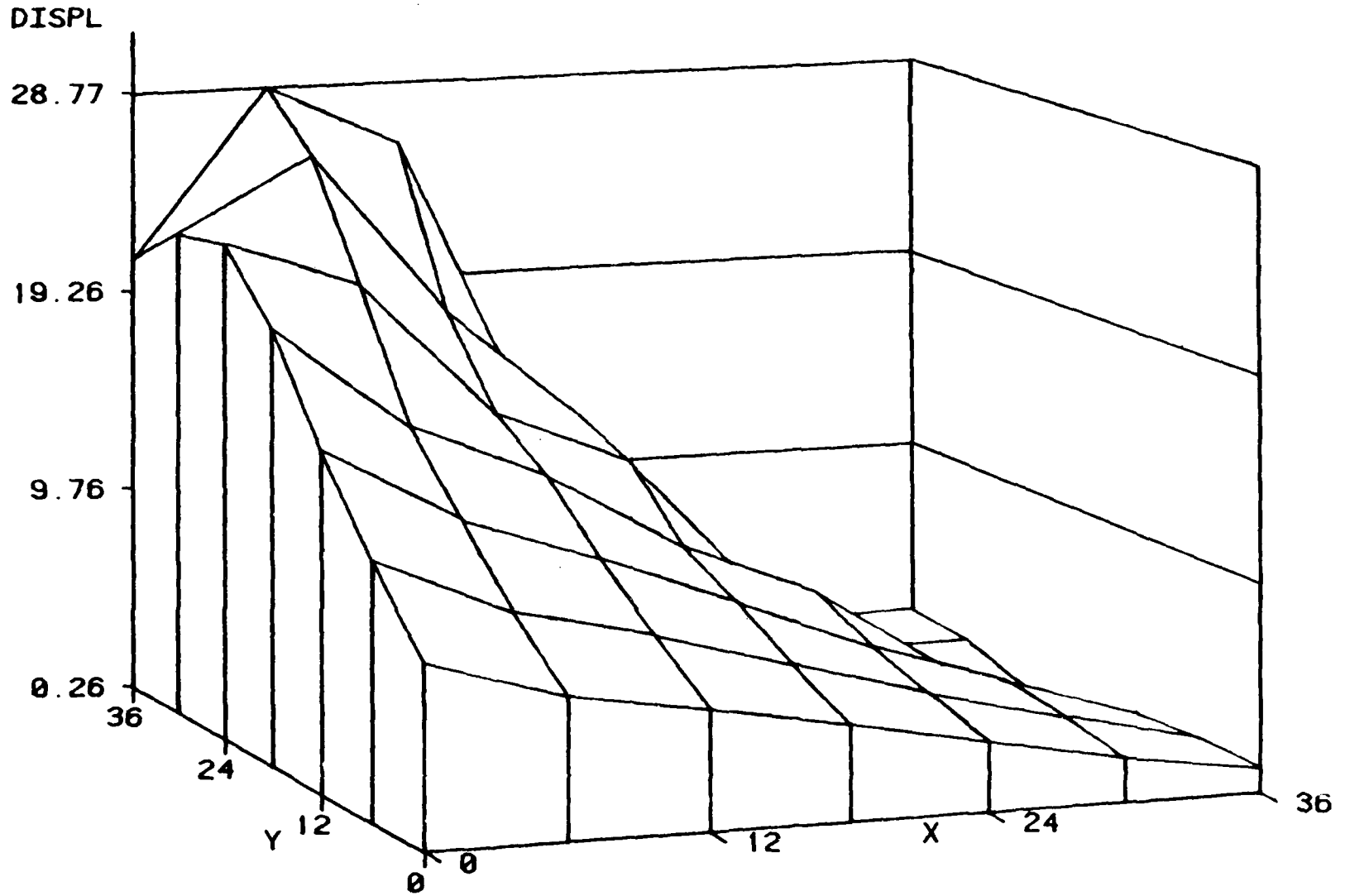

Figure 4.37 Vertical Displacement Distribution for the Large Mesh

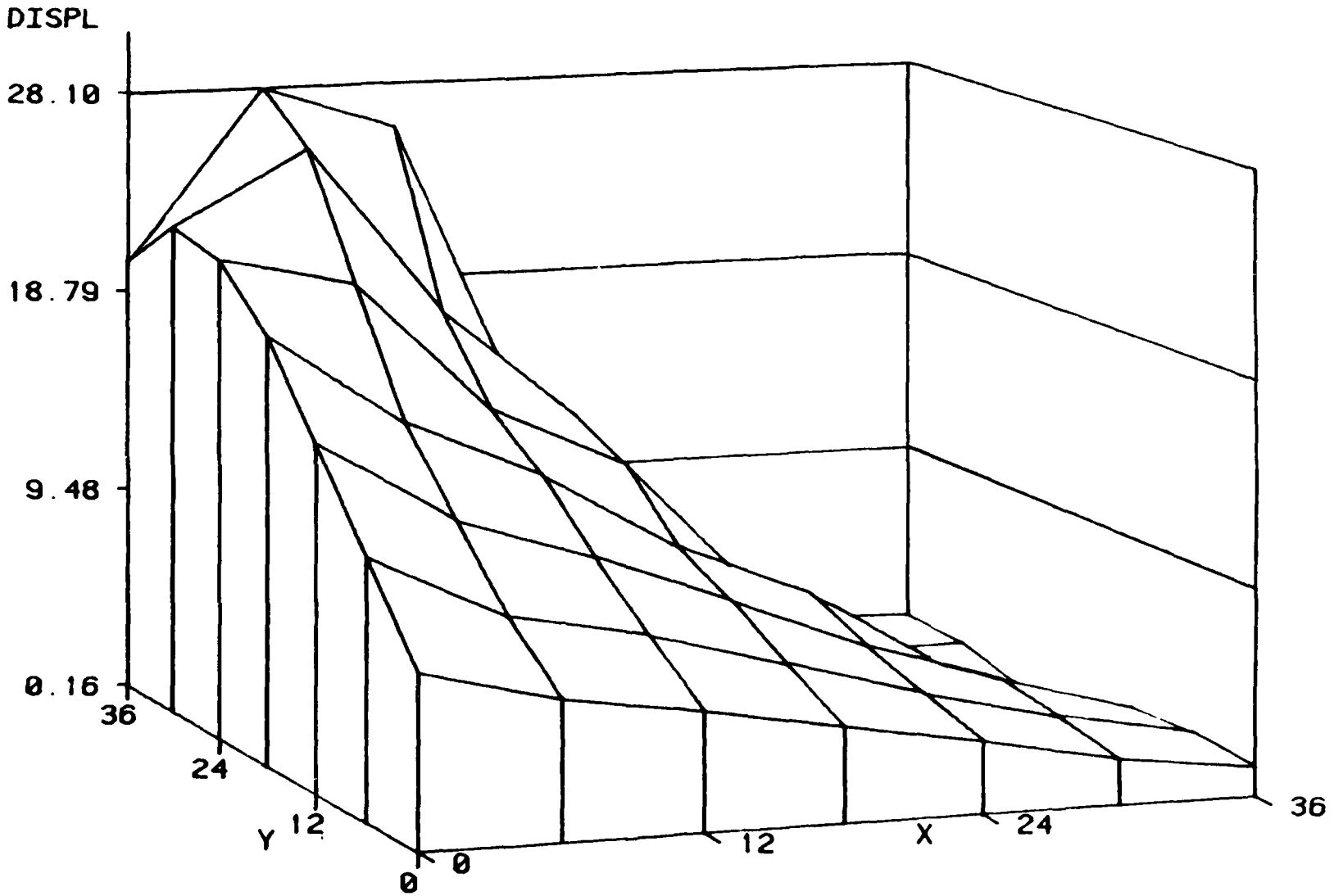

Figure 4.38 Vertical Displacement Distribution for the Small Mesh with a Nonreflecting Boundary

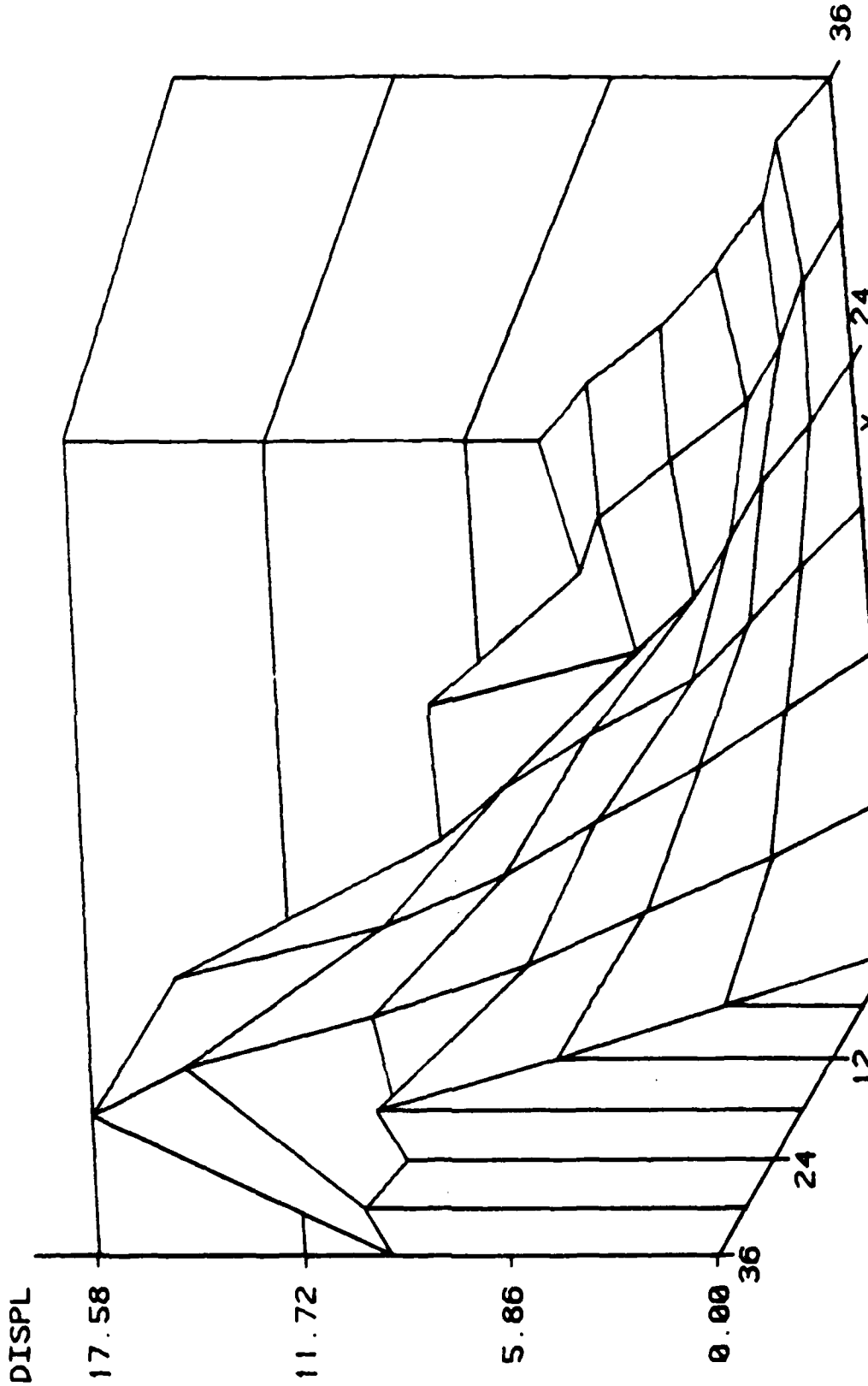

Figure 4.39 Vertical Displacement Distribution for the Small Mesh without a Nonreflecting Boundary

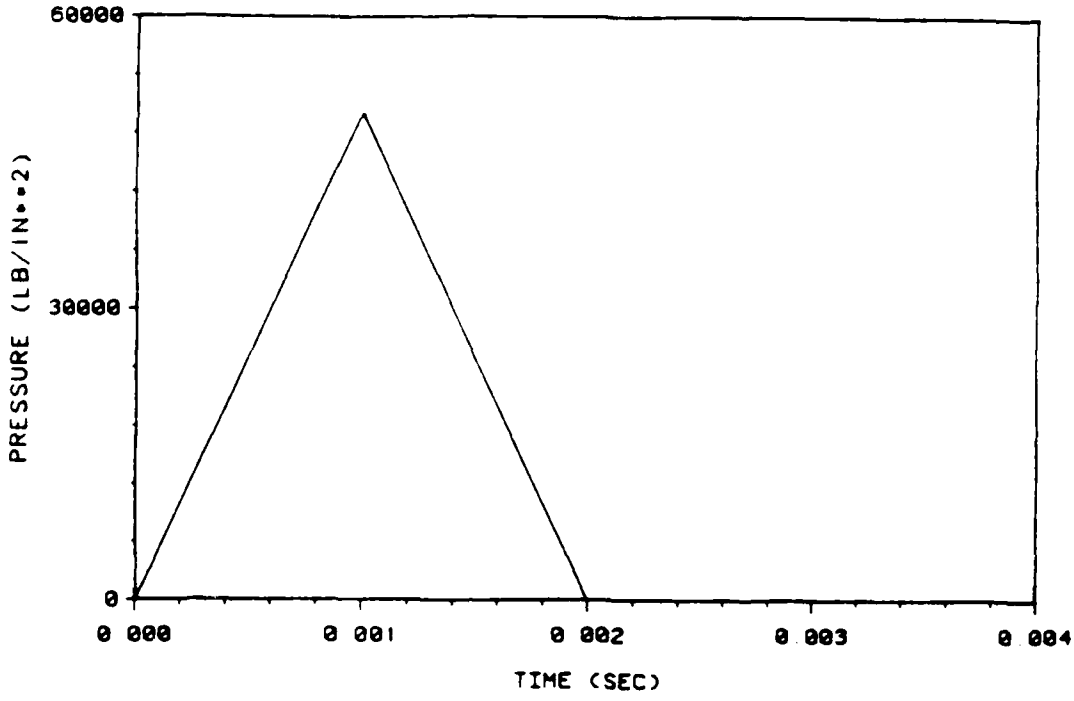

Figure 4.40 Impulse Load

Figures 4.37 and 4.38 are very similar. The vertical displacement distribution of the small mesh without the nonreflecting boundary is bounded by 17.58-in and exhibits a surface that differs slightly from the previous two plots. The vertical displacement along the bottom axis in Figure 4.39 is zero indicating that this axis is indeed fixed in the vertical direction.

The two tests demonstrate a limitation of the nonreflecting boundary. The shear absorption of the nonreflecting boundary tangent to the vertical loading in the small mesh does not adequately simulate the shear stiffness of the portion of the large mesh that is to the immediate right of the vertical load. The remaining tests in this study, will apply the load along the 18-in line measured right from the axis of symmetry.

The nonreflecting boundary has performed well for the tests utilizing a Brode nuclear airblast curve. The loading was then changed to a simple triangular impulse load shown in Figure 4.40 with a peak pressure of 50 ksi. All other parameters for both meshes have been kept the same. The graphical results of the three field variables in Figures 4.41 - 4.43 demonstrate that the form of the loading does not affect the effectiveness of the nonreflecting boundary. In this case, the results are better than the previous tests using the airblast curve. The large mesh solution and the nonreflecting boundary solution in the normal stress and shear stress versus time graphs have similar peak values of stress but are slightly out of phase with one another. The cause of this phenomena is unknown to the authors and several unsuccessful attempts were made to remedy the situation. The vertical displacement distributions of the three meshes at time = 0.004 sec are shown in Figures 4.44 - 4.46. The surfaces described by the vertical displacements of the nodes in the three meshes are similar to those in Figures 4.37 - 4.39 but are bounded by different displacements.

The remaining tests of the nonreflecting boundary incorporated fiber reinforced concrete instead of Yuma soil. The loading, once again, is the airblast curve with a peak pressure of 50 ksi. The graphical results are presented in Figures 4.47 - 4.49. Note that the termination time for the solutions is 0.0015 sec instead of 0.004 sec for Yuma soil. The stress wave speed through concrete is approximately three times faster than the stress wave speed through Yuma soil. The time of divergence for the three solutions is still greater than 1/3 the termination time. Therefore, the test is valid. The nonreflecting boundary solution correlates well with the large mesh solution for all three field variables, particularly the normal stress. The normal stress and the shear

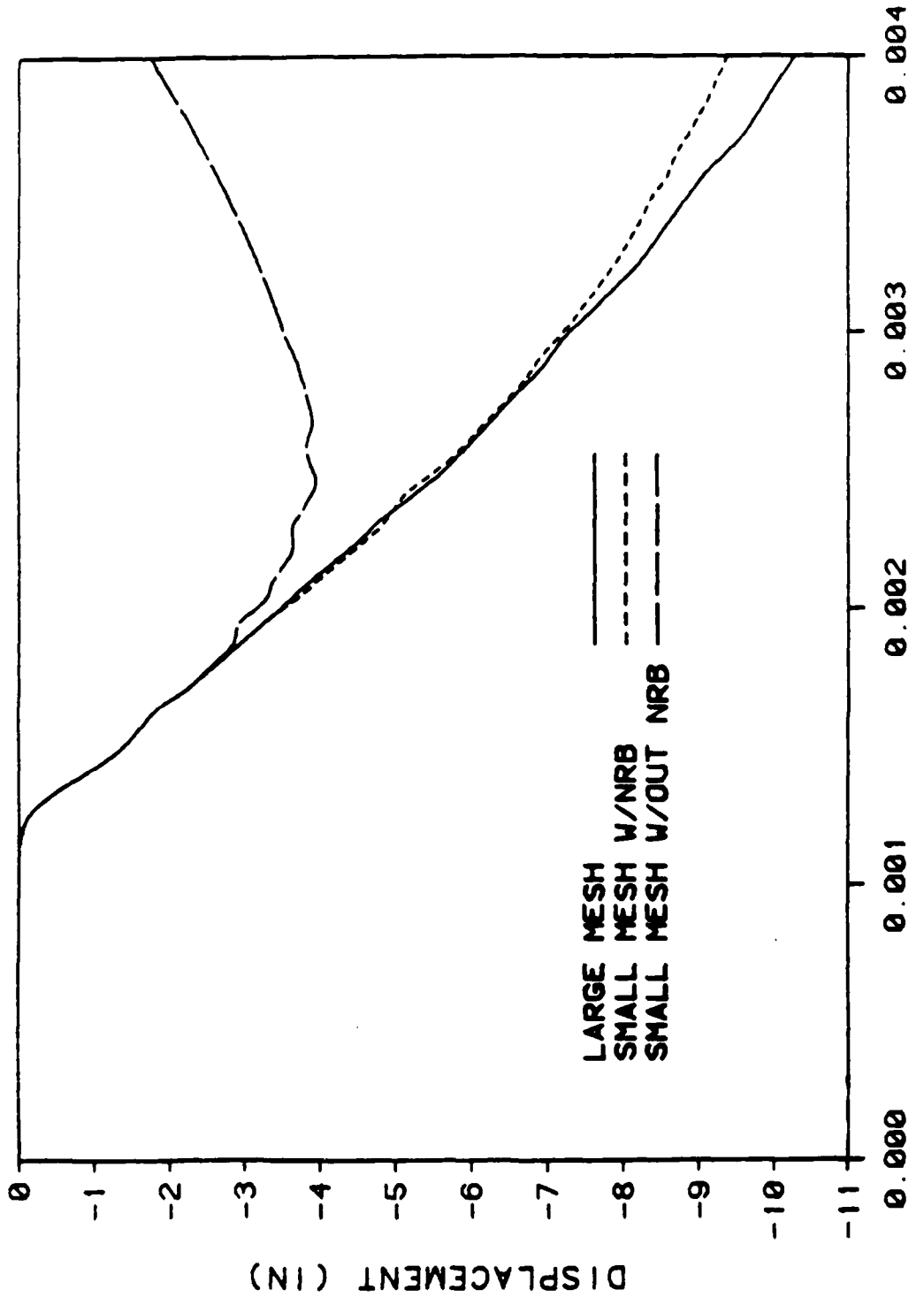

Figure 4.41 Vertical Displacement vs. Time Impulse Load

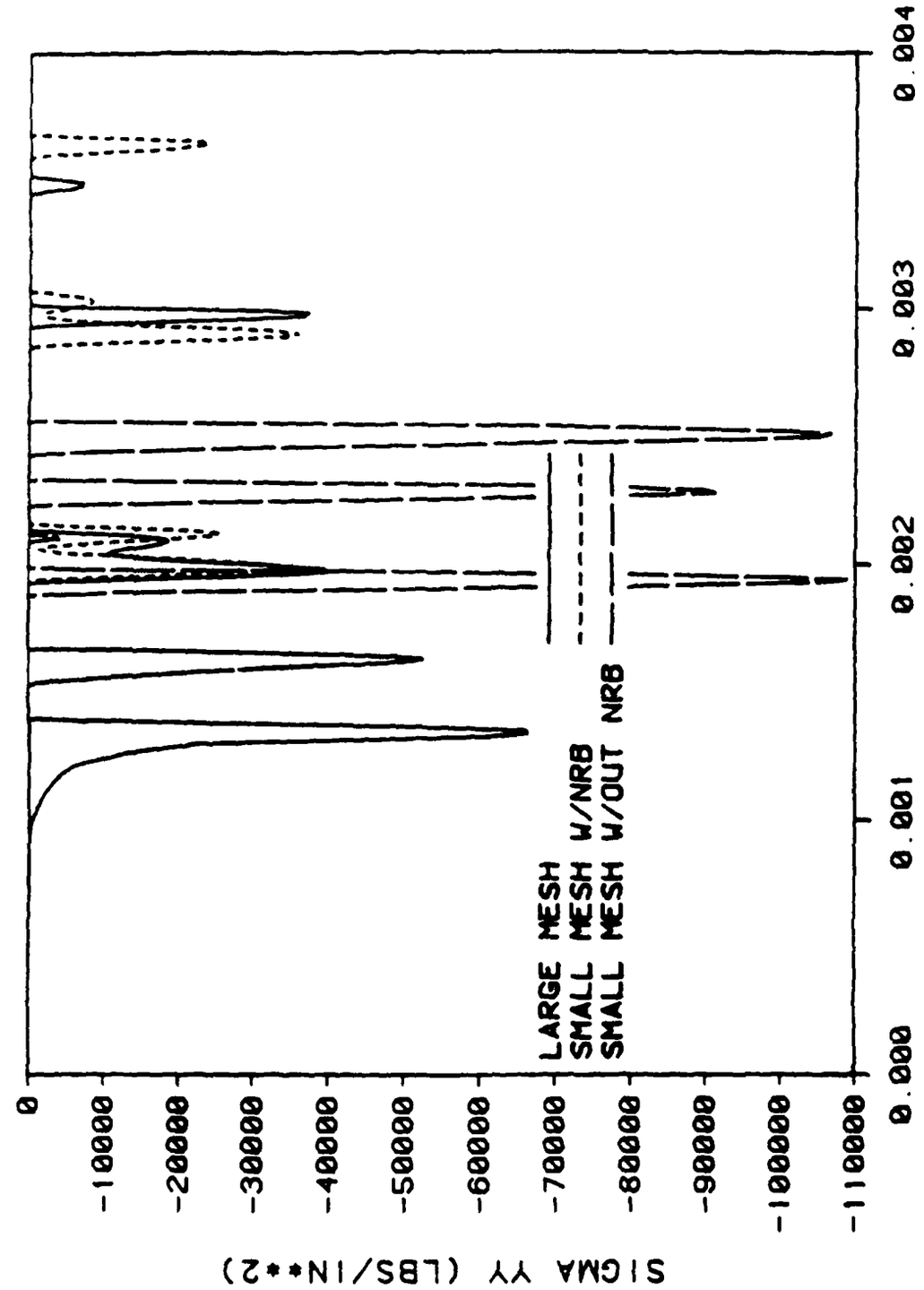

Figure 4.42 Normal Stress, σ_{yy} vs. Time Impulse Load

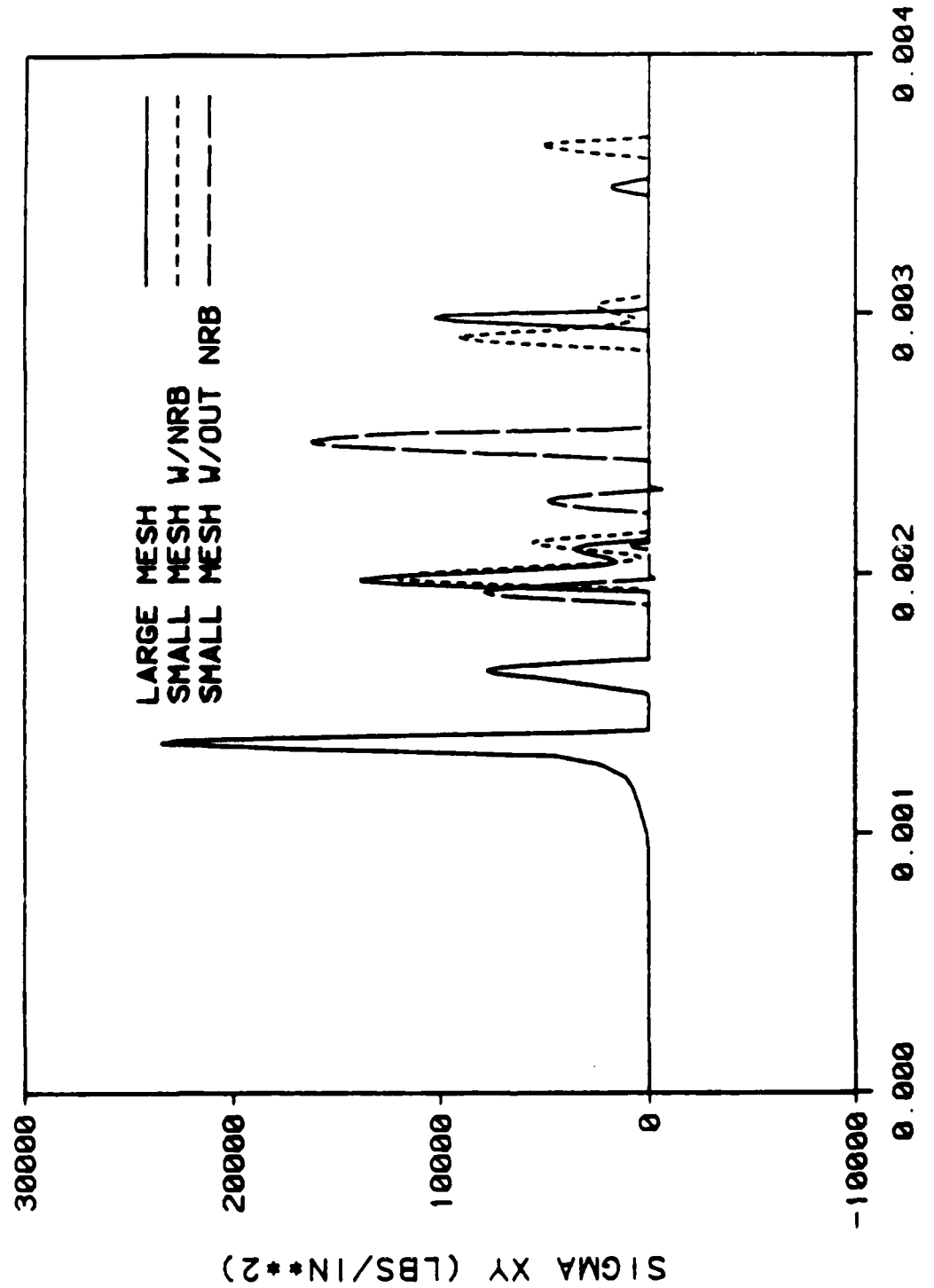

Figure 4.43 Shear Stress, σ_{xy} vs. Time Impulse Load

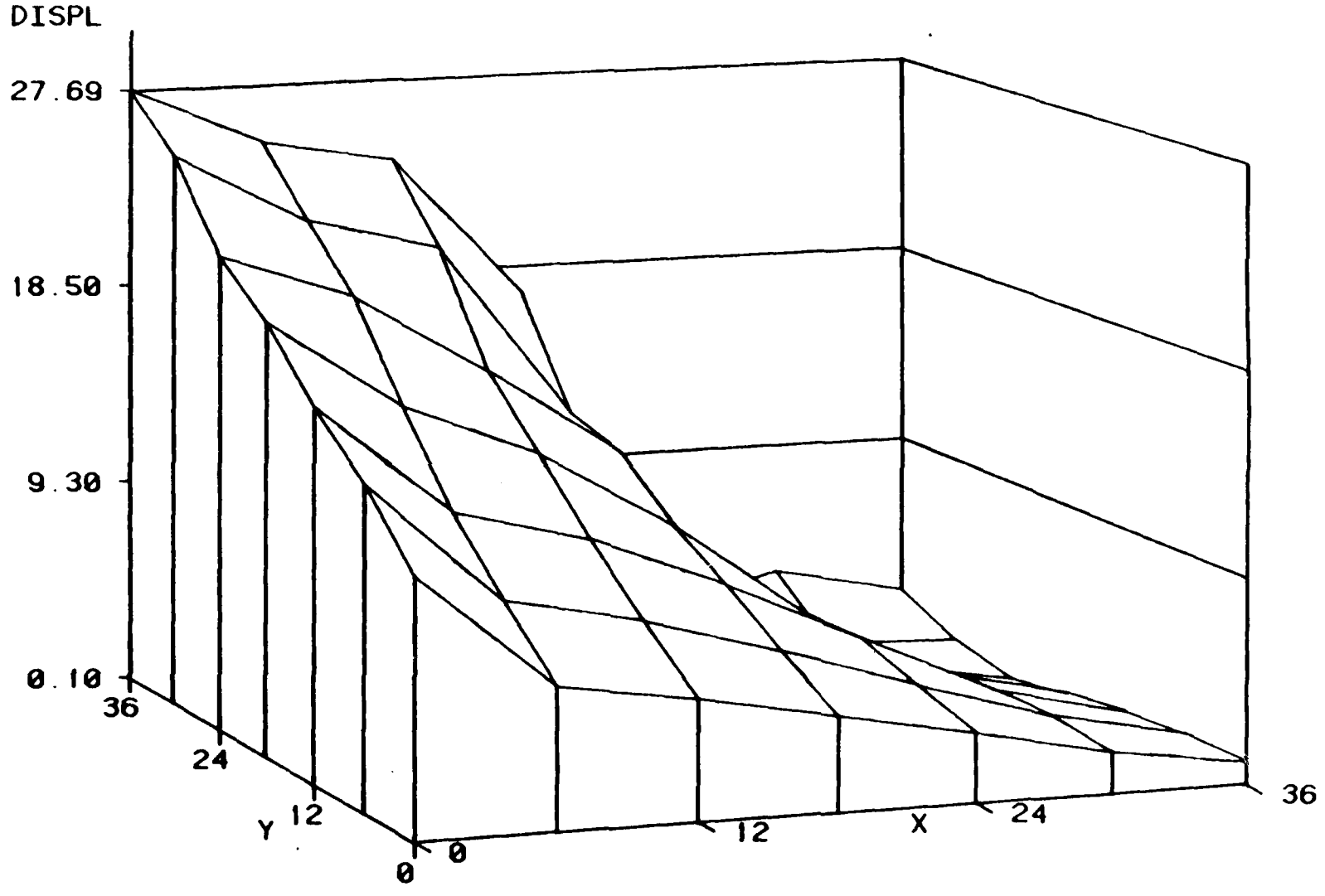

Figure 4.44 Vertical Displacement Distribution for the Large Mesh

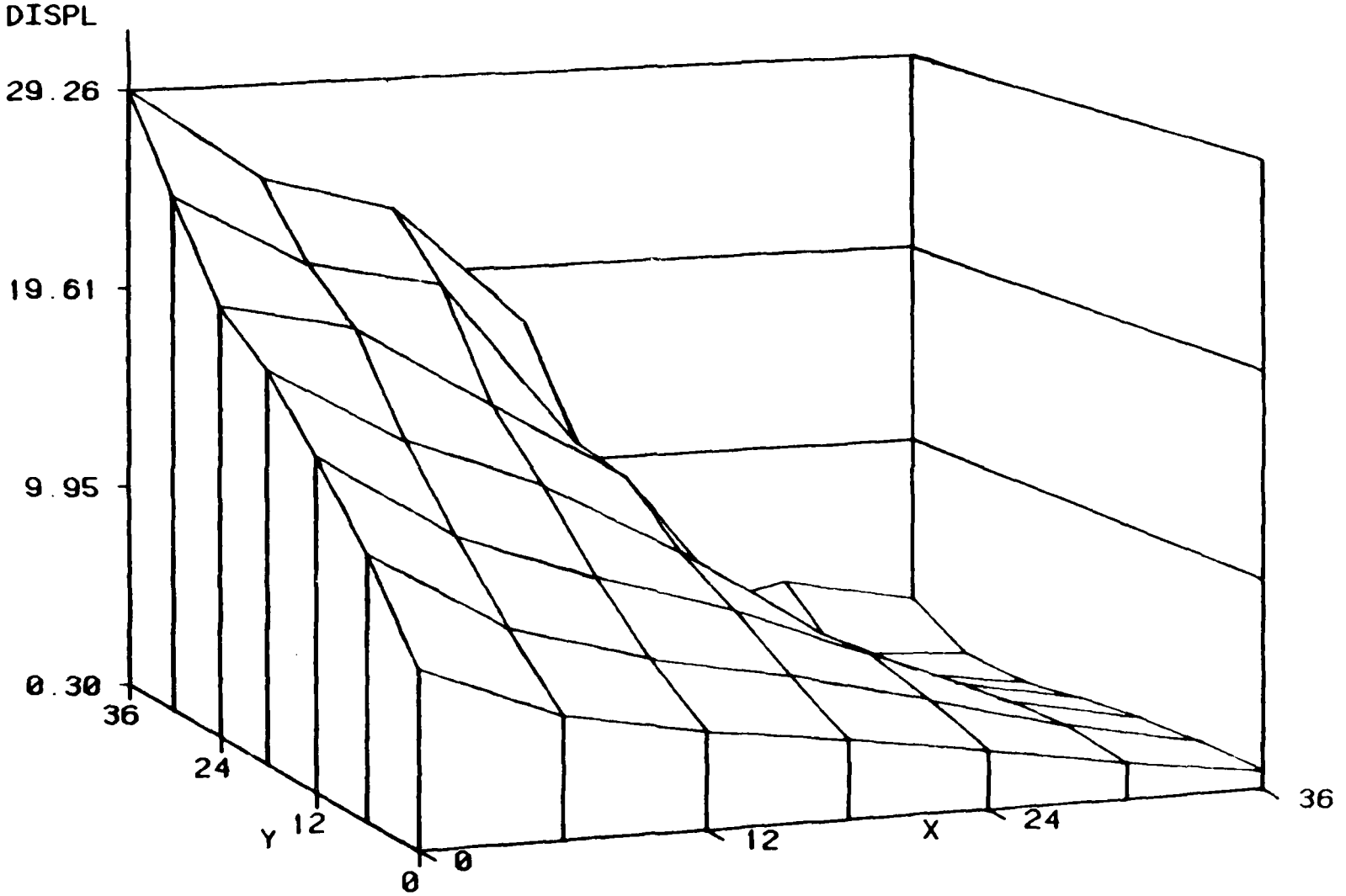

Figure 4.45 Vertical Displacement Distribution for the Small Mesh with a Nonreflecting Boundary

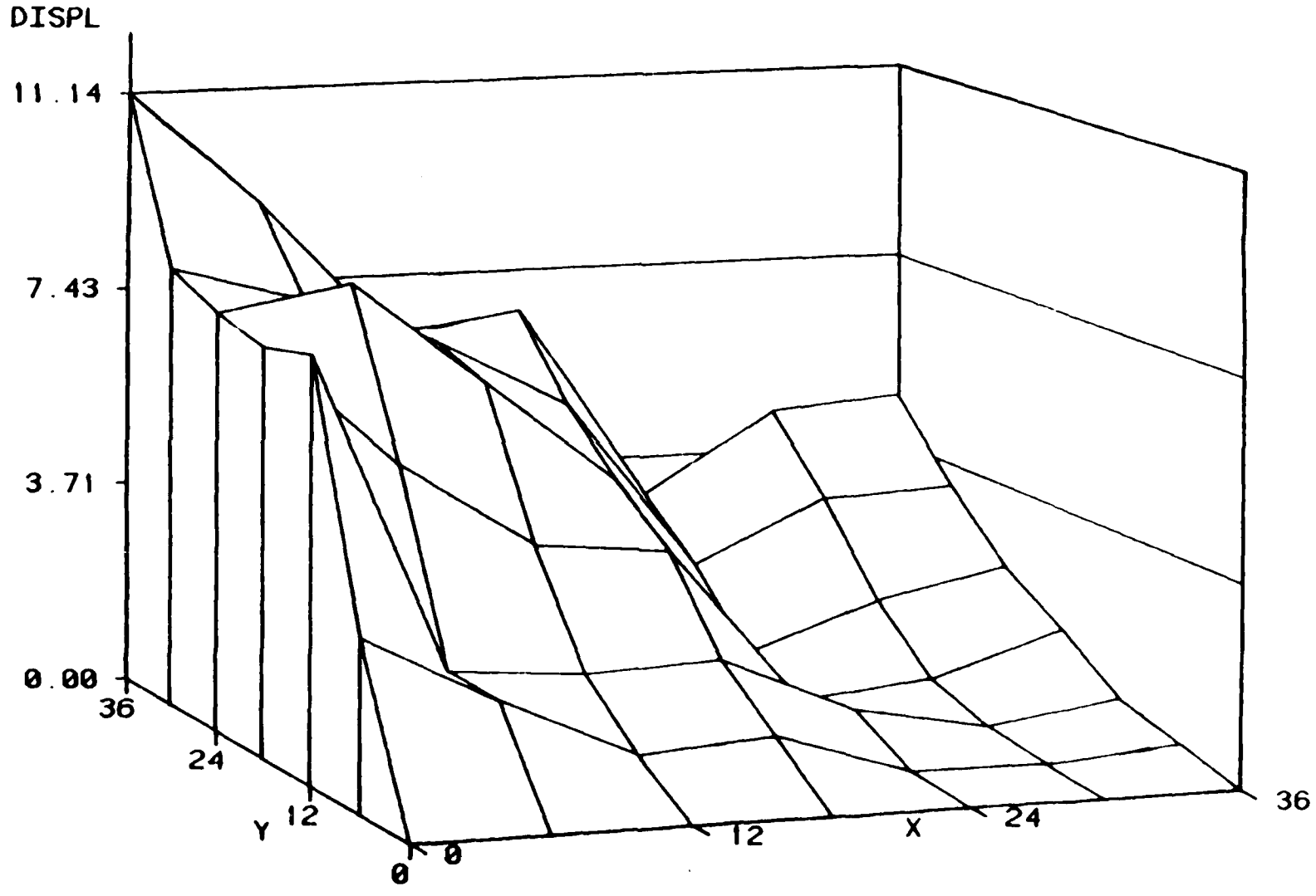

Figure 4.46 Vertical Displacement Distribution for the Small Mesh without a Nonreflecting Boundary

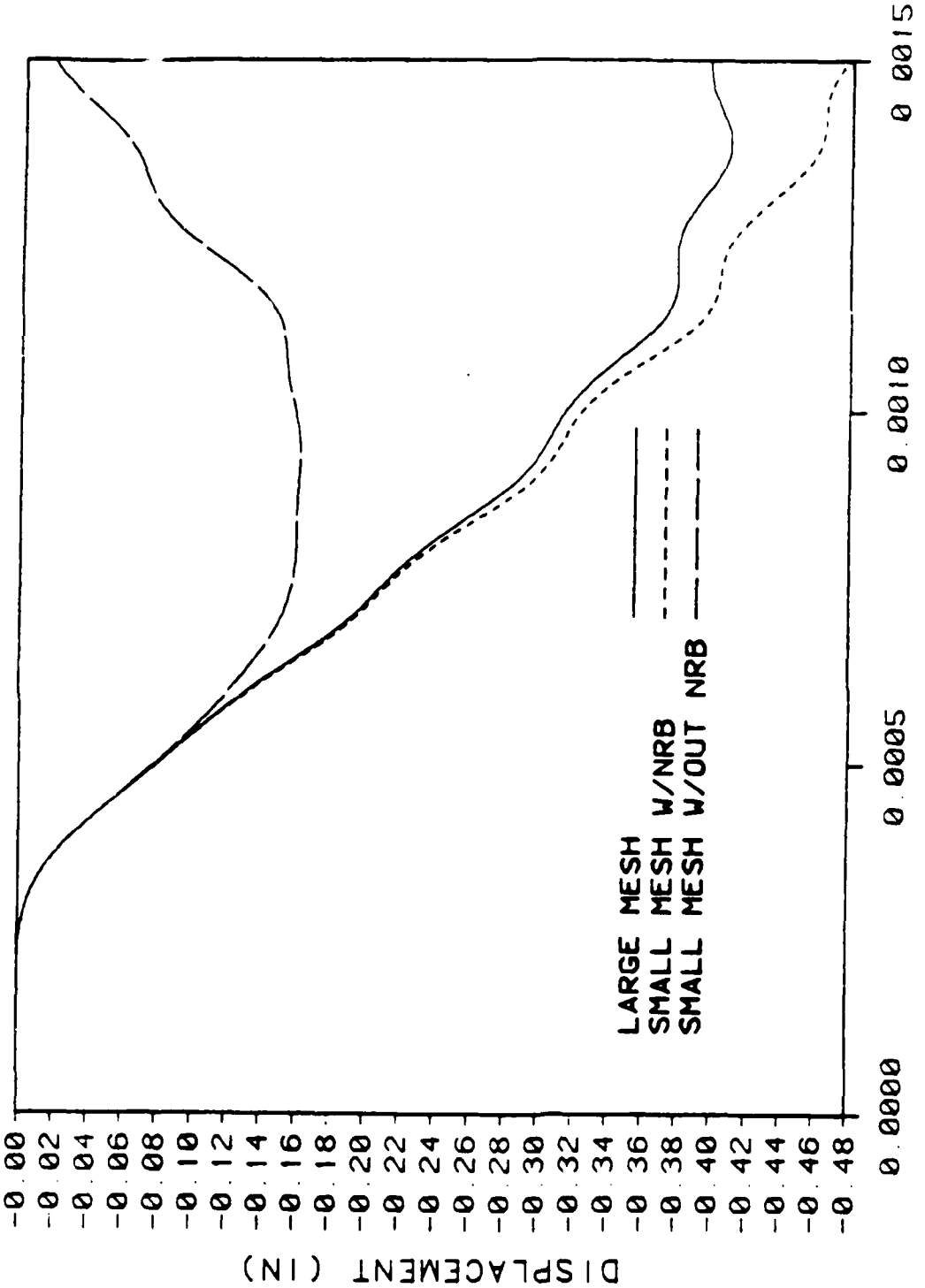

Figure 4.47 Vertical Displacement vs. Time, Fiber-Reinforced Concrete

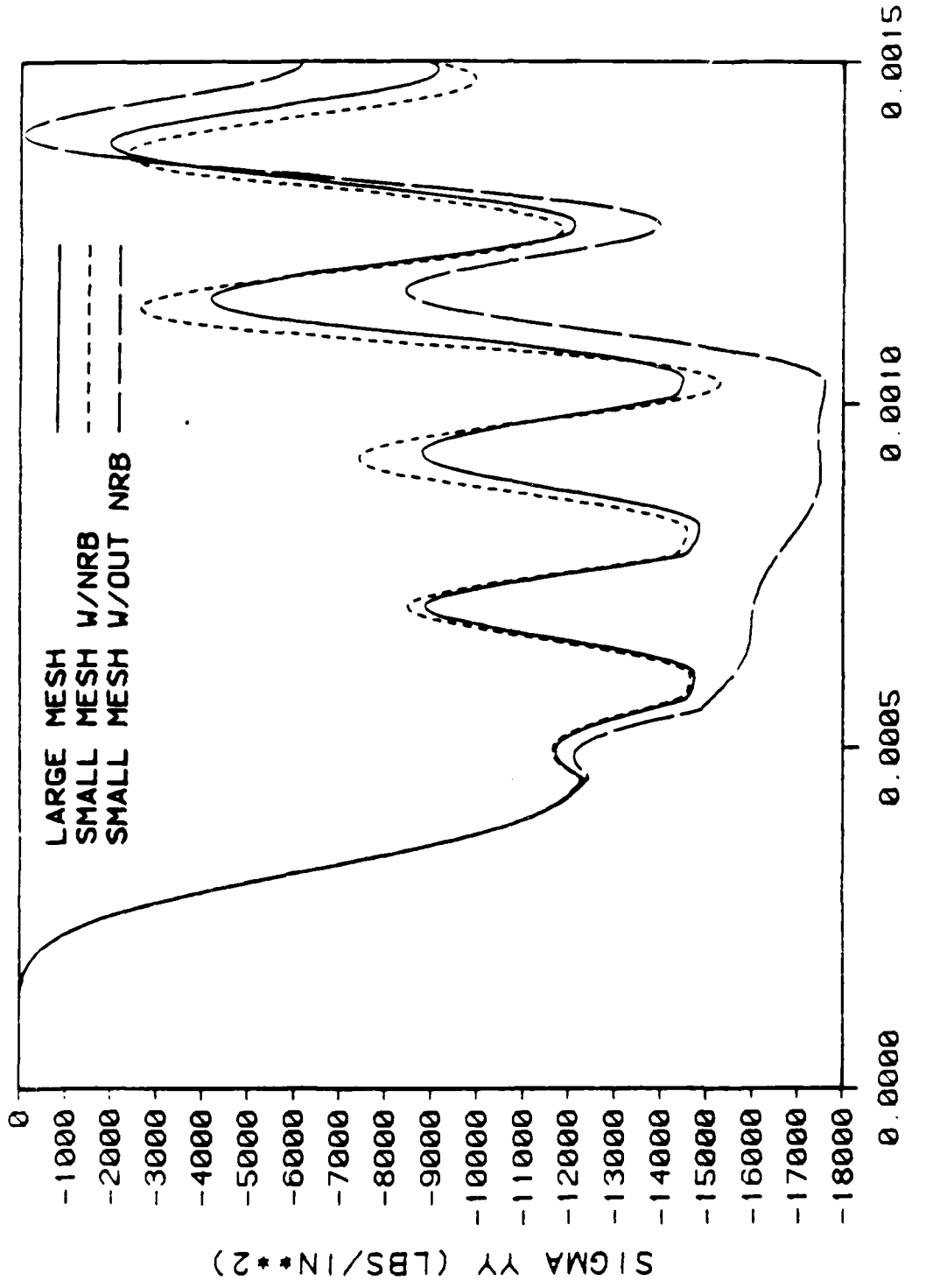

Figure 4.48 Normal Stress, σ_{yy} vs. Time. Fiber-Reinforced Concrete

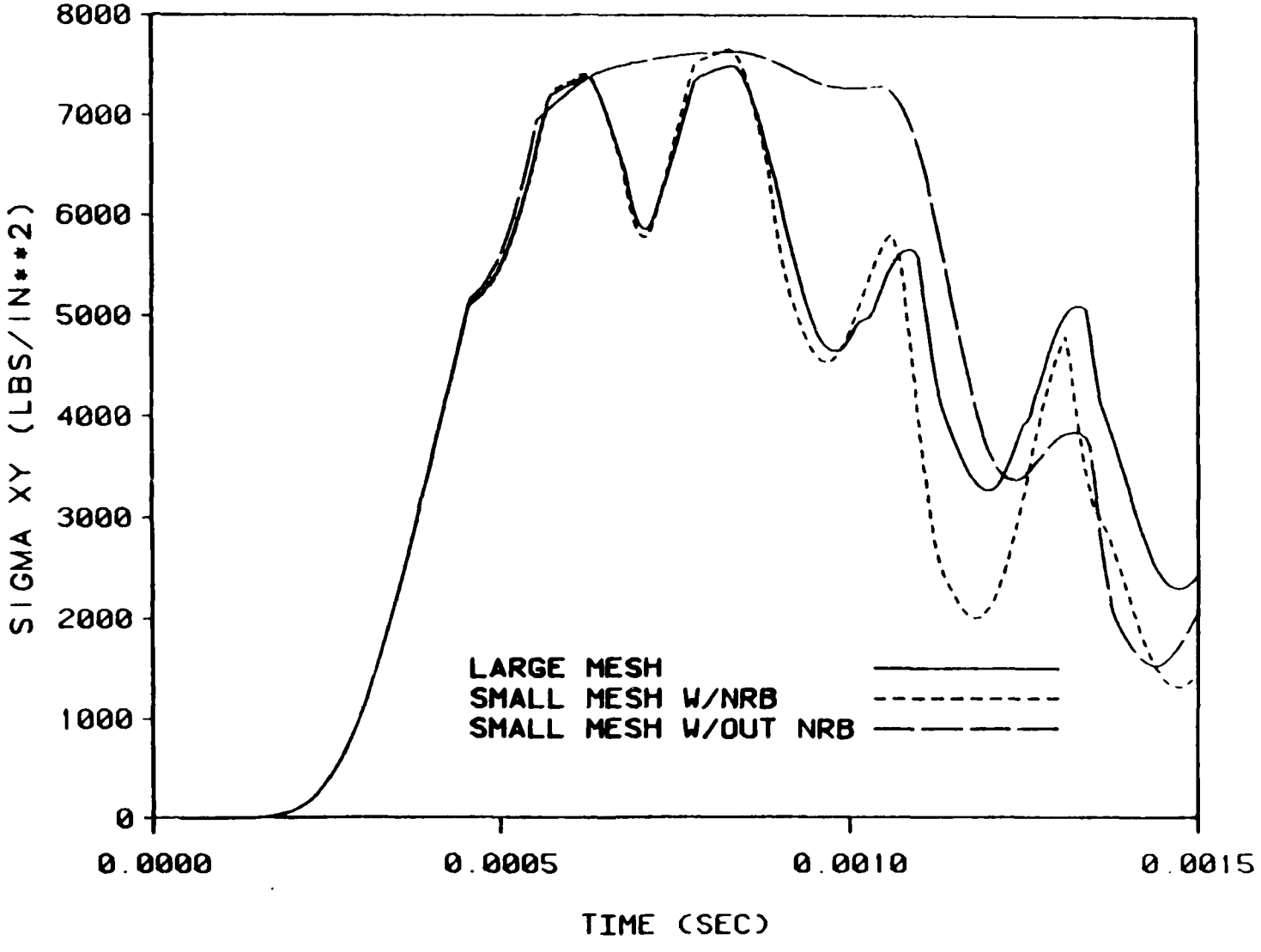

Figure 4.49 Shear Stress, σ_{xy} vs. Time. Fiber-Reinforced Concrete

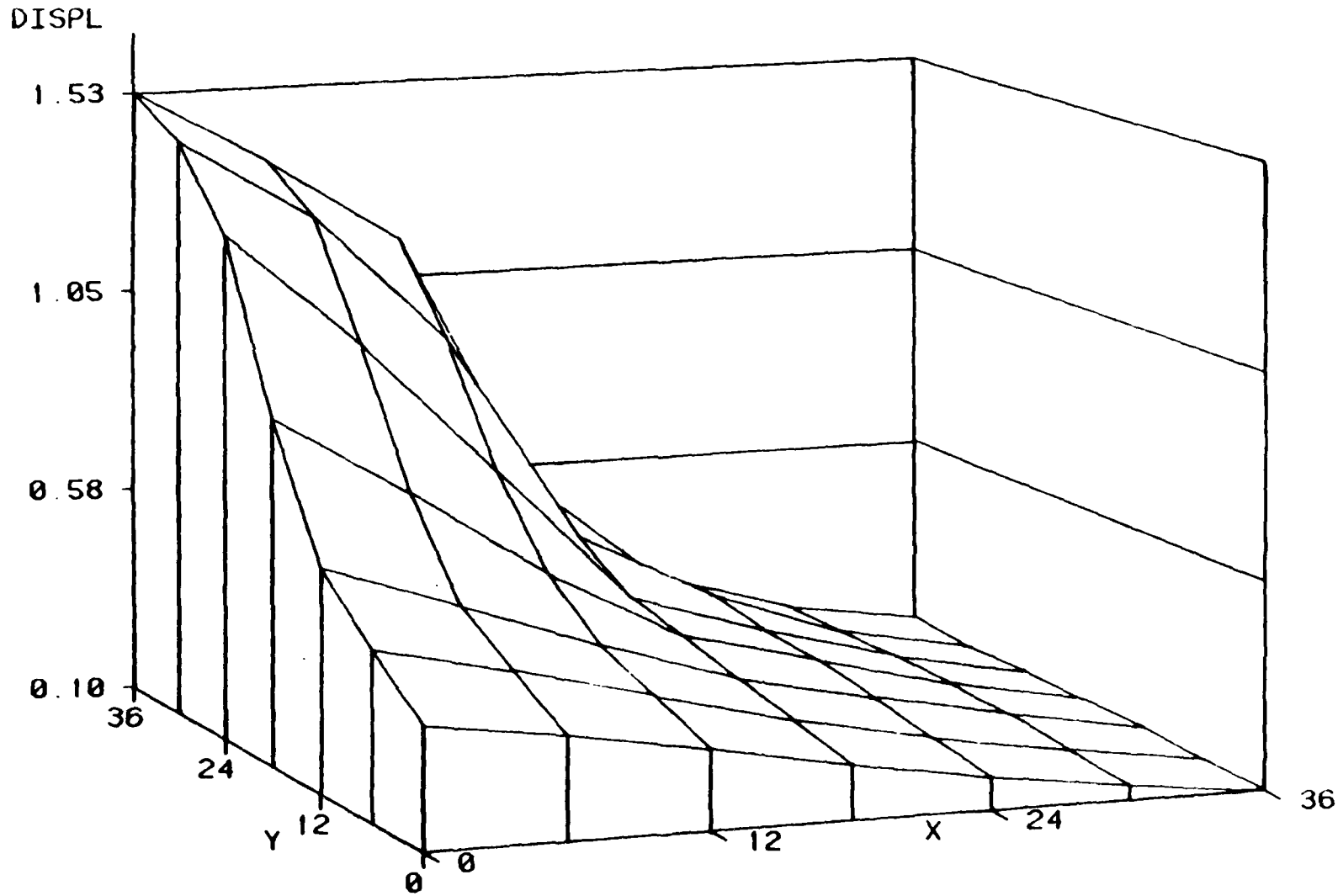

Figure 4.50 Vertical Displacement Distribution for the Large Mesh

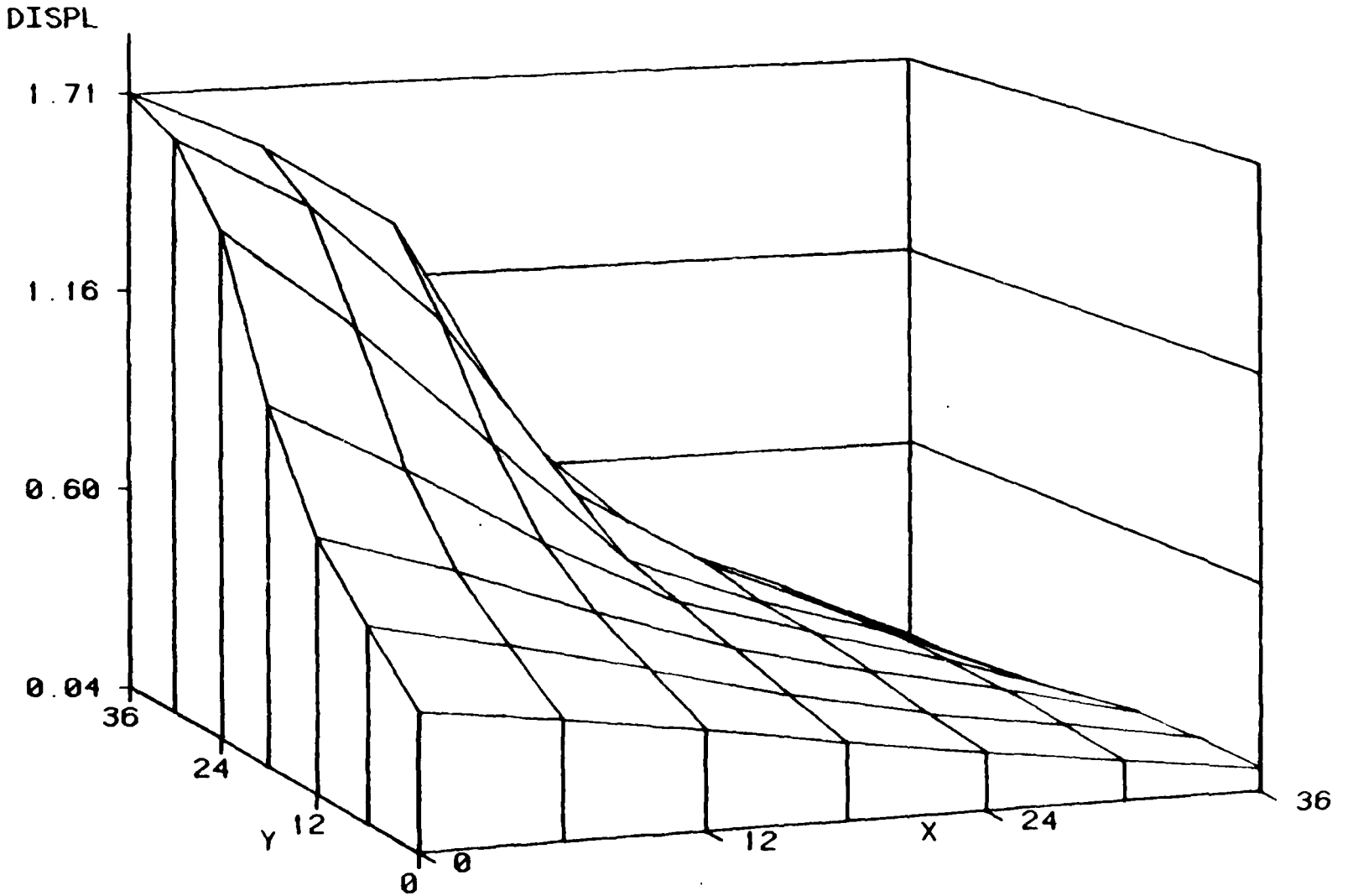

Figure 4.51 Vertical Displacement Distribution for the Small Mesh with a Nonreflecting Boundary

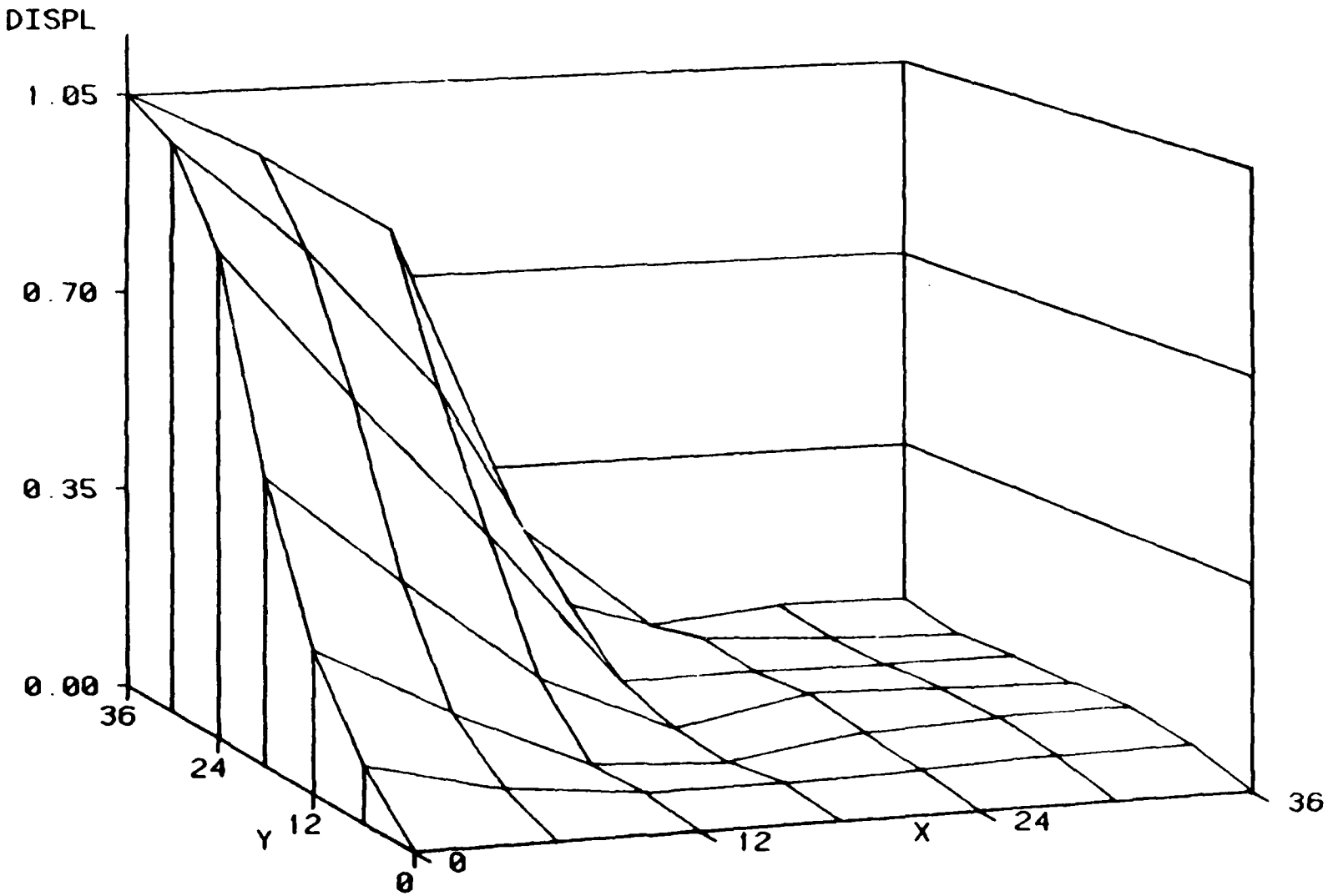

Figure 4.52 Vertical Displacement Distribution for the Small Mesh without a Nonreflecting Boundary

stress versus time graphs are not as erratic as the corresponding graphs involving Yuma soil. The vertical displacement distribution of the upper left section of the large mesh is shown in Figure 4.50. The vertical displacement distribution of the small mesh with the nonreflecting boundary is shown in Figure 4.51. The surfaces of these two plots are reasonably close to one another. This discrepancy is negligible upon observation of the vertical displacement distribution of the small mesh without the nonreflecting boundary illustrated in Figure 4.52.

All of the previous tests used loads with a peak pressure of 50 ksi. The magnitude of this peak pressure caused large inelastic deformations to occur in the meshes. The next test employed the same form of the Brode Airblast curve but with a lower peak pressure of 50 psi. For fiber-reinforced concrete, the first loading segment corresponds to the unloading segment in the hydrostatic pressure versus volumetric strain curve. At low levels of stress, the concrete mesh will remain elastic. The first loading segment for Yuma soil, however, is much different than the unloading segment. At low levels of stress, the soil will still exhibit inelastic behavior. The graphical results of the solutions involving Yuma soil at small magnitude of loading were extremely noisy. It was difficult to distinguish between the three solutions. Therefore, only the test involving concrete is included in this report for low peak pressure loadings. The displacement, normal stress, and shear stress versus time for the selected field variables were analyzed. The graphical results are presented in Figures 4.53 - 4.55. Once again, the large mesh solutions were very similar to the nonreflecting boundary solutions. The displacement versus time graph shows more variance between the three solutions while a less significant difference can be seen in the normal stress and shear stress versus

time graphs. The vertical displacement distributions of the meshes were not plotted due to the similarity to the previous test. This test is indicative of the ability of the nonreflecting boundary to absorb stress waves of varying strengths.

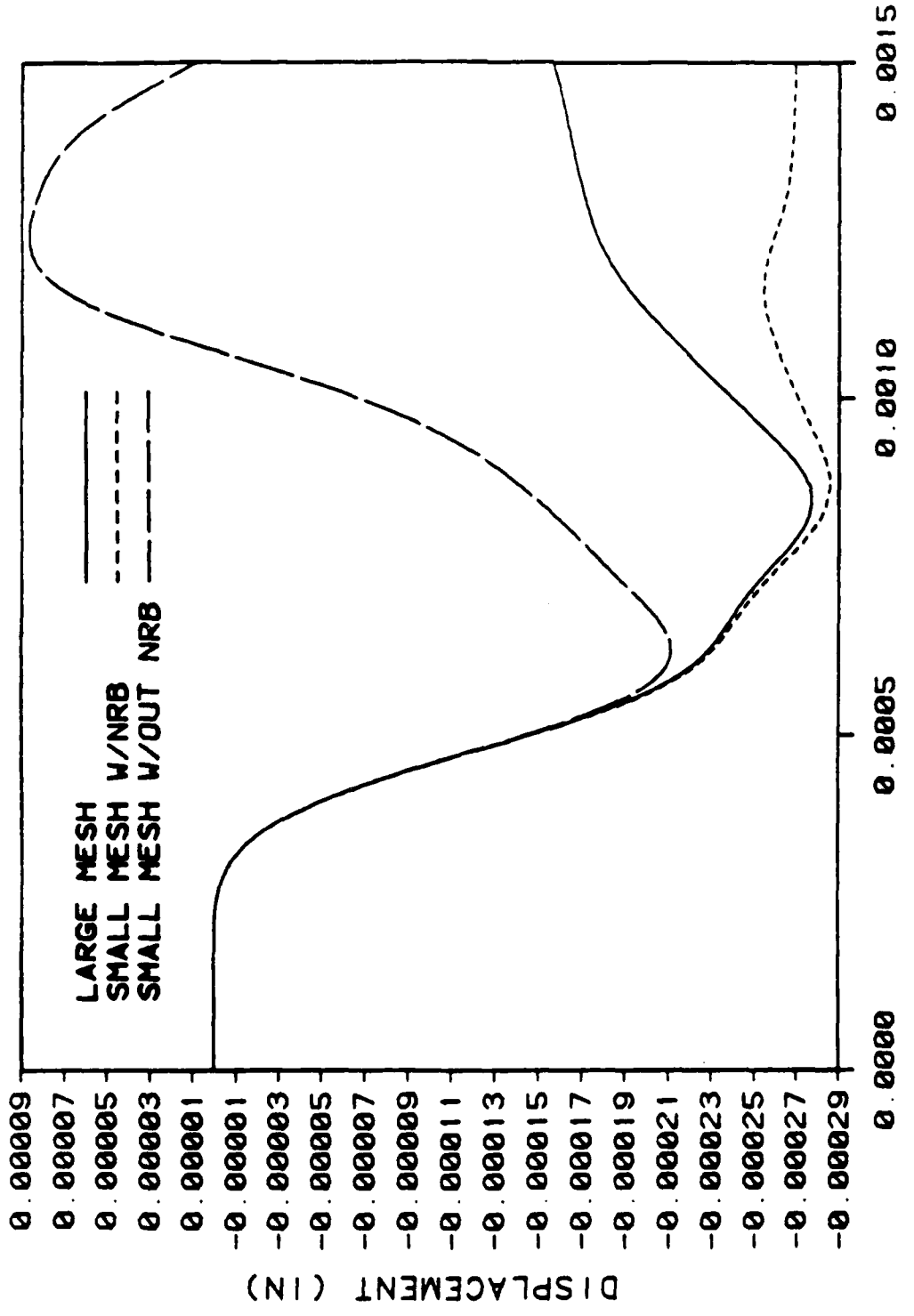

Figure 4.53 Vertical Displacement vs. Time Lower Peak Pressure

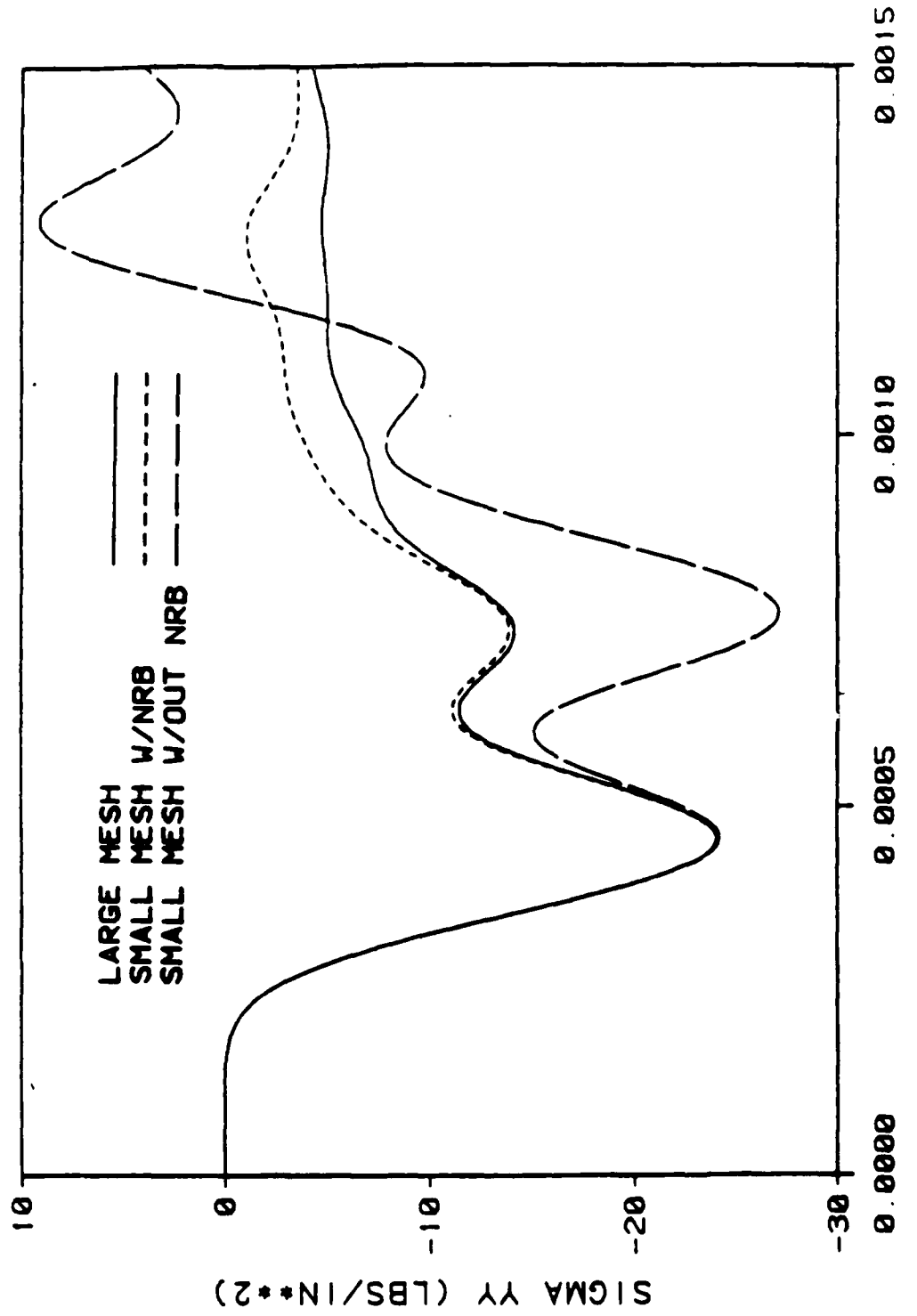

Figure 4.54 Normal Stress, σ_{yy} vs. Time Lower Peak Pressure

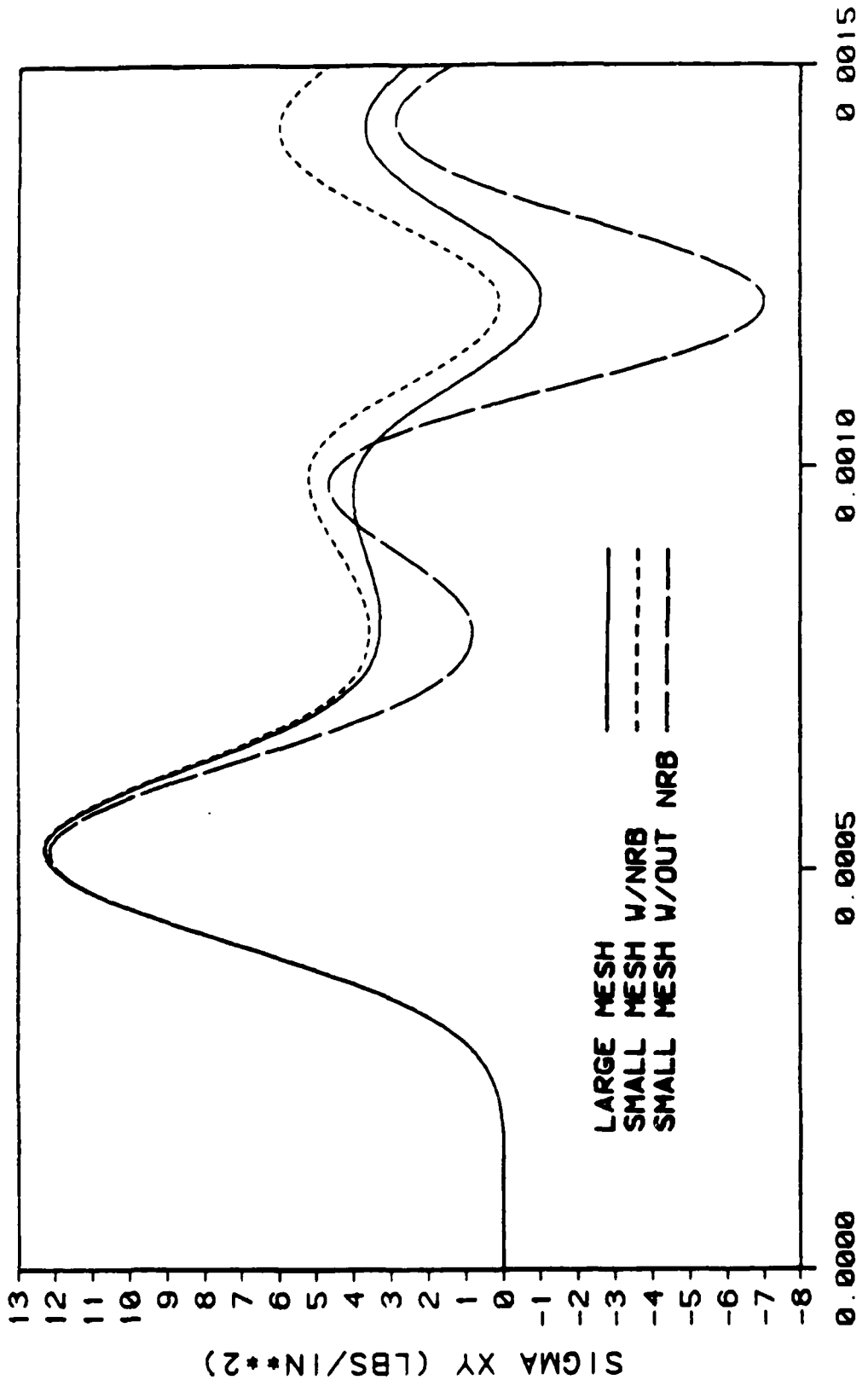

Figure 4.55 Shear Stress, σ_{xy} vs. Time Lower Peak Pressure

Chapter 5

CONCLUSIONS AND RECOMMENDATIONS

The nonreflecting boundary that has been implemented into the SAMSON2 code has proven to be very effective in the absorption of dilatational stress waves and shear stress waves under a wide range of applications. There are, however, certain limitations on the use of the nonreflecting boundary. Some of these limitations have not been fully tested and should require further analyses. There are many conclusions that can be obtained from the results of the several tests conducted in this study. Recommendations, in addition to conclusions, are presented in order to provide instruction on the proper and most efficient use of the nonreflecting boundary.

The objective of a nonreflecting boundary is to minimize the computational and storage costs for the computer and the time required by the user to prepare an input file. Because the boundary is treated as a load line, the additional computation time and storage for the input instructions for the boundary are about the same as if another load line were applied to the system. Also, the input instructions for the boundary are easily understood by users familiar with the SAMSON2 code and the format of the load line data card. The introduction of the nonreflecting boundary into the SAMSON2 code required relatively few executable statements. The additional execution time for the nonreflecting boundary is a result of the modified formulation within the subroutine READPV. The triple DO loop that retrieves the element numbers along the nonreflecting boundary involves the majority of the additional CPU time. The extra storage requirements for the nonreflecting boundary are minimal. For a

given number of nodes, N, on a nonreflecting boundary, the number of extra variables stored (the size of the array BIMP) in the program would be 2(N - 1).

For all of the tests conducted in this study, the use of the nonreflecting boundary has required a negligible increase in the CPU time. Comparing the solution time for a small mesh with a nonreflecting boundary and the solution time for a small mesh with fixed/free boundaries, the increase in CPU time was less than 3%. Sometimes the nonreflecting boundary solution actually required less time than the solution with the fixed/free boundary. A time comparison between the nonreflecting boundary solution and the large mesh solution would be inapplicable. The solution time is roughly proportional to the number of nodes in a mesh. For example, if the number of nodes in the large mesh can be reduced to half the number using a nonreflecting boundary, the solution time will also be reduced by one-half. The savings in the CPU time would depend solely upon the original dimensions of the large mesh. In other words, the larger the original mesh, the greater the savings in solution time using a small mesh with a nonreflecting boundary.

The stability of the solutions was not adversely affected in all of the wave propagation tests. However, the maximum allowable time step that could be used in the tests was not determined. Thus, the nonreflecting boundary can be deduced not to affect the stability limit of a problem to an appreciable extent, if at all. The same time step for a large mesh can be used for a small mesh with a nonreflecting boundary.

This study has shown that the nonreflecting boundary almost perfectly absorbs stress waves that impinge normal to the boundary. The effectiveness of the nonreflecting boundary does, in fact, decrease with an increase in the angle of incidence of the

stress wave. Therefore, for a problem involving two-dimensional wave propagation, the mesh should be designed such that the nonreflecting boundary is oriented normal, if possible, to the wave source.

Axisymmetric problems can be difficult to model for a nonreflecting boundary that is parallel to the axis of symmetry. For the one-dimensional wave propagation tests employing an axisymmetric bar, satisfactory results were obtained when the nonreflecting boundary parallel to the axis of symmetry was placed at a distance corresponding to an R/λ value greater than 2.0. In a two-dimensional axisymmetrical problem, the wavelengths of the radiating stress waves cannot be calculated accurately, especially in an inelastic medium. Accordingly, the value of R/λ cannot be determined. Thus, the minimum distance, or radius, the nonreflecting boundary can be from the axis of symmetry is unknown for the two-dimensional case.

Material properties that were analyzed in the one-dimensional wave propagation tests included the effect of Poisson's ratio and an anisotropic medium on the effectiveness of the nonreflecting boundary. It was concluded that the effectiveness of the nonreflecting boundary significantly decreases as Poisson's ratio nears its maximum value of 0.5. The nonreflecting boundary performs very well for values of Poisson's ratio between 0 and 0.4. The nonreflecting boundary is also very effective for a simple problem involving an anisotropic medium. However, the ability of the boundary to absorb stress waves in a two-dimensional anisotropic medium is still undetermined due to the complexity of the problem.

The material laws used in this study were material law 6, a perfectly elastic medium, and material law 9, the AFWL "engineering" model. The remaining material

laws were not included in the study. The biaxial elastic-plastic material laws, applicable only for the continuum elements, are similar to the perfectly elastic material law at low values of stress. The inelastic portion of the elastic-plastic material law will be similar to a multi-segmented AFWL "engineering" law at higher levels of stress. The endochronic, viscoplastic, and the Weidlinger Associate's cap material law, which presently exist in the code, are not recommended or verified. Further testing of the nonreflecting boundary should be conducted including these unverified material laws.

The two-dimensional wave propagation tests were performed using the AFWL "engineering" model, exclusively. The large magnitude of stress applied to the system resulted in a very nonlinear response. The dilatational impedence and shear impedence for the tests corresponded to the first loading segment, or the "elastic" section, of the hydrostatic pressure versus volumetric strain curve for the material. The use of the elastic dilatational impedence and elastic shear impedence for the nonreflecting boundary gave the best overall results. The values of the impedences are directly related to the stress wave speed in the material. If better approximations for the stress wave speeds in a problem can be determined, the impedences can be adjusted accordingly by changing the values of Young's modulus and Poisson's ratio. Although not examined in this study, this adjustment should increase the effectiveness of the nonreflecting boundary.

The nonreflecting boundary is only applicable for problems involving continuum elements along a boundary. The interior of the mesh, however, can consist of any type of element. Of all the continuum elements in the SAMSON2 finite element library,

the 4NQ works best with the nonreflecting boundary. This was evident in the one-dimensional wave propagation tests. The results from the one-dimensional tests using the 5NT and 6NT, although not contained in the report, were the least accurate of the continuum elements.

The nonreflecting boundary cannot be used in a static or quasi-static problem. This implies that the use of the dynamic relaxation feature of SAMSON2 is prohibited. When utilizing the nonreflecting boundary, the value of the low-frequency mass proportional damping parameter should be zero.

The nonreflecting boundary should not be placed adjacent to a load line. The nonreflecting boundary is only capable of absorbing impinging stress waves and not the direct stress resulting from the direct application of load.

The lone application of Rayleigh waves, without the presence of dilatational waves and shear waves, has not been included in this study. There are two reasons for this exclusion. First, the displacement time history that describes a Rayleigh wave solution is cumbersome to discretize for a SAMSON2 input file. Second, and most importantly, is that for the two-dimensional wave propagation tests, Rayleigh waves were also generated during the analyses in addition to the two body waves. The displacement and stress distribution in the mesh will be affected, in part, by the propagation of these Rayleigh waves. If the nonreflecting boundary solution compares well to the large mesh solution, the nonreflecting boundary can be assumed to be capable of also absorbing Rayleigh waves.

Fulfilling the second objective of the research, the possible errors that exist in the SAMSON2 code have been found. The anomalies discovered in the SAMSON2

code and SAMSON2 User's Manual by the authors are located in Appendix B along with recommended corrections.

The following list provides a summary of the recommendations on the use of the nonreflecting boundary presented in this chapter.

1. The nonreflecting boundary should be oriented normal to the wave source if possible.

2. The nonreflecting boundary parallel to the axis of symmetry should be located such that the distance from the boundary to the axis corresponds to an R/λ ratio greater than 2.0 if the wavelength of the stress wave can be approximated.

3. When the AFWL "engineering" material model is employed with a multi-segmented loading curve, the Young's modulus and Poisson's ratio should correspond to the first loading segment if a typical wave speed for the problem cannot be accurately determined.

4. Use of the 4NQ continuum element yields the best results for the nonreflecting boundary.

5. The nonreflecting boundary is not applicable for a static problem (i.e., the use of dynamic relaxation is not allowed).

6. The nonreflecting boundary should not be placed adjacent to a load line.

LIST OF REFERENCES

[1] Rudeen, D.K., Personal communication with regard to the slideline formulation.

[2] Lysmer, J. and Kuhlemeyer, R.L., Finite Dynamic Model for Infinite Media, *Journal of the Engineering Mechanics Division*, ASCE, **pp 859-877**, August, 1969.

[3] Vaughan, D.K., Using the FLEX Code, Weidlinger Associates, Palo Alto, California, March 1985.

[4] Vaughan, D.K., FLEX Briefing, Weidlinger Associates, Palo Alto, California, March 1986.

[5] Cohen, M. and Jennings, P.C., Silent Boundary Methods for Transient Analysis, *Computational Methods for Transient Analysis, Volume 1*, Belytschko, T. and Hughes, T.J.R., eds., Elsevier Science Publishers B.V., Amsterdam, Netherlands, 1983.

[6] White, W., Valliappan, S., and Lee, I.K., Unified Boundary for Finite Dynamic Models, *Journal of the Engineering Mechanics Division*, ASCE, **pp 949-964**, October 1977.

[7] Lysmer, J. and Waas, G., Shear Waves in Plane Infinite Structures, *Journal of the Engineering Mechanics Division*, ASCE, **pp 85-105**, February, 1972.

[8] Smith, W.D., A Nonreflecting Plane Boundary for Wave Propagation Problems, *Journal of Computational Physics*, Volume 15, **pp 492-503**, 1974.

[9] Cundall, P.A., Kunar, R.R., Carpenter, P.C., and Marti, J., Solution of Infinite Dynamic Problems by Finite Modelling in the Time Domain, *Proceedings of the 2nd International Conference on Applied Numerical Modelling*, Madrid, Spain, 1978

[10] Kunar, R.R. and Rodriguez-Ovejero, L., A Model with Nonreflecting Boundaries for the Use in Explicit Soil-Structure Interaction Analyses, *Earthquake Engineering and Structural Dynamics, Volume 8*, **pp 361-374**, 1980.

[11] Robinson, A.R., The Transmitting Boundary-Again, *Structural and Geotechnical Mechanics*, Hall, W.J., ed., Prentice-Hall, Englewood Cliffs, New Jersey, **pp 163-177**, 1977.

[12] Schreyer, H.L., Richards, C.G., Bean, J.E., and Durka, G.R., SAMSON2, A Nonlinear Two-Dimensional Structure-Media Computer Code: User's Manual

AFWL-TN-82-18, Air Force Weapons Lab, Kirtland Air Force Base, New Mexico, June 1984.

BIBLIOGRAPHY

Belytschko, T. and Robinson, R.R., SAMSON2: A Nonlinear Two-Dimensional Structure/Media Interaction Computer Code, AFWL-TR-81-109, Air Force Weapons Laboratory, Kirtland Air Force Base, New Mexico, January 1982.

Belytschko, T., Chiapetta, R.L., and Bartel, H.D., Efficient Large Scale Nonlinear Transient Analysis by Finite Elements, *International Journal for Numerical Methods in Engineering*, Volume 10, pp. 579-596, 1976.

Clough, R.W. and Penzien, J., *Dynamics of Structures*, Mcgraw-Hill, New York, 1975.

Miller, S.S., Investigation of the Higher-Order Elements in the SAMSON2 Code, M.S. Thesis, submitted to Washington State University, Pullman, Washington, August 1986.

Roesset, J.M. and Ettouney, M.M., Transmitting Boundaries: A Comparison, *International Journal for Numerical and Analytical Methods in Geomechanics*, Volume 1, pp 151-176, 1977.

Rudeen, D.K., Rath, J.S., SAMSON2, A Nonlinear Two-Dimensional Structure-Media Interaction Computer Code: User's Manual (Revised), WA11-4, New Mexico Engineering Research Institute, University of New Mexico, Albuquerque, New Mexico, September, 1986.

Satterthwaite, B., Personal communication with regard to the slideline and AFWL engineering material law formulations.

Telford, W.M., Geldart, L.P., Sheriff, R.E., and Keys, D.A., *Applied Geophysics*, Cambridge University Press, Cambridge, England, 1976.

Appendix A
REVISED LOAD LINE CONTROL DATA CARD *

CARD 10A — LOAD LINE CONTROL — READPV

FORMAT(7I5,5X,**E10.3**)

Columns	Variable	Description
1-5	I	Load line number
6-10	NDNOD	Number of nodes on load line
11-15	IVOL(1)	= -2, pressure line for axisymmetric problems = -1, pressure line for plane problems = 0, initial velocity line = 1, force line = 2, displacement history line **= 3, axisymmetric nonreflecting boundary** **= 4, plane nonreflecting boundary**
16-20	IVOL(2)	Used only when *IVOL(1) = 0* = 0, initial velocities are normal and tangent to the load line = 1, initial velocities are in the global x- and y-components
21-25	IVOL(3)	Force or displacement component code. Used only when IVOL(1) = 1 or 2 = 1, x-component is specified = 2, y-component is specified
26-30	INT1	Node generation increment
31-35	NPT	Number of points used to define the piecewise linear pressure, force, or displacement history. Not used if IVOL(1) = 0, **3, or 4**
36-40		Blank
41-50	Thick	Thickness for planar problem pressure

* modifications are printed in bold type

Appendix B

ANOMALIES IN THE SAMSON2 CODE AND USER'S MANUAL

The latest version of the SAMSON2 code was received by the authors late in the period of the research. All of the errors that were discovered in the outdated SAMSON2 code - which was used primarily in the research - were inapplicable upon receiving the new version of the code. The only anomaly that was found in the latest version of the code is located in subroutine READMA. The last executable line in the subroutine before the RETURN statement computes the value of LADD. The last term in the line subtracts one from the sum of INDXE(NUMMAT) plus LE2 plus LADD2. To be precise, two should be subtracted from the sum instead of one. However, the only advantage to this correction is a negligible savings in the storage requirement for the program. The correction is simply cosmetic.

There were typographic mistakes in the input instructions section of the revised SAMSON2 User's Manual [13]. Several card format statements in the User's Manual either do not correlate with the card column specifications or do not match the format statements in the SAMSON2 code. Some of these anomalies in the format statements are purely academic; they do not affect the column specifications at all or are simply a variation in the type of variable (Ex. F10.0 in the code might be listed as F10.3 in the User's Manual). Those anomalies that do affect the column specifications should be corrected in the next revision of the SAMSON2 User's Manual and are discussed in this appendix.

The first anomaly is on card 4 which contains the program control data. The last variable, IPPLF, is not read in the execution of the code. The reason is unknown to the authors. The column specification for the alphanumeric title in card 9B, "motion control output", should be 16-31 instead of 11-23. Likewise for card 9C, "element variable output", the column specification for the title should be 16-31 instead of 16-32. The most significant error found in the User's Manual was found on card 9D, "picture output request". The format statement should read 2I5 instead of 2I10. Also, the column specifications for the variables NTSTEP and K should be 1-5 and 6-10, respectively.

The input cards that do not have errors in their format statements are the following: card 1, "title"; card 3, "master control data"; card 4, "program control data"; card 5C, "material law parameter data"; card 8, "nodal boundary condition data"; card 9B, "motion component output"; card 9C, "element variable output"; card 9F, "node point output"; card 9G, "element output"; card 10B-1, "load line history"; card 10C, "load line nodes"; and all of the slideline cards. The correct format statements for the cards not mentioned above can be found in the latest version of the SAMSON2 code used in this study.

Appendix C

MODIFIED SUBROUTINES IN THE SAMSON2 CODE

The subroutines that have been modified by the authors are listed in this appendix. The following FORTRAN listings have been changed from the AFWL's HP9000 to be compatible to the IBM 3090 computer. The only differences occur in the initial lines at the beginning of each subroutine. The common block, character, equivalence and dimension statements in the IBM 3090 version are substituted for the include statements in the HP9000 version of the code. The modified executable lines are printed in bold type.

```
      SUBROUTINE FREEF2 (XC,YC,X1,V,FORCD,STRS,INDXS,IP,NPT,NDNOD,
     1                   IVOL,KPRES,PT,THICK, BIMP)
C-----------------------------------------------------------------
C
C     CALCULATES VELOCITY AND PRESSURE BOUNDARY CONDITIONS
C
C-----------------------------------------------------------------
      COMMON/DYNAM/ DELT,TIME,MXSTEP,NTSTEP,NTSTP1,OMEGA,WMAX,CWAVE,
     +           CBULK,CSHEAR,C1DAMP,TIMEMX,DTMIN,DTMAX,MXSUB,POISR
      COMMON/RTIME/ DATE, RUNTIM, CREATR, VRSION
      CHARACTER*8  DATE, RUNTIM, CREATR, VRSION
C
      COMMON/NUM/ NUMNP,NUMEL,NUMMAT,NUMDIS,NDGREE,NPRES,NSLID,MEQ,
     *          DELTMX,LE2,NPLOT
      COMMON/KNTRL/ISYMF,MITSF,IUN5F IT11F,IMSHF,IHISF,
     +           IQARF,IRSTF
      DIMENSION KONTRL(10)
      EQUIVALENCE (KONTRL(1),ISYMF)
C
      DIMENSION    XC(1), YC(1), X1(1), V(1), FORCD(1),STRS(1),
     1           INDXS(1), IVOL(5), KPRES(1), PT(1),  BIMP(1)
C
      IF(IVOL(1) .EQ. 0)  RETURN
      NDN = NDNOD-1
      TOTFX = 0.0
      TOTFY = 0.0
      DVOL  = 0.0
C
C**** COMPUTE NODAL FORCES FOR PRESSURE LOADINGS ****
C**** GET OLD VOLUME FOR PRESSURE LINE OR OLD TOTAL DISPLACEMENT ****
C**** GET OLD PRESSURE OR FORCE ****
C**** GET OLD EXTERNAL WORK ****
C**** GET OLD IMPULSE ****
C
      K = INDXS(NUMEL+2)+IP-1
      VOLD = STRS(K)
C
      L = INDXS(NUMEL+3)+IP-1
      POLD = STRS(L)
C
      M = INDXS(NUMEL+5)+IP-1
      WEXT = STRS(M)
C
      MM = INDXS(NUMEL+4)+IP-1
      WIM = STRS(MM)
C
C**** PRESSURE,FORCE, DISPLACEMENT HISTORY
      CALL PRESS(  NPT,   PT,    P,  TIME)
      IF (IVOL(1) .EQ. 1) THEN
C-----------------------------------------------------------------
C****    NODAL FORCE LOADING ****
```

```
C-------------------------------------------------
      J = IVOL(3)
C
      DO 510 I1 = 1,NDNOD
        IN1 = KPRES(I1)
        IN2 = IN1*2-2+J
        FORCD(IN2) = FORCD(IN2)+P
C
C****     COMPUTE TOTAL FORCE * DELT X ****
        TOTFX = TOTFX+V(IN2)
 510   CONTINUE
C
C****   STORE NEW FORCE,IMPULSE, TOTAL WORK IN STRS ARRAY
C
      STRS(L)  = P
      STRS(MM) = WIM+(P+POLD)*NDNOD*.5*DELT
      STRS(M)  = WEXT+(P+POLD)*.5*TOTFX*DELT
C
    ELSEIF (IVOL(1) .EQ. 2) THEN
C-------------------------------------------------
C****   DISPLACEMENT TIME GIVEN ****
C****     COMPUTE VELOCITY ****
C-------------------------------------------------
      J = IVOL(3)
      DO 610 I1 = 1,NDNOD
        IN1 = KPRES(I1)
        IN2 = IN1*2-2+J
        V(IN2)  = (P-X1(IN2))/DELT
        X1(IN2) = P
 610   CONTINUE
C
    ELSEIF ((IVOL(1) .EQ. -1) .OR. (IVOL(1) .EQ. -2)) THEN
C-------------------------------------------------
C**** PRESSURE LINE
C-------------------------------------------------
      DO 100 I1 = 1,NDN
C
C**** FIND NEXT TWO NODES NO LOAD LINE ****
        IN1 = KPRES(I1)
        IN2 = KPRES(I1+1)
        XC1 = XC(IN1)+X1(2*IN1-1)
        XC2 = XC(IN2)+X1(2*IN2-1)
        YC1 = YC(IN1)+X1(2*IN1)
        YC2 = YC(IN2)+X1(2*IN2)
        SS  = XC1-XC2
        CC  = YC2-YC1
C
C**** COMPUTE CHANGE IN VOLUME ****
        PP = (YC(IN2)-YC(IN1))*(X1(2*IN1-1)+X1(2*IN2-1))
   1       -(XC(IN2)-XC(IN1))*(X1(2*IN1)+X1(2*IN2))
   2       +X1(2*IN1-1)*X1(2*IN2)-X1(2*IN1)*X1(2*IN2-1)
        FX = 0.5*CC*P*THICK
```

```
        FY = 0.5*SS*P*THICK
        IF (IVOL(1) .NE. -1) THEN
C
C**** AXISYMMETRIC LOADING ****
          CC = 0.5*(XC1+XC2)
          PP = PP*CC
          FX = FX*CC
          FY = FY*CC
        ENDIF
        DVOL = DVOL+0.5*PP
C
C**** STORE EXTERNAL FORCE ****
        TOTFX = TOTFX+FX
        TOTFY = TOTFY+FY
        FORCD(2*IN1-1) = FORCD(2*IN1-1)+FX
        FORCD(2*IN2-1) = FORCD(2*IN2-1)+FX
        FORCD(2*IN1)   = FORCD(2*IN1)+FY
        FORCD(2*IN2)   = FORCD(2*IN2)+FY
 100    CONTINUE
C
C**** STORING VOLUME CHANGE,WORKDONE BY PRESSURE, PRESSURE, IMPULSE
C**** IN STRS
C
      STRS(K) = DVOL
      STRS(M) = WEXT+0.5*(POLD+P)*(DVOL-VOLD)
      STRS(L) = P
      IF (P .NE. 0.0) THEN
        TOTFX = SQRT(TOTFX*TOTFX+TOTFY*TOTFY)*DELT*(1.0+POLD/P)*.5
C
C****     LAST TERM IS AN APPROXIMATION TO F+FOLD ****
        STRS(MM) = WIM + TOTFX
      ENDIF
C
    ELSE
C-------------------------------------------------
C**** NONREFLECTING BOUNDARY
C-------------------------------------------------
      DO 200 I1 = 1,NDN
C
C**** FIND NEXT TWO NODES NO LOAD LINE ****
        IN1 = KPRES(I1)
        IN2 = KPRES(I1+1)
        XC1 = XC(IN1)+X1(2*IN1-1)
        XC2 = XC(IN2)+X1(2*IN2-1)
        YC1 = YC(IN1)+X1(2*IN1)
        YC2 = YC(IN2)+X1(2*IN2)
        SS  = XC2-XC1
        CC  = YC2-YC1
C
        REFP=BIMP(NDNOD+2*I1-1)
        REFV=BIMP(NDNOD+2*I1)
C
```

```
C**** COMPUTE CHANGE IN VOLUME ****
        PP = (YC(IN2)-YC(IN1))*(X1(2*IN1-1)+X1(2*IN2-1))
     1       -(XC(IN2)-XC(IN1))*(X1(2*IN1)+X1(2*IN2))
     2       +X1(2*IN1-1)*X1(2*IN2)-X1(2*IN1)*X1(2*IN2-1)
C
        V1X=V(2*IN1-1)
        V1Y=V(2*IN1)
        V2X=V(2*IN2-1)
        V2Y=V(2*IN2)
C
        FX1=-(2./6.*V1X +1./6.*V2X)*(CC*REFP +SS*REFV)*THICK
        FX2=-(1./6.*V1X +2./6.*V2X)*(CC*REFP +SS*REFV)*THICK
        FY1=-(2./6.*V1Y +1./6.*V2Y)*(SS*REFP +CC*REFV)*THICK
        FY2=-(1./6.*V1Y +2./6.*V2Y)*(SS*REFP +CC*REFV)*THICK
        IF (IVOL(1) .EQ. 3) THEN
C
C**** AXISYMMETRIC LOADING ****
          CC = 0.5*(XC1+XC2)
          PP = PP*CC
          FX1 = FX1*CC
          FY1 = FY1*CC
          FX2 = FX2*CC
          FY2 = FY2*CC
        ENDIF
        DVOL = DVOL+0.5*PP
C
C**** STORE EXTERNAL FORCE ****
        TOTFX = TOTFX+FX1+FX2
        TOTFY = TOTFY+FY1+FY2
        FORCD(2*IN1-1) = FORCD(2*IN1-1)+FX1
        FORCD(2*IN2-1) = FORCD(2*IN2-1)+FX2
        FORCD(2*IN1)   = FORCD(2*IN1)+FY1
        FORCD(2*IN2)   = FORCD(2*IN2)+FY2
C
        WEXT = WEXT + ABS(FX1*X1(2*IN1-1))
        WEXT = WEXT + ABS(FX2*X1(2*IN1))
        WEXT = WEXT + ABS(FY1*X1(2*IN2-1))
        WEXT = WEXT + ABS(FY2*X1(2*IN2))
C
 200    CONTINUE
C
C**** STORING VOLUME CHANGE,WORKDONE BY PRESSURE, PRESSURE, IMPULSE
C**** IN STRS
C
      STRS(K) = DVOL
      STRS(M) = WEXT
      TOTFX = SQRT(TOTFX*TOTFX+TOTFY*TOTFY)*DEL T
C
C****     LAST TERM IS AN APPROXIMATION TO F+FOLD ****
        STRS(MM) = WIM + TOTFX
C
    ENDIF
```

```
      RETURN
      END
```

```
      SUBROUTINE FREEFD (   XC,    YC,    X1,     V, FORCD,
     1                   STRS, INDXS,    IP,   NPT, NDNOD,
     2                   IVOL, KPRES,    PT, THICK,  BIMP)
C-------------------------------------------------------
C
C**** THIS ROUTINE WILL COMPUTE THE LOADING CONDITIONS AS A FUNCTION****
C**** OF TIME.  INITIAL CONDITIONS ARE COMPUTED IF FREEFD IS CALLED ****
C**** PRESSURE LOADINGS ARE COMPUTED IF FREEF2 IS CALLED.
C****                                                  ****
C     1. COMPUTES NODAL FORCES FOR A GIVEN PRESSURE LINE WITH
C        PIECEWISE LINEAR PRESSURE TIME HISTORY
C     2. COMPUTES NODAL FORCES THAT ARE DIRECTLY SPECIFIED WITH
C        PIECEWISE LINEAR TIME HISTORY
C     3. SETS NONZERO INITIAL VELOCITIES FOR IMPULSE LOADING
C        NORMAL TO LOAD LINE OR IN GLOBAL X,Y DIRECTIONS
C     4. COMPUTES NONZERO PRESCRIBED DISPLACEMENTS FROM PIECEWISE
C        LINEAR INPUT
C
C     XC,YC = GLOBAL (ORIGINAL) X,Y COORDINATE ARRAYS
C     BIMP  = BOUNDARY IMPEDENCE ARRAY
C     X1    = NODAL DISPLACEMENT ARRAY
C     V     = NODAL VELOCITY ARRAY
C     FORCD = GLOBAL EXTERNAL FORCE ARRAY , F-EXT
C     STRS  = ELEM.STORAGE ARRAY
C     INDXS = LOCATOR FOR STRS
C     IP    = LOAD LINE NO.
C     NPT   = NO.OF PTS.FOR PIECEWISE LINEAR DESCRIPTION OF FORCES
C           OR DISPLACEMENTS ON LOAD LINE
C     NDNOD = NO.OF NODES ON LOAD LINE
C     PT    = VALUES OF FUNCTION AND TIME AT NPT POINTS
C     IVOL  = CONTROL FOR LOAD LINE ** REFER TO READPV
C     KPRES = NODES DEFINING THE LOAD LINE
C
C****   NUMDIS   NUMBER OF NODES WITH DISPLACEMENT  PRESSURE
C****            PRESCRIBED
C****   NNODE    NUMBER OF NODES IN PROBLEM
C****   XC(N)    X COORDINATE OF NODE NUMBER N
C****   YC(N)    Y COORDINATE OF NODE NUMBER N
C****   NDNOD    NUMBER OF NODES ON LOAD LINE
C****   IVOL(1) = -1PRESSURE TIME INPUT AXISYMMETRIC
C****   IVOL(1) = 0 PRESSURE TIME INPUT PLANE
C****   IVOL(1) = 1 INITIAL VELOCITY INPUT
C****   IVOL(2) = 0 LOAD APPLIED NORMAL AND TANGENT TO LOAD LINE
C****   IVOL(2) = 1 LOAD APPLIED IN GLOBAL X AND Y DIRECTIONS
C****   IVOL(3)  USED FOR FORCE LOADING
C****           = 0 FORCE IS APPLIED IN GLOBAL X DIRECTION
C****           = 1 FORCE IS APPLIED IN GLOBAL Y DIRECTION
C****   STRS     ELEMENT STRESS ARRAY
C****   INDXS    INDEX TO ELEMENT STRESS ARRAY (STRS)
C-------------------------------------------------------
C
```

```
      COMMON/DYNAM/ DELT,TIME,MXSTEP,NTSTEP,NTSTP1,OMEGA,WMAX,CWAVE,
     +           CBULK,CSHEAR,C1DAMP,TIMEMX,DTMIN,DTMAX,MXSUB,POISR
      COMMON/RTIME/ DATE, RUNTIM, CREATR, VRSION
      CHARACTER*8  DATE, RUNTIM, CREATR, VRSION
C
      COMMON/NUM/ NUMNP,NUMEL,NUMMAT,NUMDIS,NDGREE,NPRES,NSLID,MEQ,
     *          DELTMX,LE2,NPLOT
      COMMON/KNTRL/ISYMF,MITSF,IUN5F,IT11F,IMSHF,IHISF,
     +           IQARF,IRSTF
      DIMENSION KONTRL(10)
      EQUIVALENCE (KONTRL(1),ISYMF)
C
      DIMENSION   XC(1), YC(1), X1(1), V(1), FORCD(1), STRS(1),
     1           INDXS(1), IVOL(5), KPRES(1), PT(1),  BIMP(1)
C
C**** CONTOL FOR INITIAL VALUE INPUT ****
      IF (IVOL(1) .EQ. 0) THEN
C
C****   INITIAL VELOCITY INPUT ****
        IF(IVOL(2) .EQ. 1) THEN
C
C**** GLOBAL VELOCITY LOADING ****
          DO 176 I1 = 1,NDNOD
            IN1 = KPRES(I1)
            IN2 = IN1*2
            V(IN2-1) = V(IN2-1)+PT(1)
            V(IN2)   = V(IN2)+PT(2)
 176      CONTINUE
C
        ELSE
          NDN = NDNOD-1
          DO 190 I1 = 1,NDN
C
C**** FIND CONSECUTIVE  NODES ON LOAD LINE ****
            IN1 = KPRES(I1)
            IN2 = KPRES(I1+1)
            CC  = XC(IN2)-XC(IN1)
            SS  = YC(IN2)-YC(IN1)
            AL  = SQRT(SS*SS+CC*CC)
            CC  = CC/AL
            SS  = SS/AL
C
C**** APPLY HALF VELOCITY AT EACH NODE ****
            VT = 0.5*PT(1)
            VN = 0.5*PT(2)
            VX = VT*CC+VN*SS
            VY = VT*SS-VN*CC
C
            IF (I1.EQ.1 .AND. PT(3).NE.0.0)  THEN
C
C**** IF FIRST NODE APPLY FIRST NODE FACTOR ****
              V(2*IN1-1) = V(2*IN1-1) + VX*PT(3)
```

```
            V(2*IN1)   = V(2*IN1)   + VY*PT(3)
            V(2*IN2-1) = V(2*IN2-1) + VX
            V(2*IN2)   = V(2*IN2)   + VY
          ELSEIF(I1.EQ.NDN .AND. PT(4).NE.0.0) THEN
C
C**** APPLY LAST NODE FACTOR ****
            V(2*IN1-1) = V(2*IN1-1) + VX
            V(2*IN1)   = V(2*IN1)   + VY
            V(2*IN2-1) = V(2*IN2-1) + VX*PT(4)
            V(2*IN2)   = V(2*IN2)   + VY*PT(4)
          ELSE
            V(2*IN1-1) = V(2*IN1-1) + VX
            V(2*IN1)   = V(2*IN1)   + VY
            V(2*IN2-1) = V(2*IN2-1) + VX
            V(2*IN2)   = V(2*IN2)   + VY
          ENDIF
C
 190    CONTINUE
      ENDIF
    ENDIF
C
C**** PRESSURE TIME LOADING ****
    CALL FREEF2 (XC,YC,X1,V,FORCD,STRS,INDXS,IP,NPT,NDNOD,IVOL,
   1          KPRES,PT,THICK, BIMP )
C
    RETURN
    END
```

```
      SUBROUTINE PREPRC
C-----------------------------------------------------------------------
C****
C     1. CONTROLS READING OF INPUT DATA FILE
C     2. SETS POINTERS (LVARIABLES) FOR ALL ARRAYS AND CHECKS THAT
C        Q-ARRAY SIZE IS CONSISTENT WITH AVAILABLE CORE.
C****
C
C-----------------------------------------------------------------------
      DIMENSION IQ(1)
      EQUIVALENCE (Q(1),IQ(1))
      COMMON /MAXQ/  MAXQ
      COMMON /ARRAY/ Q(1)
C
      COMMON/DYNAM/ DELT,TIME,MXSTEP,NTSTEP,NTSTP1,OMEGA,WMAX,CWAVE,
     +           CBULK,CSHEAR,C1DAMP,TIMEMX,DTMIN,DTMAX,MXSUB,POISR
      COMMON/RTIME/ DATE, RUNTIM, CREATR, VRSION
      CHARACTER*8  DATE, RUNTIM, CREATR, VRSION
C
C WARNING------ DO NOT CHANGE LOCAT  EXCEPT AFTER LTOTAL OR
C SUBROUTINE DEBUG WILL NOT WORK
      COMMON/LOCAT/ LFINT ,LXC   ,LYC   ,LNODDI,LIX   ,LX1   ,LV1   ,
     +LA1   ,LFORCD,LXO   ,LDTNOD,LSMASS,LMAP  ,LICTYP,LDTGRP,LANGLE,
     +LINDXE,LE    ,LIPLT ,LELOUT,LOUT  ,LNPOUT,LINDXP,LPRS  ,LINDXL,
     +LSLD  ,LINDXS,LSTRS ,LPSU  ,LT    ,LUU   ,LIXX  ,LIYY  ,LTOTAL
      DIMENSION LPTR(35)
      EQUIVALENCE (LPTR,LFINT)
C
      COMMON/OUTPA/ NPRU,NPRS,NPFREQ,NPIC,NKN,MXN,NPRUS
      COMMON/OUTPC/ TITLE
      CHARACTER TITLE*80
C
      COMMON/NUM/ NUMNP,NUMEL,NUMMAT,NUMDIS,NDGREE,NPRES,NSLID,MEQ,
     *          DELTMX,LE2,NPLOT
      COMMON/KNTRL/ISYMF,MITSF,IUN5F,IT11F,IMSHF,IHISF,
     +           IQARF,IRSTF
      DIMENSION KONTRL(10)
      EQUIVALENCE (KONTRL(1),ISYMF)
C
      COMMON/UNITS/LTNM,LLNM,LFNM,LWNM,GMAG,LPNM,LVNM,LDNM
      COMMON/UNITC/ TIMENM,LENGNM,FORCNM,WGTNM,PRESNM   ,VELNM,
     +  DENSNM
      CHARACTER*4   TIMENM,LENGNM,FORCNM,WGTNM,PRESNM*12,VELNM*9,
     +  DENSNM*20
      CHARACTER COMMNT*80
C
C**** PRINT BANNER,DATE, TIME AND VRSION
C
      CREATR  = 'SAMSON2'
      VRSION = '0.8'
      CALL RTIME(DATE,RUNTIM)
```

```
      WRITE (6,1000)
      WRITE (6,1001)
      WRITE (6,1002) CREATR,VRSION,DATE, RUNTIM
C
C**** INITIALIZE
C
      REWIND 1
      REWIND 2
      NDGREE  = 2
      NTSTEP  = 0
      NTSTP1 = 1
      TIME    = 0.0
      DELTMX  = 9.99E10
      NKN     = 0
C
C**** READ/WRITE USER COMMENT BLOCK, TERMINATE WITH BLANK STRING
C
      DO 90 I = 1, 100
        READ (5,110) COMMNT
        IF(COMMNT(1:2) .NE. '*/')GO TO 100
        IF(I .EQ. 1) WRITE(6,109)
        WRITE(6,111) COMMNT(3:80)
   90 CONTINUE
C
  100 BACKSPACE 5
      READ(5,110) TITLE
C
C**** CHECK FOR RESTART RUN IN FIRST PART OF PROBLEM TITLE * * *
C
      IF(TITLE(1:7).EQ.'RESTART' .OR. TITLE(1:7).EQ.'RESTART' ) THEN
        CALL RESTAR(2)
        IF(IHISF.NE.0) CALL PSTAPE

C IF THE USER HAS REQUESTED OUTPUT TO THE COMMON DATA BASE (IT11F
C IS NONZERO) THEN WRITE ALL DISCRIPTIVE INFORMATION TO TAPE11

        IF (IT11F .NE. 0) THEN
          CALL INIT11(Q(LIX),Q(LXC),Q(LMAP),Q(LIPLT))
        END IF
C
C PRINT OUT SELECTED NODES AND ELEMENT DATA ON RESTART CYCLE
C
        CALL OUTSNP(Q(LXC),Q(LYC),Q(LX1),Q(LV1),Q(LA1),Q(LINDXS),
     +          Q(LINDXE),Q(LSTRS),Q(LIX),Q(LE),Q(LMAP),Q(LICTYP))
C
C NEXT COMPUTATIONAL CYCLE IS RESTART CYCLE + 1
C
        NTSTP1 = NTSTEP + 1
        RETURN
      ENDIF
C
      WRITE (6,120) TITLE
```

```
C
C**** READ IN G-MAGNITUDE AND TIME,LENGTH,FORCE UNITS ****
C
      CALL READUN
C
C**** READ(WRITE) PROBLEM SIZE PARAMETERS * * * * *
C
      READ (5,130) NUMNP,NUMEL,NUMMAT,NUMDIS,NPRES,NSLID,MXSTEP,DELT,
     1          TIMEMX,C1DAMP
      WRITE (6,5) NDGREE,NUMNP,NUMEL,NUMMAT,NUMDIS,NPRES,NSLID,MXSTEP,
     +          DELT,TIMENM,TIMEMX,TIMENM,C1DAMP
C
C**** READ CONTROL PARAMETERS * * * * *
C
      CALL READKO
C
C**** SET NSIZE ARRAY * * * * *
C
      CALL SETNSZ
C
C**** SET ADDRESSES * * * * * *
C
      MEQ    = NDGREE*NUMNP
      LFINT  = 1
      LXC    = LFINT  + MEQ
      LYC    = LXC    + NUMNP
      LNODDI = LYC    + NUMNP
      LIX    = LNODDI + 3*(NUMDIS+1)
      LX1    = LIX    + 10*NUMEL
      LV1    = LX1    + MEQ
      LA1    = LV1    + MEQ
      LFORCD = LA1    + MEQ
      LXO    = LFORCD + MEQ
      LDTNOD = LXO    + MEQ
      IF(MITSF .LE. 0) THEN
        LSMASS = LDTNOD
      ELSE
        LSMASS = LDTNOD + NUMNP
      ENDIF
      LMAP   = LSMASS + MEQ
      LICTYP = LMAP   + NUMMAT
      LDTGRP = LICTYP + NUMMAT
      LANGLE = LDTGRP + NUMMAT
      LINDXE = LANGLE + NUMDIS + 1
      LE     = LINDXE + NUMMAT
C
C MEMADJ IS A CFTLIB ROUTINE TO ADD MEMORY TO THE END OF BLANK
C COMMON AT RUN TIME, IT RETURNS IERR  =  0 IF SUCCESSFUL
C ESTIMATE AMOUNT OF CORE NEEDED AND ADJUST ACCORDINGLY
C
      MORMEM   = LE + NUMMAT*100 + NPRES*400 + NSLID*400 + 7*NUMEL
     +         + 7*(NPRS+NPRU) + 2*NPIC
```

```
C    CALL DYNAMEM(MORMEM,MAXQ)
C
     CALL ZERO (Q,1,MAXQ)
C
C**** READ IN  MATERIAL DATA(LADD IS LENGTH OF E-ARRAY(E1 AND E2))
C****         NODAL COORDINATES ****
C****         ELEMENT DATA
C****         INITIALIZE MULT. INTEG. TIMESTEP DATA
C****         BOUNDRY CONDITIONS ****
C****         OUTPUT CODE CARDS ****
C
     CALL READMA (Q(LE),Q(LINDXE),Q(LMAP),Q(LICTYP),Q(LDTGRP),LADD)
     CALL READNO (Q(LXC),Q(LYC))
     CALL READEL (Q(LIX),Q(LMAP),Q(LDTNOD),Q(LDTGRP))
     CALL INMITS (Q(LIX),Q(LDTNOD),Q(LDTGRP))
     CALL READBC (Q(LNODDI),Q(LANGLE))
C
     READ (5,6) NPFREQ,NPRU,NPRS,NPIC
C
     LIPLT  = LE + LADD
     LELOUT = LIPLT  + NUMEL
     LOUT   = LELOUT + 6*NUMEL
     LNPOUT = LOUT + 7*(NPRU+NPRS)
C
     CALL READOU (Q(LOUT),Q(LNPOUT))
     CALL READSN
     IF(IHISF .NE. 0)CALL INITSN(Q(LXC),Q(LYC),Q(LE),Q(LMAP),
    .                Q(LINDXE),Q(LIX))
C
C**** READ IN LOADING DATA ****
C
     LINDXP = LNPOUT + 2*NPIC
     LPRS   = LINDXP + NPRES
     LADD   = 0
     IF (NPRES.NE.0) THEN
       DO 1 I = 1,NPRES
         L  = LPRS + LADD
         IQ(LINDXP+I-1) = 1 + LADD
         CALL READPV(Q(L),Q(L+5),Q(L+6),Q(L+6),LI, Q(LE),Q(LINDXE),
    .                Q(LIX),Q(L+6) )
         LADD = LADD + LI
   1   CONTINUE
     ENDIF
C
C****  READ IN SLIDE LINE DATA ****
C
     LINDXL = LPRS + LADD
     LSLD   = LINDXL + NSLID
     LADD   = 0
     IF (NSLID.NE.0) THEN
       DO 3 I = 1,NSLID
         L = LSLD + LADD
```

```
          IQ(LINDXL+I-1) = 1 + LADD
          CALL READSL(Q(L),Q(L+11),LI)
          LADD = LADD + LI
    3   CONTINUE
      ENDIF

      LINDXS = LSLD   + LADD
      LSTRS  = LINDXS + NUMEL + 6
C
C**** MORE BLANK COMMON WILL BE REQUIRED AT THIS POINT, CALL DYNAMEM
C**** ESTIMATE AMOUNT AND ADJUST ACCORDINGLY
C****  LADD  - SIZE PRINTER PLOT HISTORY ARRAYS
C****  LADDS - AMOUNT OF STORAGE IN Q-ARRAY EXCLUSIVE OF STRS ARRAY
C****  LQUES - QUESS AT FINAL SIZE OF Q-ARRAY INCLUDING STRS ARRAY
C****  ISIZE - FUNCTION TO ESTIMATE SIZE OF STRS ARRAY
C
      NQ = NPFREQ
      IF(NQ.EQ.0) NQ = 1
      LADD  = (MXSTEP+NQ-1)/NQ+2
      LADDS = LSTRS-1+4*LADD+2*(NPRU+NPRS)
      LQUES = LADDS + ISIZE(Q(LE),Q(LMAP),Q(LINDXE),Q(LICTYP),
     .        Q(LIX),Q(LINDXS))
C     MORMEM  = LQUES - MAXQ
C     CALL DYNAMEM(MORMEM,MAXQ)
C
C**** ASSMBLE LUMPED MASS MATRIX AND SET UP INDEX TO STRS ARRAY * *
C**** LADDS-INPUT TO ASSBLE IS THE TOTAL AMOUNT OF STORAGE IN Q-ARRAY
C****           EXCLUSIVE OF STRS ARRAY
C**** LADDS-OUTPUT FROM ASSBLE IS THE SIZE OF THE STRS ARRAY
C
      CALL ASSBLE (Q(LXC),Q(LYC),Q(LIX),Q(LE),Q(LSTRS),Q(LINDXS),
     .           Q(LINDXE),Q(LSMASS),LADDS,Q(LMAP),Q(LICTYP) )
      WRITE (6,126)
C
C****  LT,LUU,LIXX,LIYY,LTOTAL ARE MODIFIED IN RESTART IF CURRENT
C****  RUN IS A RESTART RUN
C
      LPSU   = LSTRS+ LADDS
      LT     = LPSU + LADD
      LUU    = LT   + LADD
      LIXX   = LUU  + NPRU + NPRS
      LIYY   = LIXX + LADD
      LTOTAL = LIYY + LADD
C
C**** PRINT L-POINTERS
C
      CALL PRINTL

C ADD MORE SPACE TO THE END OF BLANK COMMON, AT LEAST 100 WORDS

C     MORMEM  = LTOTAL - MAXQ
C     CALL DYNAMEM(MORMEM,MAXQ)
```

```
C
C**** ZERO OUT TIME DEPENDENT ARRAYS X1, V1, A1, FORCD, XO
C
      CALL ZERO(Q,LX1,LDTNOD-LX1)
C
C**** DUMP Q AT THIS POINT IF IQARF .LT. 0 ,FOR DEBUGGING RUN.
C
      IF(IQARF.LT.0) CALL DEBUG
C
C IF THE USER HAS REQUESTED OUTPUT TO THE COMMON DATA BASE (IT11F
C IS NONZERO) THEN WRITE ALL DISCRIPTIVE INFORMATION TO TAPE11

      IF (IT11F .NE. 0) THEN
        CALL INIT11(Q(LIX),Q(LXC),Q(LMAP),Q(LIPLT))
      END IF
C
C**** COMPUTE TIME STEP AND NUMBER OF TIME STEPS * * * * *
C**** CALL FRCIN W.ZERO DISPL. AND FORCES ONLY TO GET DELTMX
C
      CALL FRCIN (Q(LXC),Q(LYC),Q(LE),Q(LX1),Q(LV1),Q(LFINT),Q(LSTRS),
     .        Q(LINDXS),Q(LINDXE),Q(LMAP),Q(LIX),Q(LICTYP),Q(LDTNOD))
C
      IF (DELT .LT. 0.0) THEN
        DELT   = -DELT * DELTMX
      ELSEIF (DELT .EQ. 0.0) THEN
        DELT   =  0.5 * DELTMX
      ENDIF
      IF(TIMEMX.EQ. 0.0) TIMEMX =  DELT * MXSTEP
      IF(MXSTEP.EQ.   0) MXSTEP =  TIMEMX/DELT
      MXC = TIMEMX/DELT + 0.001
      MXSTEP = MIN0(MXC, MXSTEP)
      WRITE (6,211) DELTMX,DELT,DTMIN,DTMAX,MXSTEP,MXSUB
      IF(DELT .GT. DELTMX*0.66667) WRITE(6,214)
      IF(MITSF.GE.1) WRITE (6,212) (I,Q(LDTGRP+I-1),I=1,NUMMAT)
      WRITE (6,213)
C
      RETURN
C
C * * * * * * * * F O R M A T S * * * * * * * * * * * * * *
C
 1000 FORMAT( OMITTED )
 1002 FORMAT (//,5X,'CODE: ',A,5X,' VRSION: ',A,5X,'RUN ON:  ', A,
     .        5X,' AT:  ', A, //)
  109 FORMAT (/////,' USER COMMENTS:',/)
  111 FORMAT (15X,A)
  110 FORMAT (A)
  120 FORMAT ('1',/,' TITLE: ',A,///)
  130 FORMAT (7I5,5X,3E10.4)
    5 FORMAT (' NO. OF D. O. F.      (NDGREE)' ,I10/
     .      ' NUMBER OF NODES      (NUMNP) ' ,I10/
     .      ' NUMBER OF ELEMENTS   (NUMEL) ' ,I10/
     .      ' NUMBER OF MATERIALS  (NUMMAT)' ,I10/
```

```
     .       ' NO.OF BOUNDARY NODES (NUMDIS)' ,I10/
     .       ' NO. OF LOAD LINES    (NPRES) ' ,I10/
     .       ' SLIDING INTERFACES   (NSLID) ' ,I10/
     .       ' MAX.NO.OF TIME STEPS (MXSTEP)' ,I10/
     .       ' TIME INCREMENT       (DELT)  ' ,G14.5,1X,A/
     .       ' MAXIMUM TIME OF RUN  (TIMEMX)' ,G14.5,1X,A/
     .       ' MASS DAMPING FACTOR  (C1DAMP)' ,1X,E12.3)
   6 FORMAT (8I5)
 126 FORMAT (///)
 211 FORMAT (///,5X, 'TIME STEP INFO:',/,
     1          5X, '  MAX.TIME STEP COMPUTED BY CODE = ' ,G10.4,/,
     .          5X, '  TIME STEP USED = ',G10.4,/,
     +          5X, '  DTMIN          = ',G10.4,/,
     +          5X, '  DTMAX          = ',G10.4,/,
     +          5X, '  TOTAL NUMBER OF TIME STEPS = ' ,I10,/
     +          5X, '  NUMBER OF SUBCYCLES        = ' ,I10,/)
 212 FORMAT (  /,5X, 'MULTIPLE INTEGRATION TIMESTEPS WILL BE USED:',/
     .        ,(7X,I5,G12.4/))
 213 FORMAT (//,' END OF INPUT PROCESSING',/,
     .        1X,79('*'),/,'1')
 214 FORMAT (///,
     + ' ----------------------------------------',/
     + ' WARNING, POSSIBLE INSTABLILITY. DELT SHOULD BE',/
     + ' LESS THAN 2/3 OF DELTMX. DELTMX IS BASED ON WAVE SPEED ',/
     + ' CALCULATED FROM BULK MODULUS, ACTUAL WAVE SPEED IS PROBABLY ',/
     + ' HIGHER.',/
     + ' ----------------------------------------',//)
C
      END
```

```
      SUBROUTINE READPV(IVOL,THICK,PT,KPRES,LADD, E,INDXE,IX,BIMP )
C
C****
C**** THIS ROUTINE READS THE LOAD LINE DATA INTO ARRAYS IVOL,PT
C**** AND KPRESS FOR USE IN ROUTINE FREEFD
C****
C**** IVOL(1) = TYPE OF LOAD LINE,
C****         -2, AXISYM.PROB.PRESS.LINE
C****         -1, PLANE PROB.PRESS.LINE
C****          0, INITIAL VELOCITY LINE
C****          1, FORCE LINE
C****          2, PRESCRIBED DISPLACEMENT LINE
C****            3, AXISYM. NONREFLECTING BOUNDARY LINE
C****            4, PLANE NONREFLECTING BOUNDARY LINE
C**** IVOL(2) = INITIAL VEL.DIRECTION CODE,
C****         0, VEL.IS NORMAL AND TANGENT TO LOAD LINE.
C****         1, VEL.IS IN GLOBAL X Y DIRECTIONS
C**** IVOL(3) = COMPONENT DIRECTION CODE
C****         1, X-COMPONENT
C****         2, Y-COMPONENT
C**** IVOL(4) = NO.OF NODES FOR CURRENT LOAD LINE
C**** IVOL(5) = NO.OF TIME,PRESS.PAIRS (OR TIME,FORCE OR TIME.DISPL.)
C**** THICK   = THICKNESS FOR PLANAR PROB. PRESSURE LINE
C****         = 1.0 FOR AXISYM.PROB.LINE
C****   NPT   =  NUMBER OF(TIME,PRESSURE)DATA PAIRS
C****   PT    = (TIME,PRESSURE)PAIR DATA ** T1,P1,T2,P2,,,TNPT,PNPT
C****   NDNOD = NUMBER OF NODES ON LOAD LINE
C****   KPRES = LIST OF NODES ON LOAD LINE
C****   IPRES = LOAD LINE NUMBER
C****   LADD  = STORAGE USED IN STORING LOAD LINE INFORMATION
C****
C
      COMMON/NUM/ NUMNP,NUMEL,NUMMAT,NUMDIS,NDGREE,NPRES,NSLID,MEQ,
     *          DELTMX,LE2,NPLOT
      COMMON/KNTRL/ISYMF,MITSF,IUN5F,IT11F,IMSHF,IHISF,
     +          IQARF,IRSTF
      DIMENSION KONTRL(10)
      EQUIVALENCE (KONTRL(1),ISYMF)
C
      COMMON/UNITS/LTNM,LLNM,LFNM,LWNM,GMAG,LPNM,LVNM,LDNM
      COMMON/UNITC/ TIMENM,LENGNM,FORCNM,WGTNM,PRESNM   ,VELNM,
     +  DENSNM
      CHARACTER*4   TIMENM,LENGNM,FORCNM,WGTNM,PRESNM*12,VELNM*9,
     +  DENSNM*20
      DIMENSION IVOL(1), PT(1), KPRES(1),VOL(1), E(1),INDXE(1),
     +          IX(10,1), BIMP(1)
C
C**** READ AND WRITE THE LOAD LINE DESCRIPTION DATA****
C
      READ (5,8) IPRES,IVOL(4),(IVOL(I),I = 1,3),INT1,IVOL(5),THICK
      IF(THICK.LE.0.0) THICK = 1.0
```

```
      WRITE(6,9) IPRES,IVOL(4),IVOL(1),IVOL(2)
      WRITE(6,3) IVOL(3),INT1,IVOL(5),THICK
      NDNOD = IVOL(4)
C
C**** READ IN THE INITIAL VELOCITY LINE DATA IF IVOL(1) = 0****
C**** ELSE, READ IN FUNCTION-TIME PAIRS ****
C
      IF (IVOL(1) .EQ. 0)  THEN
        READ (5,10) (PT(J),J = 1,4)
        WRITE(6,111)
C
        IF(IVOL(2).EQ.0) THEN
          WRITE(6,14) PT(1),VELNM,PT(2),VELNM,(PT(J),J=3,4)
        ELSEIF(IVOL(2).EQ.1) THEN
          WRITE(6,15) PT(1),VELNM,PT(2),VELNM,(PT(J),J=3,4)
        ENDIF
        NPT = 2
        IVOL(5) = NPT
C
      ELSEIF ((IVOL(1) .EQ. 3) .OR. (IVOL(1) .EQ. 4)) THEN
        NPT = 0
        IVOL(5) = NPT
C
      ELSE
        NPT = IVOL(5)
        I2  = 2*NPT
        READ(5,10) (PT(J),J = 1,I2)
        WRITE(6,100)
C
        IF (IVOL(1) .LT. 0) THEN
          WRITE(6,11)TIMENM,PRESNM
        ELSEIF (IVOL(1) .EQ. 1) THEN
          WRITE(6,12) TIMENM,FORCNM
        ELSEIF (IVOL(1) .EQ. 2) THEN
          WRITE(6,20) TIMENM,LENGNM
        ENDIF
C
        DO 1 K = 1,NPT
         J1 = 2*K-1
         J2 = J1+1
         WRITE (6,13) K,(PT(J),J = J1,J2)
    1   CONTINUE
C
C**** CHECK TO SEE THAT TIME POINTS ARE IN RIGHT ORDER  ****
C
        IF (NPT.GE.2)  THEN
         NN = NPT*2-3
         DO 2 J = 1,NN,2
          IF (PT(J).GE.PT(J+2))  THEN
            WRITE(6,19)
            STOP 'READPV1'
          ENDIF
```

```
   2     CONTINUE
         ENDIF
C
      ENDIF
C
C**** COMPUTE TOTAL STORAGE USED FOR LOAD LINE INFORMATION ****
C
      LADD = NDNOD+2*NPT+6
C
C****  READ IN NODES ON LOAD LINE
C**** INDEXING ON KPRES STARTS AT I1 = 2*NPT+1 - BECAUSE PT AND KPRES
C**** START AT SAME LOCATION ****
C
      I1 = 2*NPT+1
      I2 = I1+NDNOD-1
C
      IF (INT1.EQ.0)  THEN
        READ (5,7) (KPRES(J),J = I1,I2)
      ELSE
        READ (5,8) KPRES(I1)
        I3 = I2-1
        DO 6 J = I1,I3
          KPRES(J+1) = KPRES(J)+INT1
   6    CONTINUE
      ENDIF
C
      DO 21 J = I1,I2
        IF(KPRES(J).GT.NUMNP)  THEN
          WRITE(6,23) KPRES(J)
          STOP
        ENDIF
  21  CONTINUE
C
      WRITE(6,17) (KPRES(J),J = I1,I2)
C
C**** GET THE BOUNDARY IMPEDENCES NEAR THE NONREFLECTING BOUNDARY
C
      IF (IVOL(1) .EQ. 3 .OR. IVOL(1) .EQ. 4) THEN
C
      KK = 0
      DO 157 K=I1,I2-1
C
        IN1=KPRES(K)
        IN2=KPRES(K+1)
        DO 158 I=1,NUMEL
C
          N=IX(10,I)
C
C ---------------------------------------------------
C **** THREE-NODE TRIANGLE ****
C ---------------------------------------------------
C
```

```
      IF (N .EQ. 3) THEN
C
        DO 159 J=1,2
          IF (IX(J,I) .EQ. IN1 .AND. IX(J+1,I) .EQ. IN2) GOTO 700
  159   CONTINUE
          IF (IX(3,I) .EQ. IN1 .AND. IX(1,I) .EQ. IN2)  GOTO 700
        GOTO 158
C
C ------------------------------------------------------
C **** FOUR-NODE QUADRILATERAL ****
C ------------------------------------------------------
C
      ELSEIF (N .EQ. 4) THEN
C
        DO 160 J=1,3
          IF (IX(J,I) .EQ. IN1 .AND. IX(J+1,I) .EQ. IN2) GOTO 700
  160   CONTINUE
          IF (IX(4,I) .EQ. IN1 .AND. IX(1,I) .EQ. IN2)  GOTO 700
        GOTO 158
C
C ------------------------------------------------------
C **** FIVE-NODE TRIANGLE ****
C ------------------------------------------------------
C
      ELSEIF (N .EQ. 5) THEN
C
        IF ((IX(1,I) .EQ. IN1 .AND. IX(2,I) .EQ. IN2) .OR.
     .      (IX(2,I) .EQ. IN1 .AND. IX(4,I) .EQ. IN2) .OR.
     .      (IX(4,I) .EQ. IN1 .AND. IX(3,I) .EQ. IN2) .OR.
     .      (IX(3,I) .EQ. IN1 .AND. IX(5,I) .EQ. IN2) .OR.
     .      (IX(5,I) .EQ. IN1 .AND. IX(1,I) .EQ. IN2)) GOTO 700
        GOTO 158
C
C ------------------------------------------------------
C **** SIX-NODE TRIANGLE ****
C ------------------------------------------------------
C
      ELSEIF (N .EQ. 6) THEN
C
          DO 161 J=1,3
            IF (IX(J,I) .EQ. IN1 .AND. IX(J+3,I) .EQ. IN2) GOTO 700
  161     CONTINUE
          DO 162 J=4,5
            IF (IX(J,I) .EQ. IN1 .AND. IX(J-2,I) .EQ. IN2) GOTO 700
  162     CONTINUE
            IF (IX(6,I) .EQ. IN1 .AND. IX(1,I) .EQ. IN2)  GOTO 700
          GOTO 158
C
C ------------------------------------------------------
C **** EIGHT-NODE QUADRILATERAL ****
C ------------------------------------------------------
C
```

```
      ELSEIF (N .EQ. 8) THEN
C
  800    DO 163 J=1,4
          IF (IX(J,I) .EQ. IN1 .AND. IX(J+4,I) .EQ. IN2) GOTO 700
  163    CONTINUE
         DO 164 J=5,7
          IF (IX(J,I) .EQ. IN1 .AND. IX(J-3,I) .EQ. IN2) GOTO 700
  164    CONTINUE
          IF (IX(8,I) .EQ. IN1 .AND. IX(1,I) .EQ. IN2)  GOTO 700
C
      ENDIF
C
  158 CONTINUE
C
  700 J2 = INDXE(IX(9,I)) + 5
      DENS = E(J2)
      YM   = E(J2+1)
      PR   = E(J2+2)
      BIMP(K+NDNOD+KK)   = SQRT(YM*(1.-PR)/(1.+PR)/(1.-2.*PR)*DENS)
      BIMP(K+NDNOD+KK+1) = SQRT(YM/(2.*(1.+PR))*DENS)
      KK = KK + 1
C
  157 CONTINUE
C
      LADD=LADD+2*(NDNOD-1)
      ENDIF
C
     RETURN
C
C********FORMATS************
C
    7 FORMAT (16I5)
    8 FORMAT (7I5,5X,E10.3)
    9 FORMAT(//1X,79('*')/,' LOAD LINE NO.',I5,/, ' NO. OF NODES',I5,/,
     . ' CONTROL 1 = ',I3,'  (TYPE OF LOAD LINE)',/,
     .    18X,'= -2, AXISYMM.PROB.PRESS.LINE'    ,/,
     .    18X,'= -1, PLANE PROB.PRESS.LINE'      ,/,
     .    18X,'=  0, INITIAL VELOCITY LINE'      ,/,
     .    18X,'=  1, FORCE LINE'                 ,/,
     .    18X,'=  2, PRESCRIBED DISPLACEMENT LINE',/,
     .    18X,'=  3, AXISYM. NONREFL. BOUNDARY'  ,/,
     .    18X,'=  4, PLANE NONREFL. BOUNDARY'    ,//,
     .' CONTROL 2 = ',I3,' (NEEDED ONLY WHEN CONTROL 1 = 0 )',/,
     .    18X,'=  0, INITIAL VEL.IS NORMAL AND TANG.TO LOAD LINE',/,
     .    18X,'=  1, INITIAL VEL.IS IN X,Y DIRECTIONS',//,)
    3 FORMAT(' CONTROL 3 = ',I3,' (COMPONENT I.D. , NEEDED ONLY WHEN ',
     .          'CONTROL 1  =  1 OR 2 )',/,
     .    18X,'=  1(OR 2), X(OR Y) COMPONENT SPECIFIED',//,
     .' NODE INTERVAL = ',I4,' (FOR GENERATION OF NODES ON LOAD LINE)',/
     .' NO.OF FN.PTS. = ',I4,' (NO.OF PIECEWISE LINEAR POINTS USED',
     .                 ' FOR PRESS.,',/,
     .    23X,'FORCE,ETC.HISTORY - NOT USED IF CONTROL 1 = 0)',/,
```

```
     .' THICK = ',E10.3,', THICKNESS OF PLANAR PROB.PRESS.LINE',/
     . )
C
  111 FORMAT(/ '  ** VELOCITY SPECIFICATION **')
   14 FORMAT(/7X,'VEL-TANGENT        ',1PG20.5,A/
     .       7X,'VEL-NORMAL         ',G20.5,A/
     .       7X,'FIRST NODE FACTOR',G20.5/
     .       7X,'LAST NODE FACTOR ',G20.5)
C
   15 FORMAT(/,6X,'VELOCITY-X        ',1PG20.5,A/
     .        6X,'VELOCITY-Y        ',G20.5,A/
     .        6X,'FIRST NODE FACTOR',G20.5/
     .        6X,'LAST NODE FACTOR ',G20.5)
C
   10 FORMAT (8E10.0)
  100 FORMAT (/' ** FUNCTION HISTORY DATA **')
   11 FORMAT (3X,'PT.',9X, 'TIME,' ,A, 2X,'PRESSURE,', A)
   12 FORMAT (3X,'PT.',9X, 'TIME,' ,A, 5X,'FORCE,',A)
   20 FORMAT (2X,'PT.',9X, 'TIME,' ,A, 4X,'DISPLACEMENT,' ,A)
   13 FORMAT (1X,I4,1PG19.4,G15.4)
   19 FORMAT (/,5X,'READPV ** ERROR, TIME POINTS OUT OF ORDER')
   23 FORMAT (/,5X,'READPV ** ERROR, NODE',I5,' IS OUT OF RANGE')
   17 FORMAT (//'  ** NODES ON LOAD LINE **' /(1X,20I5))
C
      END
```

```
      SUBROUTINE SOLVE
     .(XC    ,YC    ,XO    ,X1    ,V1    ,A1    ,SMASS ,FINT  ,FORCD ,
     . INDXS ,STRS  ,INDXE ,E     ,MAP   ,ICTYP ,IX    ,OUT   ,
     . NODDIS,ANGLE ,DTNOD ,NPOUT ,PSU   ,T     ,UU    ,IXX   ,IYY   ,
     . ELOUT ,IPLT  ,INDXP ,PR    ,INDXL ,SL    )
C-----------------------------------------------------------------
C     THIS IS THE MAIN CALCULATION CONTROLLING SUBROUTINE. IT CONTAINS
C    THE TIME LOOP, THE MULTIPLE TIMESTEP SUB-LOOP, AND THE CALLS TO
C    ALL THE MAJOR CALCULATING ROUTINES AS FOLLOWS:
C
C       FREEFD  -  INITIAL BOUNDARY CONDITIONS
C       FREEF2  -  TIME DEPENDENT EXTERNAL LOADS(FORCD)
C       FRCIN   -  INTERNAL STRESS VIA EOS ROUTINES
C       SLIDER  -  SLIDING INTERFACE ROUTINE
C       MOTION  -  EQUATIONS OF MOTION AND TIME INTEGRATOR
C
C    THE FOLLOWING OUTPUT, POSTPROCESSING AND UTILITY ROUTINES ARE
C    ALSO CALLED:
C
C       OUTPUT  -  SELECTED OUTPUT
C       ZERO    -  ZEROES AN ARRAY
C       STENGY  -  CALCULATES ENERGY TERMS
C-----------------------------------------------------------------
C
      DIMENSION XC(1)    ,YC(1)    ,XO(1)    ,X1(1)    ,V1(1)    ,
     . A1(1)    ,SMASS(1) ,FINT(1)  ,FORCD(1) ,INDXS(1) ,STRS(1)  ,
     . INDXE(1) ,E(1)     ,MAP(1)   ,ICTYP(1) ,IX(1)    ,OUT(1)   ,
     . NODDIS(1),ANGLE(1) ,DTNOD(1) ,NPOUT(1) ,PSU(1)   ,
     . T(1)     ,UU(1)    ,IXX(1)   ,IYY(1)   ,ELOUT(1) ,IPLT(1)  ,
     . SL(1)    ,PR(1)    ,INDXP(1) ,INDXL(1)
      INTEGER PR
C
      DIMENSION IQ(1)
      EQUIVALENCE (Q(1),IQ(1))
      COMMON /MAXQ/  MAXQ
      COMMON /ARRAY/ Q(1)
C
      COMMON/DYNAM/ DELT,TIME,MXSTEP,NTSTEP,NTSTP1,OMEGA,WMAX,CWAVE,
     +           CBULK,CSHEAR,C1DAMP,TIMEMX,DTMIN,DTMAX,MXSUB,POISR
      COMMON/RTIME/ DATE, RUNTIM, CREATR, VRSION
      CHARACTER*8  DATE, RUNTIM, CREATR, VRSION
C
C WARNING------ DO NOT CHANGE LOCAT  EXCEPT AFTER LTOTAL OR
C SUBROUTINE DEBUG WILL NOT WORK
      COMMON/LOCAT/ LFINT ,LXC   ,LYC   ,LNODDI,LIX   ,LX1   ,LV1   ,
     +LA1   ,LFORCD,LXO   ,LDTNOD,LSMASS,LMAP  ,LICTYP,LDTGRP,LANGLE,
     +LINDXE,LE    ,LIPLT ,LELOUT,LOUT  ,LNPOUT,LINDXP,LPRS  ,LINDXL,
     +LSLD  ,LINDXS,LSTRS ,LPSU  ,LT    ,LUU   ,LIXX  ,LIYY  ,LTOTAL
      DIMENSION LPTR(35)
      EQUIVALENCE (LPTR,LFINT)
C
```

```
      COMMON/OUTPA/ NPRU,NPRS,NPFREQ,NPIC,NKN,MXN,NPRUS
      COMMON/OUTPC/ TITLE
      CHARACTER TITLE*80
C
      COMMON/NUM/ NUMNP,NUMEL,NUMMAT,NUMDIS,NDGREE,NPRES,NSLID,MEQ,
     *          DELTMX,LE2,NPLOT
      COMMON/KNTRL/ISYMF,MITSF,IUN5F,IT11F,IMSHF,IHISF,
     +          IQARF,IRSTF
      DIMENSION KONTRL(10)
      EQUIVALENCE (KONTRL(1),ISYMF)
C
C
C**** SET AND PRINT INITIAL CONDITIONS WHEN NTSTP1=1* * * * *
C
      IF(NTSTP1 .EQ. 1) THEN
        IF(NPRES.GT.0) THEN
          DO 244 IP = 1,NPRES
            L1   = INDXP(IP)
            NPT  = PR(L1+4)
            NNOD = PR(L1+3)
            L2   = L1 + 6
            L3   = L2 + 2*NPT
            CALL FREEFD (XC,YC,X1,V1,FORCD,STRS,INDXS,IP,NPT,
     .           NNOD,PR(L1),PR(L3),PR(L2),PR(L1+5), PR(L3) )
 244      CONTINUE
        ENDIF
C
        CALL OUTPUT(XC,YC,X1,V1,A1,IX,E,INDXS,INDXE,OUT,NPOUT,STRS,
     .            PSU,T,MAP,ICTYP,UU,IXX,IYY,ELOUT,IPLT)
      ENDIF
C
      CALL CPTIME(CPU1)
C
C**** START OF INTEGRATION LOOP * * * * *
C
      DO 260 NTSTEP = NTSTP1, MXSTEP
C
C**** MULTIPLE TIME STEP INTEGRATION  LOOP
C
        DO 1250 NSUB = 1, MXSUB
          TIME = TIME + DTMIN
C
C**** COMPUTE EXTERNAL LOAD * * * * *
C
          CALL ZERO(FORCD,1,MEQ)
          IF(NPRES.GT.0) THEN
            DO 264 IP = 1,NPRES
              L1   = INDXP(IP)
              NPT  = PR(L1+4)
              NNOD = PR(L1+3)
              L2   = L1 + 6
              L3   = L2 + 2*NPT
```

```
            CALL FREEF2(XC,YC,X1,V1,FORCD,STRS,INDXS,IP,NPT,
     .           NNOD,PR(L1),PR(L3),PR(L2),PR(L1+5), PR(L3) )
  264       CONTINUE
          ENDIF
C
C**** COMPUTE INTERNAL LOADS VIA ELEMENT MODEL AND CONSTUTIVE LAW
C
          CALL FRCIN (XC,YC,E,X1,V1,FINT,STRS,INDXS,INDXE,MAP,
     .           IX,ICTYP,DTNOD)
C
C**** SLIDE LINE PROCESSING
C
          IF(NSLID.GT.0) THEN
            DO 320 JSLID = 1,NSLID
              L1 = INDXL(JSLID)
              L2 = L1 + 11
              CALL SLIDER(XC,YC,SL(L1),SL(L2),X1,XO,V1,SMASS,A1,
     .             FINT,FORCD,NODDIS,JSLID)
  320       CONTINUE
          ENDIF
C
C**** SOLVE FOR NEW DISPLACEMENTS,VELOCITIES AND ACCELERATIONS * *
C
          CALL MOTION(NODDIS,SMASS,XC,YC,XO,X1,V1,A1,FORCD,FINT,
     .           ANGLE,DTNOD)
C
 1250   CONTINUE
C
C**** TIME IS RECALCULATED TO AVOID ACCUMMULATION OF ROUNDOFF ERROR
C**** PARTICULARLY FOR PROBLEMS USING MITS
C
        TIME = NTSTEP*DTMAX
C
C**** COMPUTE AND STORE ENERGIES * * * * *
C
        CALL STENGY(INDXE,E,INDXS,STRS,V1,SMASS,ENERGY)
C
C**** WRITE OUT AND STORE RESPONSE * DUMP CORE IF REQD.STEP * * *
C
        CALL OUTPUT(XC,YC,X1,V1,A1,IX,E,INDXS,INDXE,OUT,NPOUT,STRS,
     .           PSU,T,MAP,ICTYP,UU,IXX,IYY,ELOUT,IPLT)
C
 260 CONTINUE
C
C**** PRINT TIMING SUMMARY
C
      CALL CPTIME(CPU2)
      CP  = CPU2 - CPU1
      CP1 = CP/(NUMEL*NTSTEP)
      CP2 = CP/(NUMNP*NTSTEP)
      NP1 = 1.0 / CP1
      NP2 = 1.0 / CP2
```

```
      WRITE(6,1000) CPU1,CPU2,NP1,NP2,CP1,CP2
C
      RETURN
 1000 FORMAT(///,' TIMING SUMMARY:',//,
     +       '   SETUP TIME(S)= ',1PG12.4,/,
     +       '   END TIME(S)  = ', G12.4,//,
     +       '   ELEMENTS/SEC = ', I6,/,
     +       '   NODES/SEC    = ', I6,//,
     +       '   SEC/ELEMENT  = ', G12.4,/,
     +       '   SEC/ NODE    = ', G12.4)
      END
```

Appendix D
SAMPLE INPUT FILES FOR SAMSON2

1-D WAVE PROPAGATION, DILATATIONAL WAVE, SHORT BAR W/NRB

```
 12   6   1   3   2   0 200          0.25
  1   0   5   0   0  -1   0   0   1
  1   6   4
    0.00      1.0
    1.0       1.0       0.0       0.00
  1           0.0       0.0
  4           6.0       0.0
  5           0.0       2.0
  8           6.0       2.0
  9           0.0       4.0
 12           6.0       4.0
  1   1   2   6   5                     1
  3   3   4   8   7                     1
  4   5   6  10   9                     1
  6   7   8  12  11                     1
  1  21
 -9  21           4

  1   1   1   1
  6
  2
  1   3   2       1   4  10
     0.        0.        2.   8.0E-5       4.  2.93E-3       6.  6.17E-3
     8.        .01      10.  1.383E-2      12.  1.707E-2      14.  1.924E-2
    16.        .02      35.        .02
  1
  2   3   4           4
  4
```

1-D WAVE PROPAGATION, SHEAR WAVE, SHORT BAR W/NRB

```
12   6   1  12   2   0 200        0.25
 1   0   5   0   0  -1   0   0   1
 1   6   4
  0.00     1.0
   1.0     1.0     0.0     0.00
 1         0.0     0.0
 4         6.0     0.0
 5         0.0     2.0
 8         6.0     2.0
 9         0.0     4.0
12         6.0     4.0
 1   1   2   6   5                  1
 3   3   4   8   7                  1
 4   5   6  10   9                  1
 6   7   8  12  11                  1
 1  12
-9  12          4
 2  10
-4  10
 6  10
-8  10
 10 10
-12 10

 1   1   1   1
 6
 2
 1   3   2       2   4  10
    0.      0.      2.   8.0E-5      4.  2.93E-3      6.  6.17E-3
    8.     .01     10. 1.383E-2      12. 1.707E-2      14. 1.924E-2
   16.     .02     35.     .02
 1
 2   3   4           4
 4
```

AXISYMMETRIC 1-D WAVE PROPAGATION, R/L = 2.0, SHORT BAR W/NRB

```
12   6   1   3   2   0 200          0.25
 0   0   5   0   0  -1   0   0   1
 1   6  14
   0.00
    1.0      1.0      0.0      0.00
 1           58.0      0.0
 4           64.0      0.0
 5           58.0      2.0
 8           64.0      2.0
 9           58.0      4.0
12           64.0      4.0
 1   1   2   6   5                    1
 3   3   4   8   7                    1
 4   5   6  10   9                    1
 6   7   8  12  11                    1
 1  21
-9  21           4

 1   1   1   1
 6
 2
 1   3   2        1   4  10
    0.       0.       2.   8.0E-5       4.  2.93E-3       6.  6.17E-3
    8.       .01      10. 1.383E-2       12. 1.707E-2       14. 1.924E-2
   16.       .02      35.       .02
 1
 2   3   3            4
 4
```

1-D WAVE PROPAGATION, 8NQ ELEMENTS, SHORT BAR W/NRB

```
 18   3   1   3   2   0 200          0.25
  1   0   5   0   1  -1   0   0   1
  1   6   4
    2.0      1.0
    1.0      1.0      0.0      0.00
  1          0.0      0.0
  3          0.0      4.0
  4          1.0      0.0
  5          1.0      4.0
  6          2.0      0.0
  8          2.0      4.0
  9          3.0      0.0
 10          3.0      4.0
 11          4.0      0.0
 13          4.0      4.0
 14          5.0      0.0
 15          5.0      4.0
 16          6.0      0.0
 18          6.0      4.0
  1   1   6   8   3   4   7   5   2   1
  3  11  16  18  13  14  17  15  12   1
  1  21
 -3  21

  1   1   1   1
  7
  2
  1   3   2        1   1  10
    0.       0.       2.   8.0E-5       4.  2.93E-3       6.  6.17E-3
    8.      .01       10.  1.383E-2      12.  1.707E-2      14.  1.924E-2
   16.      .02       35.      .02
  1
  2   3   4            1
 16
```

ANISOTROPIC 1-D WAVE PROPAGATION, DILATATIONAL WAVE, SHORT BAR W/ NRB

```
 12   6   2   3   2   0 200        0.25
  1   0   5   0   0  -1   0   0   1
  1   6   4
   0.00      1.0
    1.0      1.0      0.0      0.00
  2   6   4
   0.00      1.0
    1.0      4.0      0.0      0.00
 1           0.0      0.0
 4           6.0      0.0
 5           0.0      2.0
 8           6.0      2.0
 9           0.0      4.0
12           6.0      4.0
 1   1   2   6   5                   1
 3   3   4   8   7                   1
 4   5   6  10   9                   2
 6   7   8  12  11                   2
 1  21
-9  21           4

 1   1   1   1
 6
 2
 1   3   2       1   4  10
    0.       0.       2.   8.0E-5      4.  2.93E-3      6.  6.17E-3
    8.      .01      10. 1.383E-2      12. 1.707E-2      14. 1.924E-2
   16.      .02      35.      .02
 1
 2   3   4           4
 4
```

1-D WAVE PROPAGATION, DILATATIONAL WAVE, LONG BAR

```
 63  40   1   3   1   0 200          0.25
  1   0   5   0   0  -1   0   0   1
  1   6   4
    0.00      1.0
    1.0       1.0      0.00      0.00
  1           0.0      0.0
 21          40.0      0.0
 22           0.0      2.0
 42          40.0      2.0
 43           0.0      4.0
 63          40.0      4.0
  1   1   2  23  22                    1
 20  20  21  42  41                     1
 21  22  23  44  43                     1
 40  41  42  63  62                     1
  1  21
-43  21          21

  1   1   1   1
 23
  2
  1   3   2        1  21  10
     0.       0.       2.   8.0E-5      4.  2.93E-3      6.  6.17E-3
     8.      .01      10.  1.383E-2      12.  1.707E-2     14.  1.924E-2
    16.      .02      35.      .02
  1
```

SMALL MESH W/NRB, SOIL, SHORTENED BLAST LOAD

```
 49  36   1   7   2   0 4000       0.10E-5
  0   0   5   0   0  -1   0   0   0
  1   9  14              YUMA SOIL PARAMETERS
    0.00
0.173E-3 0.1904E5     0.38      0.01      5.0       1.0       2.0
    0.0       1.0
0.2644E5   -0.122      0.38
0.4429E5   -0.156      0.38
0.1553E6   -0.192      0.38
0.3442E6   -0.212      0.38
0.2199E7   -0.999      0.38
0.2199E7      0.0      0.38
    0.0  0.7249E2
 -0.1E7    0.65E6
  1          0.00      0.00
  2          0.00      6.00
  3          0.00     12.00
  4          0.00     18.00
  5          0.00     24.00
  6          0.00     30.00
  7          0.00     36.00
  8          6.00      0.00
  9          6.00      6.00
 10          6.00     12.00
 11          6.00     18.00
 12          6.00     24.00
 13          6.00     30.00
 14          6.00     36.00
 15         12.00      0.00
 16         12.00      6.00
 17         12.00     12.00
 18         12.00     18.00
 19         12.00     24.00
 20         12.00     30.00
 21         12.00     36.00
 22         18.00      0.00
 23         18.00      6.00
 24         18.00     12.00
 25         18.00     18.00
 26         18.00     24.00
 27         18.00     30.00
 28         18.00     36.00
 29         24.00      0.00
 30         24.00      6.00
 31         24.00     12.00
 32         24.00     18.00
 33         24.00     24.00
 34         24.00     30.00
 35         24.00     36.00
```

36	30.00	0.00
37	30.00	6.00
38	30.00	12.00
39	30.00	18.00
40	30.00	24.00
41	30.00	30.00
42	30.00	36.00
43	36.00	0.00
44	36.00	6.00
45	36.00	12.00
46	36.00	18.00
47	36.00	24.00
48	36.00	30.00
49	36.00	36.00

1	1	8	9	2	1
2	2	9	10	3	1
3	3	10	11	4	1
4	4	11	12	5	1
5	5	12	13	6	1
6	6	13	14	7	1
7	8	15	16	9	1
8	9	16	17	10	1
9	10	17	18	11	1
10	11	18	19	12	1
11	12	19	20	13	1
12	13	20	21	14	1
13	15	22	23	16	1
14	16	23	24	17	1
15	17	24	25	18	1
16	18	25	26	19	1
17	19	26	27	20	1
18	20	27	28	21	1
19	22	29	30	23	1
20	23	30	31	24	1
21	24	31	32	25	1
22	25	32	33	26	1
23	26	33	34	27	1
24	27	34	35	28	1
25	29	36	37	30	1
26	30	37	38	31	1
27	31	38	39	32	1
28	32	39	40	33	1
29	33	40	41	34	1
30	34	41	42	35	1
31	36	43	44	37	1
32	37	44	45	38	1
33	38	45	46	39	1
34	39	46	47	40	1
35	40	47	48	41	1
36	41	48	49	42	1

1	10
-7	10

```
                1
 4000   1
99999  10   1   1
  17
  15
   1   4  -2          7   9
     0.0      0.0   0.2E-3    0.5E5   0.4E-3   0.25E5  0.12E-2   0.15E5
   0.3E-2    7000.   0.6E-2    3000. 0.1020E-1    2200. 0.2020E-1    1000.
 0.402E-1     500.
   7
   2  13   3
   1   8  15  22  29  36  43  44  45  46  47  48  49
```

SMALL MESH W/NRB, SOIL, IMPULSE LOAD

```
 49   36    1    7    2    0 4000       0.10E-5
  0    0    5    0    0   -1    0    0    0
  1    9   14              YUMA SOIL PARAMETERS
    0.05
0.173E-3 0.1904E5     0.38      0.01       5.0       1.0       2.0
    0.0       1.0
0.2644E5    -0.122     0.38
0.4429E5    -0.156     0.38
0.1553E6    -0.192     0.38
0.3442E6    -0.212     0.38
0.2199E7    -0.999     0.38
0.2199E7       0.0     0.38
    0.0  0.7249E2
 -0.1E7    0.65E6
  1          0.00      0.00
  2          0.00      6.00
  3          0.00     12.00
  4          0.00     18.00
  5          0.00     24.00
  6          0.00     30.00
  7          0.00     36.00
  8          6.00      0.00
  9          6.00      6.00
 10          6.00     12.00
 11          6.00     18.00
 12          6.00     24.00
 13          6.00     30.00
 14          6.00     36.00
 15         12.00      0.00
 16         12.00      6.00
 17         12.00     12.00
 18         12.00     18.00
 19         12.00     24.00
 20         12.00     30.00
 21         12.00     36.00
 22         18.00      0.00
 23         18.00      6.00
 24         18.00     12.00
 25         18.00     18.00
 26         18.00     24.00
 27         18.00     30.00
 28         18.00     36.00
 29         24.00      0.00
 30         24.00      6.00
 31         24.00     12.00
 32         24.00     18.00
 33         24.00     24.00
 34         24.00     30.00
 35         24.00     36.00
```

```
36          30.00     0.00
37          30.00     6.00
38          30.00    12.00
39          30.00    18.00
40          30.00    24.00
41          30.00    30.00
42          30.00    36.00
43          36.00     0.00
44          36.00     6.00
45          36.00    12.00
46          36.00    18.00
47          36.00    24.00
48          36.00    30.00
49          36.00    36.00
 1   1   8   9   2                1
 2   2   9  10   3                1
 3   3  10  11   4                1
 4   4  11  12   5                1
 5   5  12  13   6                1
 6   6  13  14   7                1
 7   8  15  16   9                1
 8   9  16  17  10                1
 9  10  17  18  11                1
10  11  18  19  12                1
11  12  19  20  13                1
12  13  20  21  14                1
13  15  22  23  16                1
14  16  23  24  17                1
15  17  24  25  18                1
16  18  25  26  19                1
17  19  26  27  20                1
18  20  27  28  21                1
19  22  29  30  23                1
20  23  30  31  24                1
21  24  31  32  25                1
22  25  32  33  26                1
23  26  33  34  27                1
24  27  34  35  28                1
25  29  36  37  30                1
26  30  37  38  31                1
27  31  38  39  32                1
28  32  39  40  33                1
29  33  40  41  34                1
30  34  41  42  35                1
31  36  43  44  37                1
32  37  44  45  38                1
33  38  45  46  39                1
34  39  46  47  40                1
35  40  47  48  41                1
36  41  48  49  42                1
 1  10
-7  10
```

```
                1
 4000   1
99999  10   1   1
  17
  15
   1   4  -2          7   3
     0.0      0.0    0.001  50000.0    0.002      0.0
   7
   2  13   3
   1   8  15  22  29  36  43  44  45  46  47  48  49
```

SMALL MESH W/NRB, CONCRETE, SMALL BLAST LOAD

```
 49   36   1   7   2   0 3000       0.50E-6
  0    0   5   0   0  -1   0   0   0
  1    9  14              FIBER REINF. CONC. PARAMETERS
    0.05
0.2516E-3 0.1755E7     0.24      0.01      4.0       1.0       3.0
     0.0       1.0
0.1125E7  -0.6E-2      0.24
0.1940E6 -0.32E-1      0.24
 .1380E6  -0.5E-1      0.24
 .2700E7   -0.999      0.24
0.1125E7  0.625E3      0.24
  0.2E3     0.4E3
-0.47E4    0.81E4
-0.268E5  0.2916E5
  1          0.00      0.00
  2          0.00      6.00
  3          0.00     12.00
  4          0.00     18.00
  5          0.00     24.00
  6          0.00     30.00
  7          0.00     36.00
  8          6.00      0.00
  9          6.00      6.00
 10          6.00     12.00
 11          6.00     18.00
 12          6.00     24.00
 13          6.00     30.00
 14          6.00     36.00
 15         12.00      0.00
 16         12.00      6.00
 17         12.00     12.00
 18         12.00     18.00
 19         12.00     24.00
 20         12.00     30.00
 21         12.00     36.00
 22         18.00      0.00
 23         18.00      6.00
 24         18.00     12.00
 25         18.00     18.00
 26         18.00     24.00
 27         18.00     30.00
 28         18.00     36.00
 29         24.00      0.00
 30         24.00      6.00
 31         24.00     12.00
 32         24.00     18.00
 33         24.00     24.00
 34         24.00     30.00
 35         24.00     36.00
```

```
36        30.00    0.00
37        30.00    6.00
38        30.00   12.00
39        30.00   18.00
40        30.00   24.00
41        30.00   30.00
42        30.00   36.00
43        36.00    0.00
44        36.00    6.00
45        36.00   12.00
46        36.00   18.00
47        36.00   24.00
48        36.00   30.00
49        36.00   36.00
 1   1   8   9   2                1
 2   2   9  10   3                1
 3   3  10  11   4                1
 4   4  11  12   5                1
 5   5  12  13   6                1
 6   6  13  14   7                1
 7   8  15  16   9                1
 8   9  16  17  10                1
 9  10  17  18  11                1
10  11  18  19  12                1
11  12  19  20  13                1
12  13  20  21  14                1
13  15  22  23  16                1
14  16  23  24  17                1
15  17  24  25  18                1
16  18  25  26  19                1
17  19  26  27  20                1
18  20  27  28  21                1
19  22  29  30  23                1
20  23  30  31  24                1
21  24  31  32  25                1
22  25  32  33  26                1
23  26  33  34  27                1
24  27  34  35  28                1
25  29  36  37  30                1
26  30  37  38  31                1
27  31  38  39  32                1
28  32  39  40  33                1
29  33  40  41  34                1
30  34  41  42  35                1
31  36  43  44  37                1
32  37  44  45  38                1
33  38  45  46  39                1
34  39  46  47  40                1
35  40  47  48  41                1
36  41  48  49  42                1
 1  10
-7  10
```

```
            1
 3000   1
99999  10   1   1
  17
  15
   1   4  -2          7   9
     0.0      0.0   0.2E-3     50.0   0.4E-3     25.0  0.12E-2     15.0
   0.3E-2      7.0   0.6E-2      3.0 0.1020E-1      2.2 0.2020E-1      1.0
 0.402E-1      0.5
   7
   2  13   3
   1   8  15  22  29  36  43  44  45  46  47  48  49
```

LARGE MESH, SOIL, SHORTENED BLAST LOAD

```
256 225   1  48   1   0 4000       0.10E-5
  0   0   5   0   0  -1   0   0   0
  1   9  14              YUMA SOIL PARAMETERS
    0.00
0.173E-3 0.1904E5     0.38     0.01      5.0      1.0      2.0
    0.0      1.0
0.2644E5   -0.122     0.38
0.4429E5   -0.156     0.38
0.1553E6   -0.192     0.38
0.3442E6   -0.212     0.38
0.2199E7   -0.999     0.38
0.2199E7      0.0     0.38
    0.0  0.7249E2
 -0.1E7   0.65E6
  1          0.00     0.00
  2          0.00     6.00
  3          0.00    12.00
  4          0.00    18.00
  5          0.00    24.00
  6          0.00    30.00
  7          0.00    36.00
  8          0.00    42.00
  9          0.00    48.00
 10          0.00    54.00
 11          0.00    60.00
 12          0.00    66.00
 13          0.00    72.00
 14          0.00    78.00
 15          0.00    84.00
 16          0.00    90.00
 17          6.00     0.00
 18          6.00     6.00
 19          6.00    12.00
 20          6.00    18.00
 21          6.00    24.00
 22          6.00    30.00
 23          6.00    36.00
 24          6.00    42.00
 25          6.00    48.00
 26          6.00    54.00
 27          6.00    60.00
 28          6.00    66.00
 29          6.00    72.00
 30          6.00    78.00
 31          6.00    84.00
 32          6.00    90.00
 33         12.00     0.00
 34         12.00     6.00
 35         12.00    12.00
```

36	12.00	18.00
37	12.00	24.00
38	12.00	30.00
39	12.00	36.00
40	12.00	42.00
41	12.00	48.00
42	12.00	54.00
43	12.00	60.00
44	12.00	66.00
45	12.00	72.00
46	12.00	78.00
47	12.00	84.00
48	12.00	90.00
49	18.00	0.00
50	18.00	6.00
51	18.00	12.00
52	18.00	18.00
53	18.00	24.00
54	18.00	30.00
55	18.00	36.00
56	18.00	42.00
57	18.00	48.00
58	18.00	54.00
59	18.00	60.00
60	18.00	66.00
61	18.00	72.00
62	18.00	78.00
63	18.00	84.00
64	18.00	90.00
65	24.00	0.00
66	24.00	6.00
67	24.00	12.00
68	24.00	18.00
69	24.00	24.00
70	24.00	30.00
71	24.00	36.00
72	24.00	42.00
73	24.00	48.00
74	24.00	54.00
75	24.00	60.00
76	24.00	66.00
77	24.00	72.00
78	24.00	78.00
79	24.00	84.00
80	24.00	90.00
81	30.00	0.00
82	30.00	6.00
83	30.00	12.00
84	30.00	18.00
85	30.00	24.00
86	30.00	30.00
87	30.00	36.00

88	30.00	42.00
89	30.00	48.00
90	30.00	54.00
91	30.00	60.00
92	30.00	66.00
93	30.00	72.00
94	30.00	78.00
95	30.00	84.00
96	30.00	90.00
97	36.00	0.00
98	36.00	6.00
99	36.00	12.00
100	36.00	18.00
101	36.00	24.00
102	36.00	30.00
103	36.00	36.00
104	36.00	42.00
105	36.00	48.00
106	36.00	54.00
107	36.00	60.00
108	36.00	66.00
109	36.00	72.00
110	36.00	78.00
111	36.00	84.00
112	36.00	90.00
113	42.00	0.00
114	42.00	6.00
115	42.00	12.00
116	42.00	18.00
117	42.00	24.00
118	42.00	30.00
119	42.00	36.00
120	42.00	42.00
121	42.00	48.00
122	42.00	54.00
123	42.00	60.00
124	42.00	66.00
125	42.00	72.00
126	42.00	78.00
127	42.00	84.00
128	42.00	90.00
129	48.00	0.00
130	48.00	6.00
131	48.00	12.00
132	48.00	18.00
133	48.00	24.00
134	48.00	30.00
135	48.00	36.00
136	48.00	42.00
137	48.00	48.00
138	48.00	54.00
139	48.00	60.00

140	48.00	66.00
141	48.00	72.00
142	48.00	78.00
143	48.00	84.00
144	48.00	90.00
145	54.00	0.00
146	54.00	6.00
147	54.00	12.00
148	54.00	18.00
149	54.00	24.00
150	54.00	30.00
151	54.00	36.00
152	54.00	42.00
153	54.00	48.00
154	54.00	54.00
155	54.00	60.00
156	54.00	66.00
157	54.00	72.00
158	54.00	78.00
159	54.00	84.00
160	54.00	90.00
161	60.00	0.00
162	60.00	6.00
163	60.00	12.00
164	60.00	18.00
165	60.00	24.00
166	60.00	30.00
167	60.00	36.00
168	60.00	42.00
169	60.00	48.00
170	60.00	54.00
171	60.00	60.00
172	60.00	66.00
173	60.00	72.00
174	60.00	78.00
175	60.00	84.00
176	60.00	90.00
177	66.00	0.00
178	66.00	6.00
179	66.00	12.00
180	66.00	18.00
181	66.00	24.00
182	66.00	30.00
183	66.00	36.00
184	66.00	42.00
185	66.00	48.00
186	66.00	54.00
187	66.00	60.00
188	66.00	66.00
139	66.00	72.00
190	66.00	78.00
191	66.00	84.00

192	66.00	90.00
193	72.00	0.00
194	72.00	6.00
195	72.00	12.00
196	72.00	18.00
197	72.00	24.00
198	72.00	30.00
199	72.00	36.00
200	72.00	42.00
201	72.00	48.00
202	72.00	54.00
203	72.00	60.00
204	72.00	66.00
205	72.00	72.00
206	72.00	78.00
207	72.00	84.00
208	72.00	90.00
209	78.00	0.00
210	78.00	6.00
211	78.00	12.00
212	78.00	18.00
213	78.00	24.00
214	78.00	30.00
215	78.00	36.00
216	78.00	42.00
217	78.00	48.00
218	78.00	54.00
219	78.00	60.00
220	78.00	66.00
221	78.00	72.00
222	78.00	78.00
223	78.00	84.00
224	78.00	90.00
225	84.00	0.00
226	84.00	6.00
227	84.00	12.00
228	84.00	18.00
229	84.00	24.00
230	84.00	30.00
231	84.00	36.00
232	84.00	42.00
233	84.00	48.00
234	84.00	54.00
235	84.00	60.00
236	84.00	66.00
237	84.00	72.00
238	84.00	78.00
239	84.00	84.00
240	84.00	90.00
241	90.00	0.00
242	90.00	6.00
243	90.00	12.00

244			90.00	18.00	
245			90.00	24.00	
246			90.00	30.00	
247			90.00	36.00	
248			90.00	42.00	
249			90.00	48.00	
250			90.00	54.00	
251			90.00	60.00	
252			90.00	66.00	
253			90.00	72.00	
254			90.00	78.00	
255			90.00	84.00	
256			90.00	90.00	
1	1	17	18	2	1
2	2	18	19	3	1
3	3	19	20	4	1
4	4	20	21	5	1
5	5	21	22	6	1
6	6	22	23	7	1
7	7	23	24	8	1
8	8	24	25	9	1
9	9	25	26	10	1
10	10	26	27	11	1
11	11	27	28	12	1
12	12	28	29	13	1
13	13	29	30	14	1
14	14	30	31	15	1
15	15	31	32	16	1
16	17	33	34	18	1
17	18	34	35	19	1
18	19	35	36	20	1
19	20	36	37	21	1
20	21	37	38	22	1
21	22	38	39	23	1
22	23	39	40	24	1
23	24	40	41	25	1
24	25	41	42	26	1
25	26	42	43	27	1
26	27	43	44	28	1
27	28	44	45	29	1
28	29	45	46	30	1
29	30	46	47	31	1
30	31	47	48	32	1
31	33	49	50	34	1
32	34	50	51	35	1
33	35	51	52	36	1
34	36	52	53	37	1
35	37	53	54	38	1
36	38	54	55	39	1
37	39	55	56	40	1
38	40	56	57	41	1
39	41	57	58	42	1

40	42	58	59	43	1
41	43	59	60	44	1
42	44	60	61	45	1
43	45	61	62	46	1
44	46	62	63	47	1
45	47	63	64	48	1
46	49	65	66	50	1
47	50	66	67	51	1
48	51	67	68	52	1
49	52	68	69	53	1
50	53	69	70	54	1
51	54	70	71	55	1
52	55	71	72	56	1
53	56	72	73	57	1
54	57	73	74	58	1
55	58	74	75	59	1
56	59	75	76	60	1
57	60	76	77	61	1
58	61	77	78	62	1
59	62	78	79	63	1
60	63	79	80	64	1
61	65	81	82	66	1
62	66	82	83	67	1
63	67	83	84	68	1
64	68	34	85	69	1
65	69	85	86	70	1
66	70	86	87	71	1
67	71	87	88	72	1
68	72	88	89	73	1
69	73	89	90	74	1
70	74	90	91	75	1
71	75	91	92	76	1
72	76	92	93	77	1
73	77	93	94	78	1
74	78	94	95	79	1
75	79	95	96	80	1
76	81	97	98	82	1
77	82	98	99	83	1
78	83	99	100	84	1
79	84	100	101	85	1
80	85	101	102	86	1
81	86	102	103	87	1
82	87	103	104	88	1
83	88	104	105	89	1
84	89	105	106	90	1
85	90	106	107	91	1
86	91	107	108	92	1
87	92	108	109	93	1
88	93	109	110	94	1
89	94	110	111	95	1
90	95	111	112	96	1
91	97	113	114	98	1

92	98	114	115	99	1
93	99	115	116	100	1
94	100	116	117	101	1
95	101	117	118	102	1
96	102	118	119	103	1
97	103	119	120	104	1
98	104	120	121	105	1
99	105	121	122	106	1
100	106	122	123	107	1
101	107	123	124	108	1
102	108	124	125	109	1
103	109	125	126	110	1
104	110	126	127	111	1
105	111	127	128	112	1
106	113	129	130	114	1
107	114	130	131	115	1
108	115	131	132	116	1
109	116	132	133	117	1
110	117	133	134	118	1
111	118	134	135	119	1
112	119	135	136	120	1
113	120	136	137	121	1
114	121	137	138	122	1
115	122	138	139	123	1
116	123	139	140	124	1
117	124	140	141	125	1
118	125	141	142	126	1
119	126	142	143	127	1
120	127	143	144	128	1
121	129	145	146	130	1
122	130	146	147	131	1
123	131	147	148	132	1
124	132	148	149	133	1
125	133	149	150	134	1
126	134	150	151	135	1
127	135	151	152	136	1
128	136	152	153	137	1
129	137	153	154	138	1
130	138	154	155	139	1
131	139	155	156	140	1
132	140	156	157	141	1
133	141	157	158	142	1
134	142	158	159	143	1
135	143	159	160	144	1
136	145	161	162	146	1
137	146	162	163	147	1
138	147	163	164	148	1
139	148	164	165	149	1
140	149	165	166	150	1
141	150	166	167	151	1
142	151	167	168	152	1
143	152	168	169	153	1

144	153	169	170	154	1
145	154	170	171	155	1
146	155	171	172	156	1
147	156	172	173	157	1
148	157	173	174	158	1
149	158	174	175	159	1
150	159	175	176	160	1
151	161	177	178	162	1
152	162	178	179	163	1
153	163	179	180	164	1
154	164	180	181	165	1
155	165	181	182	166	1
156	166	182	183	167	1
157	167	183	184	168	1
158	168	184	185	169	1
159	169	185	186	170	1
160	170	186	187	171	1
161	171	187	188	172	1
162	172	188	189	173	1
163	173	189	190	174	1
164	174	190	191	175	1
165	175	191	192	176	1
166	177	193	194	173	1
167	178	194	195	179	1
168	179	195	196	180	1
169	180	196	197	181	1
170	181	197	198	182	1
171	182	198	199	183	1
172	183	199	200	184	1
173	184	200	201	185	1
174	185	201	202	186	1
175	186	202	203	187	1
176	187	203	204	188	1
177	188	204	205	189	1
178	189	205	206	190	1
179	190	206	207	191	1
180	191	207	208	192	1
181	193	209	210	194	1
182	194	210	211	195	1
183	195	211	212	196	1
184	196	212	213	197	1
185	197	213	214	198	1
186	198	214	215	199	1
187	199	215	216	200	1
188	200	216	217	201	1
189	201	217	218	202	1
190	202	218	219	203	1
191	203	219	220	204	1
192	204	220	221	205	1
193	205	221	222	206	1
194	206	222	223	207	1
195	207	223	224	208	1

```
 196  209  225  226  210                1
 197  210  226  227  211                1
 198  211  227  228  212                1
 199  212  228  229  213                1
 200  213  229  230  214                1
 201  214  230  231  215                1
 202  215  231  232  216                1
 203  216  232  233  217                1
 204  217  233  234  218                1
 205  218  234  235  219                1
 206  219  235  236  220                1
 207  220  236  237  221                1
 208  221  237  238  222                1
 209  222  238  239  223                1
 210  223  239  240  224                1
 211  225  241  242  226                1
 212  226  242  243  227                1
 213  227  243  244  228                1
 214  228  244  245  229                1
 215  229  245  246  230                1
 216  230  246  247  231                1
 217  231  247  248  232                1
 218  232  248  249  233                1
 219  233  249  250  234                1
 220  234  250  251  235                1
 221  235  251  252  236                1
 222  236  252  253  237                1
 223  237  253  254  238                1
 224  238  254  255  239                1
 225  239  255  256  240                1
   1   10
 -16   10
   1   01
-241   01          16
 241   10
-256   10
                1
4000    1
99999   10   1   1
  44
  4
   1   4  -2          16   9
     0.0      0.0   0.2E-3    0.5E5   0.4E-3   0.25E5  0.12E-2   0.15E5
  0.3E-2    7000.   0.6E-2    3000. 0.1020E-1    2200. 0.2020E-1    1000.
 0.402E-1     500.
  16
```